Review of the finite difference Hartree–Fock method for atoms and diatomic molecules, and its implementation in the x2dhf program

Jacek Kobus[a,*], Susi Lehtola[b]

[a]*Instytut Fizyki, Uniwersytet Mikołaja Kopernika, Grudziądzka 5, 87-100 Toruń, Poland*
[b]*Department of Chemistry, University of Helsinki, P.O. Box 55 (A. I. Virtasen aukio 1), FI-00014 University of Helsinki, Finland*

Abstract

We present an extensive review of the two-dimensional finite difference Hartree–Fock (FD HF) method, and present its implementation in the newest version of x2dhf, the FD HF program for atoms and diatomic molecules. The program was originally published in this journal in 1996, and was last revised in 2013. x2dhf can be used to obtain HF limit values of total energies and multipole moments for a wide range of diatomic molecules and their ions, using either point nuclei or a finite nuclear model. Polarizabilities (α_{zz}) and hyperpolarizabilities (β_{zzz}, γ_{zzzz}, $A_{z,zz}$, $B_{zz,zz}$) can also be computed by the program with the finite-field method. x2dhf has been extensively used in the literature to assess the accuracy of existing atomic basis sets and to help in developing new ones. As a new feature since the last revision, the program can now also perform Kohn–Sham density functional calculations with local and generalized gradient exchange-correlation functionals with the Libxc library of density functionals, enabling new types of studies. Furthermore, the initialization of calculations has been greatly simplified. As before, x2dhf can also perform one-particle calculations with (smooth) Coulomb, Green–Sellin–Zachor and Krammers–Henneberger potentials, while calculations with a superposition of atomic potentials have been added as a new feature. The program is easy to install from the GitHub repository and build via CMake using the x2dhfctl script that facilitates creating its single- and multiple-

---

[*]Corresponding author.
E-mail address: jacek.kobus@umk.pl

threaded versions, as well as building in Libxc support. Calculations can be carried out with `x2dhf` in double- or quadruple-precision arithmetic.

Keywords: Schrödinger equation of one-electron atomic and diatomic systems, restricted open-shell Hartree–Fock method, atoms, diatomic molecules, density functional theory, exchange–correlation, fully numerical solution, local density approximations, generalized gradient approximations, Hooke's atom with exchange-correlation functionals, superposition of atomic potentials, Gauss and Fermi nuclear charge distributions, finite-field method, prolate spheroidal coordinates, eighth order discretization, (multi-colour) successive overrelaxation, parallelisation via OpenMP, parallelisation via Portable Operating System Interface threads (pthreads)

NEW VERSION PROGRAM SUMMARY

Program Title: `x2dhf`
CPC Library link to program files: (to be added by Technical Editor)
Developer's repository link: https://github.com/x2dhf/x2dhf
Code Ocean capsule: (to be added by Technical Editor)
Licensing provisions(please choose one): GPLv3
Programming language: Fortran 95, C
Supplementary material:
Journal reference of previous version: [1]
Does the new version supersede the previous version?: Yes
Reasons for the new version:
Code modularisation with Fortran 95, parallelisation via OpenMP and Portable Operating System Interface threads (pthreads), support for density functional theory using the Libxc library [2], simplified initialization of calculations, build process facilitated by CMake and `x2dhfctl` (a Bash script), testing facilitated by `testctl` (a Bash script) and a host of test suites.
Summary of revisions:
Code overhauled, modularised and streamlined with Fortran 95 standard, parallelisation of the self-consistent field (SCF) process and the successive overrelaxation (SOR) algorithm, corrected implementation of GGA functionals and support for the Libxc library of density functionals [2], improved initialisation of the SCF process via HF or LDA atomic orbitals and the superposition of atomic potentials [3], an enlarged test suite of input data and the corresponding outputs (235 in all) and `xhf` and `testctl` scripts to run and examine the tests. Script `x2dhfctl` added to control the build process via CMake, `pecctl` to automate calculations of potential energy curves and `elpropctl` to calculate (hyper)polarisabilities.
Nature of problem:

The program finds numerically exact solutions of the HF or Kohn–Sham density functional equations for atoms, diatomic molecules, and their ions by determining the lowest energy eigenstates of a given irreducible representation and spin. Density functional calculations can be carried out using various exchange and correlation functionals provided by the Libxc library [2]. The program can also be used to perform independent particle calculations with the (smooth) Coulomb, Green–Sellin–Zachor, Krammers–Henneberger, and superposition of atomic potentials [3], as well as two-particle HF calculations for the harmonium atom.

Solution method:

Factoring out the analytical angular solution around the bond axis, two-dimensional numerical single-particle functions (orbitals) are used to construct an antisymmetric many-electron wave function according to the restricted open-shell HF or density functional theory (DFT) model. The HF/DFT equations are written as coupled two-dimensional second-order (elliptic) partial differential equations (PDEs), which are discretized by an eighth order central difference stencil on a two-dimensional grid, whereas quadrature is performed with a Newton–Cotes rule. The resulting large and sparse system of linear equations are solved by the (multicolour) successive overrelaxation ((MC)SOR) method, and the orbitals and potentials are solved by simultaneous SOR iterations on the corresponding Poisson equations. The convergence of the SCF procedure is monitored with that of the orbital energies and normalisation factors. The precision of the obtained solutions depends on the grid and the system under consideration, and one can typically obtain orbitals that yield total and orbital energies with up to 12 significant figures using double precision arithmetic. If more precise results are needed, `x2dhf` can also be compiled in quadruple precison floating-point arithmetic.

Additional comments including restrictions and unusual features:

CMake (ver. 3) and gfortran/ifort compiler are required to compile and build the program. The incomplete gamma function is needed to evaluate hydrogenic orbitals and its values are calculated by means of the `dgamit.F` subroutine written by Fullerton [4] which uses FORTRAN 90 versions of `d1mach` and `i1mach` functions.

References

[1] J. Kobus, A finite difference Hartree–Fock program for atoms and diatomic molecules, Comput. Phys. Commun. 184 (2013) 799–811. `doi:10.1016/j.cpc.2012.09.033`.

[2] S. Lehtola, C. Steigemann, M. J. T. Oliveira, M. A. L. Marques, Recent developments in LIBXC—a comprehensive library of functionals for density functional theory, SoftwareX 7 (2018) 1–5. `doi:10.1016/j.softx.2017.11.002`.

[3] S. Lehtola, Assessment of initial guesses for self-consistent field calculations. superposition of atomic potentials: Simple yet efficient, J. Chem. Theory Comput. 15 (2019) 1593–1604. `arXiv:1810.11659`, `doi:10.1021/acs.jctc.8b01089`.

[4] W. Fullerton, Netlib, July 1977 edition, C3, Los Alamos Scientific Lab.

Contents

1. Introduction

A great deal of effort has been spent over the last 50 years on the development of computational methods to model the electronic structure of atoms

and molecules. Thanks to the resulting improvements in the ease of use and accuracy of these models, electronic structure calculations are nowadays routine, and a significant part of the computing power available to the scientific community is used to extract atomistic understanding of the physical and chemical behaviour of molecular and solid state systems with a range of methods.

Practically all ab initio electronic structure calculations start out by solving the Hartree–Fock (HF) or Kohn–Sham [2] equations for the molecular orbitals. Naturally, these unknown functions have to be discretized in some way to allow for a computational solution. In mainstream computational chemistry, the molecular orbitals are typically expressed as linear combinations of atomic basis functions, since this makes modeling systems of any composition and geometry straightforward, and the resulting method easily scales to calculations on large systems.

However, atomic basis sets are usually far from complete. Accordingly, any computed properties suffer from basis set truncation errors, which can be difficult to assess and control. Atomic-orbital basis sets do have a major benefit here, in that they tend to benefit from systematic error cancellation for many types of observables, such as reaction or excitation energies and other types of molecular properties. In specific, as errors made in the energetically important core region will be similar across geometries and electronic states, they cancel out when computing such observables.

To work around the limitations posed by basis set truncation error, atomic basis sets typically come in families that span various sizes, commonly ranging from split-valence or double-ζ quality to polarized triple-ζ or polarized quadruple-ζ quality, some families going even further to quintuple-ζ, hextuple-ζ, or beyond. The access to different sized basis sets allows users to find the sweet spot in cost and accuracy for their application. Several families of atomic orbital basis sets have been developed over many decades in order to make calculations of various systems and properties feasible and credible [3–6].

Typical basis set families also offer further variants that have been augmented with diffuse functions for modeling extended electronic states, such as those found in many anionic species. Although these functions typically have little effect on total energies of neutral species in their ground state, they are also often important for the reliable modeling of electronic excited states, which may even require the addition of several sets of diffuse functions to obtain a converged result. Similarly, reliable modeling of the response of

the ground state to an external electric field also usually requires the inclusion of diffuse functions, and multiple augmentation may again be necessary to reach a numerically converged result.

As the quality of a computational solution critically depends on two things—the discretization error and the error inherent in the computational model itself—it is important to separate these two when examining and developing novel discretizations of the electronic structure problem for a given level of theory. Knowing the right result—the complete basis set (CBS) limit—for the studied quantum chemical model is key to the design of new discretizations, or families of basis sets that approach the CBS limit in a systematic and error-balanced sequence.

The design of atomic orbital basis sets therefore often starts from establishing fully numerical reference values at the CBS limit. Comparison to fully numerical reference values enables one to assess the accuracy of the designed approximate atomic basis sets, and this knowledge is useful for designing cost-balanced basis sets.

As we will shortly review, fully numerical calculations on atoms and diatomic molecules have been possible for a long time, and an extensive review of the topic has been recently published [7]. In the following, we will go over the key studies leading to the approach used in the x2dhf program for fully numerical calculations on atoms and diatomic molecules; for further references and other approaches, we invite the reader to read the discussion in ref. 7. We will also undertake a review of further related literature later on in this work (see section 5).

The proper description of the nuclear Coulomb cusp is key to the numerical accuracy of any electronic structure method, as most of the total energy of an atom can be found close to the nucleus. Atoms feature a high degree of symmetry, and the polar spherical coordinate system allows for an efficient handling of atomic problems, as the one-electron solutions can be written as a product of a radial function with an analytic angular solution in terms of spherical harmonics. The radial problem is straightforward to solve by numerical methods, since the singular Coulomb potential is regularized by the r^2 factor in the volume element of the coordinate system, and the resulting one-dimensional problem is facile to solve to high accuracy. As a result, fully numerical calculations on atoms were feasible already in the 1950s [8].

Riding on the success of the atomic approach, there were attempts in the early 1960s to solve the HF problem for molecules with one-center expansions [9–13]. However, as polyatomic calculations lack the symmetry of the

7

atomic problem, the off-center nuclear Coulomb singularities are not killed off by the r^2 Jacobian, and as a result, the one-center expansions converge extremely slowly with respect to the angular expansion, which is where the off-center nuclear Coulomb cusp problem lies. Alternative avenues for poly-atomic molecules are thereby needed.

Like all linear molecules, diatomic molecules have cylindrical symmetry that allows one to factor out the "angular" part of the problem and solve it analytically [7]. However, what makes diatomic molecules special is that they can be fully described within the prolate spheroidal coordinate sys-tem, where there are no issues with nuclear cusps: the volume factor in this coordinate system turns out to be proportional to $dV \propto r_A r_B$, which again regularizes the singularities in the Coulomb nuclear attraction terms $-Z_A/r_A^{-1}$ and $-Z_B/r_B^{-1}$ that are the bane of general three-dimensional ap-proaches for atoms and molecules [7]. This elimination of the nuclear cusps in the prolate spheroidal coordinates enables facile numerical approaches to the diatomic problem, as well, leading to a two-dimensional problem instead of the one-dimensional radial problem found in atoms.

Let us now delve a bit deeper. Let us place nuclei A and B in Carte-sian coordinates along the z axis at points $\mathbf{R}_A = (0, 0, -R/2)$ and $\mathbf{R}_B = (0, 0, +R/2)$, R being the internuclear distance. The prolate spheroidal co-ordinates are then given by the "radial" coordinate

$$\xi = (r_A + r_B)/R, \tag{1}$$

the "relative" coordinate

$$\eta = (r_A - r_B)/R, \tag{2}$$

and the azimuthal angle θ ($0 \leq \theta \leq 2\pi$) measured around the z axis, where $r_A = |\mathbf{r} - \mathbf{R}_A|$ and $r_B = |\mathbf{r} - \mathbf{R}_B|$ are the distances of a given point $\mathbf{r}$ from the two nuclei.

McCullough made the first successful numerical attempt to solve the (multi-configuration) HF equations for diatomic molecules by the so-called partial-wave self-consistent-field method (PWSCF) [14, 15] in this coordi-nate system. As a result of the cylindrical symmetry, the molecular orbitals and the corresponding Coulomb and exchange potentials can be expressed in the form $f(\eta, \xi)e^{im\theta}$, where m is an integer, and the three-dimensional HF equations for diatomic molecules reduce to a set of two-dimensional problems defined by the functions $f(\eta, \xi)$ for each m.

In the PWSCF method, the function f is expanded in η in terms of an orthonormal polynomial basis set,

$$f(\eta, \xi) = \sum_{l=m}^{l_{\max}} X^{ml}(\xi) P_l^m(\eta) \tag{3}$$

where $P_l^m(\eta)$ are associated Legendre polynomials. McCullough then solved the unknown functions $X^{ml}(\xi)$ with finite differences on a grid.

Since the expansion in eq. (3) is in terms of Legendre polynomials while $X^{ml}(\xi)$ was solved on a grid, McCullough referred to this method as *semi-numerical*. However, the expansion in P_l^m is in principle a completely valid fully numerical technique, which typically rely on the use of orthonormal polynomials: calculations can be straightforwardly converged to the CBS limit by studying larger and larger values for the truncation parameter $l_{\max}$. Of course, also the finite difference grid for ξ needs to be converged to reach the CBS limit.

Following McCullough, Becke developed a numerical approach for solving density functional equations for f in a basis of cubic polynomial splines on a two-dimensional grid in the early 1980s [16–19]. Importantly, Becke proposed using a transformed coordinate system [16]: employing the (ν, μ, θ) system of coordinates given by

$$\nu = \cos^{-1} \eta \tag{4}$$

and

$$\mu = \cosh^{-1}(\xi) \tag{5}$$

instead of the (η, ξ, θ) coordinates originally employed by McCullough, exponential functions centered at the nuclei become Gaussians, and molecular orbitals have a definite parity in ν. A combination of this coordinate system, the idea of the original PWSCF approach, and high-order finite elements for the $X^{ml}(\mu)$ expansion has been recently discussed by Lehtola [20], and is available in the HelFEM program [21].

Laaksonen, Pyykkö, and Sundholm joined the effort on fully numerical solutions of diatomic molecules in the early 1980s. Following proof-of-concept work [22, 23], Laaksonen, Pyykkö, and Sundholm quickly found the coordinate system proposed by Becke to be useful in a number of studies at the HF and multiconfiguration self-consistent field levels of theory [24–26] (see ref. 7 for further references). Laaksonen, Pyykkö, and Sundholm chose to employ two-dimensional finite differences for the solution of $f(\nu, \mu)$. The second-

order partial differential equations for the orbitals and potentials were discretized by means of the sixth-order cross-like stencil, and the ensuing large and sparse systems of linear equations were solved by the iterative successive overrelaxation (SOR) method [27]. This approach will be referred to as the finite difference HF (FD HF) method in the remainder of this work.

The first author got interested in the FD HF method in the late 1980s and has been involved in its development and applications ever since [28–30], taking over the work begun by Laaksonen, Pyykkö, and Sundholm. An improved version of the FD HF program was announced in 1996 [31], and it was again revised in 2013 [1]. In this work, we present the current version (3.0) of the x2dhf program; this work is thus an update to the two earlier papers describing previous versions of the program [1, 31].

In short, the content of the paper is as follows. We begin with a thorough discussion of the theory behind x2dhf, and present the latest revisions to the method: various improvements have resulted in a considerable increase in its efficiency. We then present the internal organization of the program; the refactorings performed in the code allow for further development to take place wherever necessary. Next, we review the literature applications of the program, and then demonstrate its capabilities with some example calculations: the method can now be routinely and confidently applied to medium-size diatomic molecules, *i.e.*, systems with 35–45 electrons.

In specific, the layout is the following. The introduction is followed by a general description of the restricted open-shell HF method for diatomic molecules in section 2, which can also be used to solve the Kohn–Sham equations. Also model potentials, such as the Green–Sellin–Zachor and superposition of atomic potentials, as well as the Kramers–Henneberger potential can be modeled within similar approaches by omitting the dielectronic terms. The harmonium atom can be approached with minor modifications to the equations, as well.

Having written down the Fock and Kohn–Sham equations in section 2, the solution of such elliptic partial differential equations (PDE) by the SOR method is discussed in section 3. The accuracy of the discretization of the PDEs is analysed on calculations on a model Poisson equation. The handling of the proper boundary conditions is described, and the numerical stencil used to relax the solution at every inner grid point is presented. The SOR method and its multi-colour variant (MCSOR) are discussed within the context of the solution of the self-consistent field (SCF) equations in terms of macro- and micro-iterations, and the update procedure of the boundary values is also

discussed in this context. The crucial problem of choosing the overrelaxation parameter for orbitals and potentials is analysed in detail, as it is critical for the efficiency of the resulting FD HF method.

The subsequent section 4 describes the `x2dhf` program itself. Pseudocode is used to illustrate the most important routines. The evaluation of first and second derivatives over the ν and μ variables is cast into a matrix-times-vector form which can be performed efficiently on modern hardware. The script used to build the program with OpenMP and Portable Operating System Interface thread (pthread) support is also presented, and the efficiency of the parallelisation of the SCF process is discussed.

Having described the theoretical foundations and the program's structure, related literature complementing the recent review [7], such as literature applications of the `x2dhf` program, are discussed in section 5. Section 6 contains some example results obtained with `x2dhf` for the harmonium atom and Ar-C in the highly repulsive region. In addition, section 6 also contains tests of the Libxc interface for various exchange and correlation functionals on closed-shell atoms, as well as plots of the kinetic potential and its ingredients for the FH molecule at the HF and local spin density (LDA) levels of approximation. The article concludes in section 7. Hartree atomic units are used throughout the text, unless specified otherwise. Further details are discussed in the appendices (sections A.8 to A.14).

2. Problem formulation

2.1. The restricted open-shell HF method
2.1.1. General formulation

Let us study HF calculations for an open-shell diatomic molecular system. We thus approximate the solution of the Schrödinger equation with a single Slater determinant ansatz

$$\Phi = \frac{1}{\sqrt{M!}} \det |\phi_1(1), \phi_2(2), \ldots, \phi_M(M)|, \tag{6}$$

which corresponds to having the electrons occupy the M lowest-lying spin-orbitals $\phi_a = \phi_a(x, y, z, \sigma)$. The HF wave function is found by minimizing the energy functional obtained as the expectation value of the Hamiltonian

$$E[\Phi] = \langle \Phi | H | \Phi \rangle = \left\langle \Phi \left| -\sum_a \frac{1}{2}\nabla_a^2 - \frac{Z_A}{r_{aA}} - \frac{Z_B}{r_{aB}} + \sum_{a<b} \frac{1}{r_{ab}} + \frac{Z_A Z_B}{R} \right| \Phi \right\rangle \tag{7}$$

11

with respect to the orbitals, with the added constraint that the orbitals be orthonormal. This procedure leads to the HF equations (also known as Fock equations) for the occupied orbitals: they are a set of M coupled one-particle integro-differential equations of the form [1, 31, 32]

$$F_a \phi_a = \sum_{b=1}^{M} \varepsilon_{ab} \phi_b, \quad a = 1, \ldots, M, \tag{8}$$

where ε_{ab} are the Lagrangian multipliers that were introduced to enforce orbital orthonormality in the variation. The Fock equations for the orbitals are written in full as

$$-\frac{1}{2} \nabla^2 \phi_a = -\left(-\frac{Z_A}{r_{aA}} - \frac{Z_B}{r_{aB}} + \sum_b \left(V_C^b - V_x^{ab} \right) - \varepsilon_a \right) \phi_a + \sum_{b \neq a} \varepsilon_{ab} \phi_b, \tag{9}$$

where the electron-electron Coulomb V_C and exchange V_x potentials can be determined from orbital densities and orbital products, respectively, by solving the Poisson equations

$$\nabla^2 V_C^b = -4\pi \phi_b^* \phi_b, \tag{10}$$

$$\nabla^2 V_x^{ab} = -4\pi \phi_a^* \phi_b. \tag{11}$$

2.2. Solution by relaxation of Poisson equations

The Fock equations for the orbitals (eq. (9)) are solved by the iterative SCF procedure, which is started from a suitable initial guess. The right-hand side of eq. (9) is known in each SCF iteration, as it is determined by the current best estimate for the orbitals; the Coulomb and exchange potentials are also determined by the same orbitals as solutions to the Poisson equations of eqs. (10) and (11), respectively.

Note that eq. (9) is a Poisson equation, as well. This means that one only needs to iteratively solve sets of Poisson equations to solve SCF. Let us furthermore note that when the density changes considerably between SCF iterations, exact solutions of eqs. (9) to (11) are not necessary, as approximate solutions to these equations are sufficient to approach the SCF solution at a similar rate as if numerically exact solutions of eqs. (9) to (11) were used, instead: after all, the right-hand side of these equations is not accurately known at this stage anyway, since it needs to be found by the SCF procedure.

Thus, when the SCF process is far from convergence, approximate solu-

tions to the Poisson equations for the orbitals and potentials are sufficient. Then, as the SCF approaches convergence, the orbitals and potentials undergo smaller and smaller changes. And in this case, an iterative solution of the Poisson equations will also converge relatively quickly onto the exact solution.

The special feature of the FD HF method is that the SCF iterations are interwoven with a number of SOR relaxation sweeps to improve the solutions to the Poisson equations for the potentials and the orbitals (see section 3.4.3 for in-depth discussion). An analysis of numerical complexity showed the FD method to be about ten-fold more efficient than analogous partial-wave self-consistent-field and finite-element methods due to this interweaving [32].

2.2.1. Angular and radial discretization

As was discussed in the Introduction, the prolate spheroidal coordinate system defined by eqs. (4) and (5) is attractive for discretizing the electronic structure of diatomic molecules: not only does the nuclear Coulomb cusp not pose a problem in this coordinate system, but the choice of the (ν, μ) coordinates also guarantees that ϕ_a is a quadratic function of μ and ν in the vicinity of the z axis.[1]

As was also mentioned in the Introduction, the cylindrical symmetry of diatomic systems allows for handling the θ part of the orbitals and the potentials analytically by expressing them in the factorized form

$$
\left.\begin{array}{c}
\phi_a \\
V_C^a \\
V_x^{ab}
\end{array}\right\} = f(\nu, \mu)e^{im\theta}. \tag{12}
$$

In this equation, m defines the rotation symmetry of the orbital or the potential: for example, σ, π, δ and φ orbitals correspond to $m = 0$, $m = \pm 1$, $m = \pm 2$, and $m = \pm 3$, respectively. Orbitals of higher symmetry than φ are not relevant for the ground states of ordinary diatomic molecules at the HF level of theory.

Since the angle θ does not appear in the Hamiltonian, it is known that the orbitals with $m = \pm|m|$ have the same radial part in exact theory. Although

---

[1]$\mu = 0$ corresponds to the Cartesian coordinates $(0, 0, -R/2 \leq z \leq R/2)$, $\nu = 0$ to $(0, 0, z \geq R/2)$ and $\nu = \pi$ to $(0, 0, z \leq -R/2)$); see section 3.3.2 for details.

this symmetry can be broken in HF as well as in DFT, in `x2dhf` the orbitals with $m = \pm|m|$ are handled as same-shell orbitals, that is, the same $f(\nu, \mu)$ expansion is used for both.

The orbitals are also spin-unpolarized, which is why the resulting method is referred to as restricted open-shell HF (ROHF), which reduces to restricted HF (RHF) for a closed-shell configuration. As a result, while σ orbitals can fit up to 2 electrons, other types of orbitals can fit up to 4 electrons, since they consist of two separate spatial orbitals for $\pm|m|$.

We note that spin-polarized as well as broken-symmetry solutions can be targeted with `HelFEM` [20], which supports calculations with unrestricted HF as well as DFT calculations with LDA, generalized gradient approximation (GGA), and meta-GGA functionals.

2.2.2. Working equations

Now, the total energy expression for the ROHF method reads

$$E = \sum_a q_a \left\langle \phi_a \left| -\frac{1}{2}\nabla^2 + V_n \right| \phi_a \right\rangle + \sum_{a,b} U_{ab} \left\langle \phi_a \left| V_C^b \right| \phi_a \right\rangle - \sum_{a,b} W_{ab} \left\langle \phi_a \left| V_x^{ab} \right| \phi_b \right\rangle$$

(13)

where $V_n = -Z_A/r_A - Z_B/r_B$ is the nuclear potential energy operator, q_a is the occupation number for orbital a, and U_{ab} and W_{ab} are the corresponding occupation-number-dependent factors for the Coulomb and exchange energy contributions. Their values are configuration dependent, and are determined by the Slater–Condon rules for evaluating the expectation values of the two-particle operators with the single Slater determinant wave function.

In the transformed prolate spheroidal coordinates (ν, μ, θ), the "radial" part of the Laplacian reads

$$\frac{4}{R^2(\xi^2 - \eta^2)} \left\{ \frac{\partial^2}{\partial \mu^2} + \frac{\xi}{\sqrt{\xi^2 - 1}} \frac{\partial}{\partial \mu} + \frac{\partial^2}{\partial \nu^2} + \frac{\eta}{\sqrt{1 - \eta^2}} \frac{\partial}{\partial \nu} - m_a^2 u(\eta, \xi) \right\} \quad (14)$$

where we have introduced the helper function

$$u(\eta, \xi) = \frac{1}{\xi^2 - 1} + \frac{1}{1 - \eta^2}. \quad (15)$$

Therefore, by multiplying the Fock equation (eq. (9)) by $-R^2(\xi^2 - \eta^2)/2 = -r_A r_B/2$, we arrive at the working equation for the spatial part of orbital a,

14

$f_a(\nu, \mu)$, in the transformed prolate spheroidal coordinates

$$
\left\{ \frac{\partial^2}{\partial \mu^2} + \frac{\xi}{\sqrt{\xi^2 - 1}} \frac{\partial}{\partial \mu} + \frac{\partial^2}{\partial \nu^2} + \frac{\eta}{\sqrt{1 - \eta^2}} \frac{\partial}{\partial \nu} - m_a^2 u(\eta, \xi) + v(\eta, \xi) \right.
$$

$$
\left. - \frac{R}{\xi}(\xi^2 - \eta^2)\tilde{V}_C + \frac{R^2}{2}(\xi^2 - \eta^2)\varepsilon_a \right\} f_a(\nu, \mu)
$$

$$
+ \frac{R}{\xi}(\xi^2 - \eta^2) \left(\tilde{V}_x^{\,a} + \frac{R\xi}{2} \sum_{b \neq a} \varepsilon_{ab} f_b(\nu, \mu) \right) = 0 \quad (16)
$$

where

$$
v(\eta, \xi) = R[(Z_A + Z_B)\xi + (Z_B - Z_A)\eta] \tag{17}
$$

is the nuclear potential term whose singularities at both nuclei have been cancelled out by the choice of the coordinate system, and the modified Coulomb ($\tilde{V}_C$) and exchange potentials ($\tilde{V}_x^a$) are defined as

$$
\tilde{V}_C = \sum_a \tilde{V}_C^a = \sum_a \frac{R\xi}{2} V_C^a, \tag{18}
$$

$$
\tilde{V}_x^a = \sum_{b \neq a} \tilde{V}_x^{ab} f_b(\nu, \mu) = \sum_{b \neq a} \frac{R\xi}{2} V_x^{ab} f_b(\nu, \mu). \tag{19}
$$

The diagonal orbital energy parameters ε_a in eq. (16) are calculated as

$$
\varepsilon_a = \langle \phi_a | h_a | \phi_a \rangle = \left\langle \phi_a \left| -\frac{1}{2}\nabla^2 + V_n + \frac{2}{R\xi}(\tilde{V}_C - \tilde{V}_x^a) \right| \phi_a \right\rangle, \tag{20}
$$

while the off-diagonal parameters ε_{ab} are obtained as

$$
\varepsilon_{ab} = \frac{q_b}{q_b + q_a} \left(\langle \phi_b | h_a | \phi_a \rangle + \langle \phi_a | h_b | \phi_b \rangle \right), \tag{21}
$$

where q_a and q_b are again the occupation numbers of orbitals a and b. The formulae for evaluating the kinetic and nuclear potential energy terms as well as the Coulomb and exchange energy contributions in eq. (20) are given in section A.9.

We note here that x2dhf program can also perform calculations with finite nuclear models, wherein the nuclear charge distribution is described by either a Gaussian or Fermi distribution instead of a point nucleus. As the

potentials of such spherically symmetric nuclear charge distributions can be written in the form

$$V(r) = -\frac{Z(r)}{r}, \quad r > 0, \tag{22}$$

the finite-nucleus implementation is as simple as replacing $Z_A \to Z_A(r_A)$ and $Z_B \to Z_B(r_B)$ in eq. (17). The parameters of the finite nuclear models have been taken from the table of atomic masses of Wapstra and Audi [33, 34] (see section A.8 for details on the implementation).

The working equation for the exchange potentials is obtained in an analogous manner to the Fock equation. The Poisson equation (eq. (11)) reads in the transformed prolate spheroidal coordinates as

$$\left\{ \frac{\partial^2}{\partial \mu^2} + \left(\frac{1}{\sqrt{\xi^2 - 1}} - \frac{2\sqrt{\xi^2 - 1}}{\xi} \right) \frac{\partial}{\partial \mu} + \frac{\partial^2}{\partial \nu^2} + \frac{\eta}{\sqrt{1 - \eta^2}} \frac{\partial}{\partial \nu} - \frac{2}{\xi^2} \right.$$
$$\left. - (m_a - m_b)^2 u(\eta, \xi) \right\} \tilde{V}_x^{ab} = -\frac{\pi R^3}{2} \xi(\xi^2 - \eta^2) f_a(\nu, \mu) f_b(\nu, \mu) \tag{23}$$

and is solved by overrelaxation, like the Poisson equation for the orbitals (eq. (16)).

It can be seen from eqs. (10) and (11) that the expression for the Coulomb potential can be obtained from that for the exchange by setting $a = b$. The expression is thus obtained from eq. (23) by setting $a = b$ and removing the vanishing term, obtaining

$$\left\{ \frac{\partial^2}{\partial \mu^2} + \left(\frac{1}{\sqrt{\xi^2 - 1}} - \frac{2\sqrt{\xi^2 - 1}}{\xi} \right) \frac{\partial}{\partial \mu} + \frac{\partial^2}{\partial \nu^2} + \frac{\eta}{\sqrt{1 - \eta^2}} \frac{\partial}{\partial \nu} - \frac{2}{\xi^2} \right\} \tilde{V}_C^a$$
$$= -\frac{\pi R^3}{2} \xi(\xi^2 - \eta^2) f_a^2(\nu, \mu). \tag{24}$$

We note here in passing that the variational solution of Poisson's equation in the prolate spheroidal coordinate system has been discussed by Csavinszky [35].

2.3. DFT method

The method described in the previous subsection can be tailored to solve a few other problems of interest. In particular, eq. (9) can adapted for solving

16

the Kohn–Sham [2] equations of density functional theory (DFT) [2, 36]

$$-\frac{1}{2}\nabla^2\phi_a = -\left(-\frac{Z_A}{r_{aA}} - \frac{Z_B}{r_{aB}} + \sum_b V_C^b - v_{xc}^\sigma[n_\alpha, n_\beta] - \varepsilon_a\right)\phi_a + \sum_{b\neq a}\varepsilon_{ab}\phi_b \quad (25)$$

where $v_{xc}^\sigma[n_\alpha, n_\beta]$ is the exchange–correlation (xc) potential.

x2dhf has long supported [31] calculations within the so-called Hartree–Fock–Slater (HFS) model [37], but the details of implementation have not been described in the previous publications [1, 31]. Since the HFS model may not be familiar to most readers, we point out that it is obtained from Hartree–Fock theory by replacing the exact exchange term with Slater's $X\alpha$ functional [37]. However, as the $X\alpha$ functional is just scaled LDA exchange [38, 39], the HFS model can be thought of as a variant of exchange-only LDA.

Importantly, the HFS implementation in x2dhf employs an atom-specific weighting of the $X\alpha$ functional that is optimized to lead to the best agreement with Hartree–Fock total energies [40]. The parameter corresponding to the heavier atom in the molecule is chosen for the calculation in x2dhf. The original aim of such a system dependent functional was to provide a faster alternative to Hartree–Fock, since there is no need to relax exchange potentials in this method. However, this system-dependent HFS model is obviously not a good starting point for computing binding energies $\Delta E_{XY} = E(X) + E(Y) - E(XY)$, for example, as there will be no systematic error cancellation if two different functionals are used to evaluate the terms.

Although the LDA exchange functional itself [38, 39]—whose definition is not system dependent—is also available in x2dhf, many density functional approximations whose definition is not system dependent like the HFS model and that are also more accurate than the LDA have been developed in recent decades. As a new feature in x2dhf, the xc potential can be evaluated with Libxc [41] from the total densities for the spin-up (α) and spin-down (β) electrons

$$n_\alpha = \sum_b q_b \phi_b^{*\alpha} \phi_b^\alpha, \qquad n_\beta = \sum_b q_b \phi_b^{*\beta} \phi_b^\beta, \qquad (26)$$

respectively, for self-consistent calculations with LDA or GGA functionals. While LDAs require no special consideration, GGA functionals introduce dependence on the density gradients ∇n_α and ∇n_β, which needs to be taken into account when solving eq. (25); the relevant details are discussed in section A.10. Note that although some GGA functionals were included in the previous version of the program [1], the gradient dependence of the potential

17

was not considered, and as a result, GGA results obtained with old versions of the program do not reproduce the correct ground state.

Finally, although eq. (25) has been written in the form for semi-local functionals, global hybrid functionals such as B3LYP [42]—which also include a fraction of exact exchange—are also supported in `x2dhf`, following the methodology already presented above in section 2.2.2.

We will verify and exemplify the DFT implementation and Libxc interface below in section 6.4 for calculations with various semi-local and hybrid LDA and GGA functionals.

2.4. Atomic model potentials

Independent particle model potentials are often useful for understanding the arrangement of energy levels in diatomic molecules. Calculations with such potentials avoid the need to solve SCF equations, instead obtaining orbitals and orbital energies from simple model potentials that reproduce the atoms' electronic shell structure. While such models do not yield estimates for total energies due to the lack of interatomic Pauli repulsion effects, they do tend to yield quite reasonable orbitals and orbital energies.

In the model potential approach, the Hamiltonian of eq. (7) is replaced by the following one-electron Hamiltonian

$$E[\Phi] = \langle \Phi | H | \Phi \rangle = \left\langle \Phi \left| -\sum_a \frac{1}{2} \nabla_a^2 - \frac{Z_A^{\text{eff}}(r_{aA})}{r_{aA}} - \frac{Z_B^{\text{eff}}(r_{aB})}{r_{aB}} \right| \Phi \right\rangle \qquad (27)$$

where the effective nuclear charges now depend on the radial distance from the nuclei (cf. eq. (22)). The implementation of this model within the FD HF approach is extremely straightforward, as there is no need to solve for Coulomb or exchange potentials. Instead, the value of the one-particle potential can straightaway be tabulated on the (ν, μ) grid.

In the late 1960s, Green, Sellin, and Zachor (GSZ) [43, 44] proposed a simple radial potential for phenomenological studies

$$Z_A^{\text{eff}}(r) = (Z_A - 1)\Omega(r) + 1 \qquad (28)$$

that was found to yield good agreement with experiment in early studies on diatomic molecules [45–47]. The function Ω in eq. (28) is given by

$$\Omega(r) = \frac{1}{H(\exp(r/d) - 1) + 1} \qquad (29)$$

18

and fitting to atomic HFS calculations led to

$$H = d\alpha(Z - 1)^\nu \tag{30}$$

with $\nu = 0.4$ and $\alpha \approx 1.05$ [43]. The d parameter in eq. (30) is atom-specific, and suitable values have been determined by optimizing the HF energy of the resulting wave function [43]. Support for the GSZ potential in `x2dhf` was already briefly mentioned in the previous publication [1]. As setting $\alpha = 1$ for simplicity causes no significant loss in accuracy [43], this choice has been made in the `x2dhf` implementation.

As a new feature, `x2dhf` can now also be used to solve orbitals arising from the superposition of atomic potentials [48, 49]. The idea of this scheme is similar to that of the GSZ approach: instead of employing a potential with fixed analytic form as in eqs. (28) to (30), self-consistent radial potentials $V(r)$ that contain classical Coulomb, exchange, as well as correlation effects are instead determined in atomic calculations at the CBS limit, and then

$$Z^{\text{eff}}(r) = -rV(r) \tag{31}$$

is computed and tabulated numerically for future use. The tabulated atomic potentials in terms of $Z^{\text{eff}}(r)$ come from exchange-only LDA [38, 39] calculations in `HelFEM` [50, 51], as this level of theory is simple while yielding excellent agreement with the optimized effective potential method [49].

2.5. Kramers–Henneberger atom

Continuing with model potentials, like the previous version of the program [1], also the current version supports calculations [52] with the Kramers–Henneberger potential [53] defined in the cylindrical coordinates z and s as

$$V_{KH}(z, s) = \frac{1}{2}\left(\frac{m}{s}\right)^2 \frac{1}{T}\int_0^T V(z, \beta(t), a)\mathrm{d}t \tag{32}$$

where m is the magnetic quantum number of the state being calculated,

$$V(z, \beta, a) = \frac{-V_0}{\frac{2\pi}{\omega}\sqrt{a^2 + \beta^2 + z^2}} \tag{33}$$

where a and V_0 are the width and depth of the soft-core potential, respectively; ϵ is the intensity and ω the cycle frequency of the laser field; and

$$\beta(t) = s + \alpha_0 + \alpha_0(\cos(\omega t) - 1), \quad \alpha_0 = \epsilon/\omega^2 \tag{34}$$

is the electron's classical trajectory of oscillatory motion. The numerical integration in eq. (32) is carried out in `x2dhf` using composite Simpson quadrature.

2.6. Harmonium atom

The method for solving the HF equations for diatomic molecules can also be applied to the harmonium atom, which is also known as Hooke's (law) atom. If the Hamiltonian in eq. (7) is replaced by that of harmonium

$$\begin{aligned}
H &= -\frac{1}{2}\nabla_a^2 + \frac{1}{2}\omega^2 \boldsymbol{r}_a^2 - \frac{1}{2}\nabla_b^2 + \frac{1}{2}\omega^2 \boldsymbol{r}_b^2 + \frac{1}{|\boldsymbol{r}_a - \boldsymbol{r}_b|} \\
&= -\frac{1}{2}\nabla_a^2 - \frac{1}{2}\nabla_b^2 + \frac{1}{2}\omega^2(r_a^2 + r_b^2) + \frac{1}{r_{ab}}
\end{aligned} \tag{35}$$

we see that instead of the nuclear potential, V_n, we now have to deal with the harmonic potential $\frac{1}{2}\omega^2(r_a^2 + r_b^2)$, where r_i is the distance from the geometric centre, $r_i = \xi_i \eta_i / \sqrt{\xi_i^2 + \eta_i^2 - 1}$, and r_{ab} is the distance between the two electrons.

The Schrödinger equation for harmonium can be solved exactly, as the Hamiltonian of eq. (35) can be decoupled in the center of mass coordinate system given by the centroid $\boldsymbol{R} = \frac{1}{2}(\boldsymbol{r}_1 + \boldsymbol{r}_2)$ and the relative coordinate $\boldsymbol{r} = \boldsymbol{r}_1 - \boldsymbol{r}_2$, yielding

$$H = -\nabla_r^2 + \frac{1}{4}\omega^2 r^2 + \frac{1}{r} - \frac{1}{4}\nabla_R^2 + \omega^2 R^2. \tag{36}$$

The centroid and relative coordinates are sometimes also referred to as extra- and intracular coordinates, respectively. In the new coordinates, the eigenvalue problem can be formulated as

$$\left(-\frac{1}{2}\nabla_r^2 + \frac{1}{2}\omega_r^2 r^2 + \frac{1}{2r}\right)\psi_r(r) = \frac{1}{2}E_r\psi_r(r), \tag{37}$$

$$\left(-\frac{1}{2}\nabla_R^2 + \frac{1}{2}\omega_R^2 R^2\right)\Psi_R(r) = 2E_R\Psi_R(r), \tag{38}$$

20

where $\omega_r = \omega/2$, and $\omega_R = 2\omega$ and the eigenvalue of the original Hamiltonian is obtained as the sum of the eigenvalues E_r and E_R of the decoupled equations. The decoupling has thus split the hard-to-solve correlated two-particle problem into two independent one-dimensional one-particle Schrödinger equations, which allow either closed-form analytical or facile numerical solution to arbitrary precision with established methodologies, meaning that the full correlated problem in Hooke's atom is indeed (numerically) exactly solvable.

It has been shown that the intracular problem (eq. (37)) has analytical solutions for some values of ω_r [54]: in particular, when $\omega_r = 1/2$ (corresponding to $\omega = \sqrt{2}/2$), then $E_r = 5/4$. However, a numerical solver is necessary to find solutions for other values of ω_r. Fortunately, eq. (37) can be viewed as a simplified variant of the Fock equation (eq. (9)), and the FD HF technique can be used to solve it. The new version of `x2dhf` allows calculations on the harmonium atom as a novel feature; examples will be discussed below in section 6.2.

3. Solving elliptic PDEs

In the previous section, we saw that the problem of solving the Fock and Kohn–Sham equations (eqs. (8) and (25)), the orbitals for the Green–Sellin–Zachor potential (eqs. (28) to (30)), the superposition of atomic potentials (eq. (31)), as well as the Kramers–Henneberger potential (eq. (32)), and the intracule equation for the harmonium atom (eq. (37)) involve solving second-order partial differential equations (PDEs) of the form

$$\left\{ A(\nu,\mu)\frac{\partial^2}{\partial\nu^2} + B(\nu,\mu)\frac{\partial}{\partial\nu} + C(\nu,\mu)\frac{\partial^2}{\partial\mu^2} + D(\nu,\mu)\frac{\partial}{\partial\mu} + E(\nu,\mu) \right\} f(\nu,\mu)$$
$$= F(\nu,\mu), \qquad (39)$$

where the functions are defined on a rectangular domain $(\nu,\mu) \in [0,\pi] \times [0,\mu_\infty]$ that corresponds to $(\eta,\xi) = [-1,1] \times [1,\xi_\infty]$. Within the approach used in `x2dhf`, one chooses a suitable grid (section 3.1), and approximates the first and second derivatives by finite differences of a given order (sections 3.2 and 3.3). The resulting system of linear equations is solved by the SOR or MCSOR methods, which are discussed below in section 3.4.

3.1. Grid specification

To obtain accurate, *i.e.*, HF limit solutions to the FD HF equations, one has to guarantee that all orbitals and all the corresponding Coulomb and exchange potentials have been calculated to high accuracy. In specific, this requires converging the calculations with respect to the employed grid size; we will exemplify this below in section 3.2 on a model Poisson equation.

Importantly, the domain definition also depends on the specification of a μ_∞ (or ξ_∞) parameter, which means that the calculation also has to be converged with respect to the employed μ_∞ parameter. In the `HelFEM` program [20, 50, 51, 55], this parameter only controls how far orbitals are non-zero, because `HelFEM` employs a variational approach where the orbitals are found by diagonalization and the potential is evaluated analytically. In `x2dhf`, however, the μ_∞ parameter has a double role: in addition to the above role pertaining to the finite support of the orbitals, `x2dhf` also relies on the use of asymptotic expansions of the orbitals and potentials in the region close to μ_∞ to set the boundary conditions for the relaxation procedure.

Since the isosurfaces of μ approach spheres for large μ (see fig. 1), the radial boundary value is typically chosen with the radius of such a sphere as

$$\mu_\infty = \cosh^{-1} \xi_\infty = \cosh^{-1} \frac{2r_\infty}{R}, \tag{40}$$

where r_∞ defines the employed value for the "practical infinity" [7]. While orbitals usually decay quite quickly, the potentials can sometimes deviate from their asymptotic limit in a large region. The value of r_∞ must thus be chosen large enough in `x2dhf` to guarantee that both the orbitals and potentials have reached their asymptotic behaviour, as this is used to estimate their values in points in the boundary region (see sections A.11 and A.12 for details). Calculations with `x2dhf` thereby sometimes require the use of extremely large values of r_∞ to obtain results converged to the HF limit [56].

The grid points in the ν and μ coordinates are distributed uniformly as

$$\nu_i = (i-1)h_\nu, \; h_\nu = \pi/(N_\nu - 1), \quad i = 1, 2, ..., N_\nu$$
$$\mu_i = (i-1)h_\mu, \; h_\mu = \mu_\infty/(N_\mu - 1), j = 1, 2, ..., N_\mu \tag{41}$$

where N_ν and N_μ are the number of grid points in the ν and μ variables, respectively, μ_∞ can be computed from r_∞ by eq. (40). Such a uniform distribution of the grid points in the (ν, μ) plane corresponds to a non-uniform

Figure 1: Distribution of grid points in the (z, x) plane corresponding to the uniform distribution in (ν, μ) variables on a $[50 \times 50/50a_0]$ grid. The upper plot shows the whole grid, while the lower plot is a close-up of the region around the A and B nuclei at $(-1, 0)$ and $(1, 0)$, respectively.
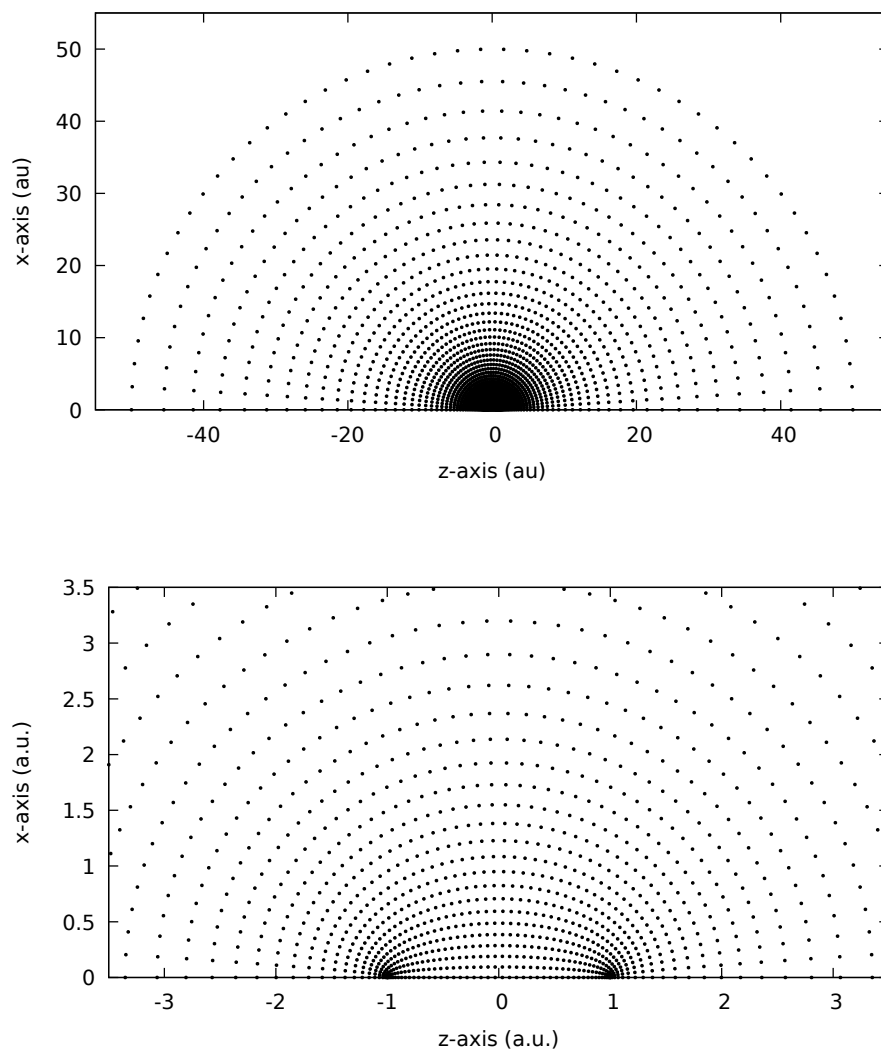
distribution in the (z, x) plane with more grid points in the vicinity of the nuclei, as shown in fig. 1, and such a grid will be denoted as $[N_\nu \times N_\mu / r_\infty]$; a similar input is used to specify the grid in `x2dhf`.

According to our experience with the FD HF method, we find that the best accuracy is typically achieved when $h_\nu \approx h_\mu$. Since the domain of the ν variable is always $\nu \in [0, \pi]$, the grid can also be specified in `x2dhf` more simply as N_ν / r_∞, as the value of N_μ that yields $h_\mu \approx h_\nu$ is easy to determine automatically within the employed discretization,[2] which will be discussed next.

3.2. Various discretizations of a model problem

Our generalized elliptic PDE of eq. (39) can be discretized on a given numerical grid by the $r + 1$ point stencil, which is based on the r-th order Stirling interpolation formula [57]. But, what order r of the discretization should one apply to eq. (39)? To try to answer this question, let us examine the following model Poisson equation

$$\frac{\partial^2 f}{\partial x^2} + \frac{\partial^2 f}{\partial y^2} = -(n+1)^2 \left[\sin((n+1)x) + \sin((n+1)y) \right] =: G(x, y) \quad (42)$$

where we have implicitly defined the source term $G(x, y)$.

We will now examine solutions of eq. (42) in the square $(x, y) = [0, \pi] \times [0, \pi]$, when we pose zero boundary conditions at the four edges: $f(0, y) = 0$, $f(\pi, y) = 0$, $f(x, 0) = 0$, and $f(x, \pi) = 0$. It is easy to see that the exact solution of eq. (42) in this region with these boundary conditions is just

$$f(x, y) = \sin[(n+1)x] + \sin[(n+1)y], \quad (43)$$

so the parameter n in eq. (42) gives the number of inner nodes ($f = 0$) in each variable in the exact solution.

Let us now discretize eq. (42) on a grid. Equation (42) is an infinite family of problems; in the following, we will study the case $n = 3$, whose solutions therefore should have three inner nodes. We will study various numerical stencils with $N_x = N_y = 100$, 200, 400, and 800 points on both axes.

The accuracy of the resulting SOR method can be assessed by checking how well the obtained numerical solution $f(x_i, y_j)$ agrees with the exact solu-

---

[2]Note the limitations on the supported grid sizes discussed below in section 3.3.

tion. The question now arises on how to check this agreement in a reasonable manner? It turns out there is an elegant solution to this question: combining eqs. (42) and (43), we see that the exact solution satisfies

$$G(x, y) = -(n + 1)^2 \sin[(n + 1)x] + \sin[(n + 1)y] = -(n + 1)^2 f(x, y), \quad (44)$$

which we can use to assess the quality of numerical solutions of eq. (42): our error metric is given by the maximal deviation from the expected result

$$\Delta f = \max_{1 \leq i \leq N_x, 1 \leq j \leq N_y} \left| f(x_i, y_j) - \frac{G(x_i, y_j)}{(n + 1)^2} \right|. \quad (45)$$

The results collected in table 1 that are displayed in fig. 2 show that—as expected—using a larger and larger grid typically leads to a more and more accurate solution. In addition to the grid size, the error also strongly depends on the employed order of the finite difference rule: a higher-order stencil affords more accurate results with exactly the same grid. The differences in accuracy between the rules of various orders are considerable. The use of low-order stencils is unattractive, since the errors remain large even with the largest 800×800 grid: $\mathcal{O}(10^{-5})$ with the second-order and $\mathcal{O}(10^{-9})$ with the fourth-order rule. The sixth order rule already reaches $\Delta f < 10^{-11}$ with the 800×800 grid, while the eighth order rule reaches such an accuracy with just the 200×200 grid, and the tenth order rule with the 100×100 grid.

When a high-order approximation is used with a large grid, the error made by approximating the PDE by the finite difference method thus starts to be insignificant, which leaves the use of finite floating point precision as the dominant remaining source of error. Contrasting the data in table 1 computed in double and quadruple precision, it becomes clear that numerical round-off effects start to show up for the sixth, eighth, and tenth-order stencils with all of the studied grids.

It can be seen from the data that the numerical error of the procedure in double precision saturates to around 4 orders of magnitude greater than machine precision, $\Delta f \approx 10^{-12}$ while $\epsilon_{\text{machine}} \approx 2.2 \times 10^{-16}$. Yet, for all practical intents and purposes, this level of precision should be sufficient; if necessary, x2dhf can also be compiled in quadruple precision.

3.3. Discretization used in x2dhf

A sixth-order stencil was originally used in the FD HF method [58]. In the first version of the present program, this stencil was replaced with the

Table 1: Accuracy (Δf) of the numerical solution of the model Poisson equation (eq. (42)) with $n = 3$ as a function of the grid size for finite difference stencils of various numerical orders. For comparison, in addition to calculations performed in double precision floating-point arithmetic, results are also included for quadruple precision arithmetic.

grid/order	100×100	200×200	400×400	800×800
	Δf (double precision)			
2	4.2×10^{-3}	1.0×10^{-3}	2.6×10^{-4}	6.5×10^{-5}
4	1.4×10^{-5}	8.6×10^{-7}	5.3×10^{-8}	3.3×10^{-9}
6	5.7×10^{-8}	8.6×10^{-10}	1.3×10^{-11}	6.7×10^{-12}
8	2.5×10^{-10}	1.2×10^{-12}	1.7×10^{-12}	3.1×10^{-12}
10	1.2×10^{-12}	2.8×10^{-13}	6.9×10^{-12}	1.1×10^{-12}
	Δf (quadruple precision)			
2	4.2×10^{-3}	1.0×10^{-3}	2.6×10^{-4}	6.5×10^{-5}
4	1.4×10^{-5}	8.6×10^{-7}	5.3×10^{-8}	4.0×10^{-9}
6	5.7×10^{-8}	6.6×10^{-10}	1.3×10^{-11}	2.1×10^{-13}
8	2.5×10^{-10}	9.5×10^{-13}	3.7×10^{-15}	1.4×10^{-17}
10	1.2×10^{-12}	1.1×10^{-15}	1.1×10^{-18}	1.0×10^{-21}

Figure 2: Comparison of the accuracy Δf of the numerical solution of the model Poisson equation (eq. (42)) in double- and quadruple-precision (dashed and solid lines, respectively). See table 1 for details.
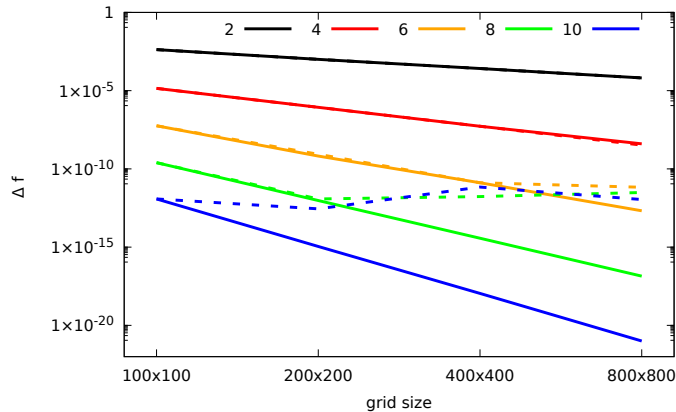
eighth-order stencil, resulting in improved accuracy and thus a substantial reduction of computational costs [31]. Although the use of even higher-order stencils would be appealing due to the greatly improved numerical accuracy and resulting savings in grid size, the application of higher-order rules is challenged by Runge's phenomenon [59] as `x2dhf` employs uniformly spaced grids: function interpolation on a uniformly spaced grid becomes numerically ill-behaved at high order. The same challenge also exists with finite element approaches that employ uniformly placed nodes [7].

We note here that modern mathematical approaches avoid the problem associated with Runge's phenomenon by employing non-uniform grids. For instance, recent works by the second author have demonstrated the feasible stability of up to 19th order schemes in electronic structure calculations [50, 60, 61], achieving significant increases in accuracy at similar computational cost. It would be desirable to pursue higher order stencils in future versions of the `x2dhf` program, as well.

The eighth-order stencil is thus still used in the current version of `x2dhf`.

This stencil is given by

$$f'_i = \frac{1}{840h} \left(3f_{i-4} - 32f_{i-3} + 168f_{i-2} - 672f_{i-1}\right.$$
$$\left. +672f_{i+1} - 168f_{i+2} + 32f_{i+3} - 3f_{i+4}\right) + O(h^8)$$
$$f''_i = \frac{1}{5040h^2} \left(-9f_{i-4} + 128f_{i-3} - 1008f_{i-2} + 8064f_{i-1} - 14350f_i\right.$$
$$\left. +8064f_{i+1} - 1008f_{i+2} + 128f_{i+3} - 9f_{i+4}\right) + O(h^8) \tag{46}$$

where $f_i = f(x_1 + ih)$ and x stands for either ν or μ. However, knowing how to differentiate is not enough: a quadrature rule is also necessary to evaluate the integrals that arise in the FD HF method. x2dhf employs the 7-point Newton–Cotes quadrature formula

$$\int_{x_1}^{x_7} f(x)\mathrm{d}x = \frac{h}{140}(41f_1 + 216f_2 + 27f_3 + 272f_4 + 27f_5 + 216f_6 + 41f_7) + \mathcal{O}(h^9) \tag{47}$$

which is therefore asymptotically more accurate than the 8 and 9 point expressions for estimating the first and second derivatives above in eq. (46). Since the quadrature rule employs 7 consecutive points at a time, it imposes a limitation for the total number of grid points in the ν and μ variables. The smallest number of grids points one could use is of course 7. The next smallest grid contains 13 points, as the last point of the first interval is the first point of the second interval. Therefore, the grid size must be of the form $6N + 1$, where N is an integer.

When the MCSOR scheme discussed below in section 3.4.2 is used, a further restriction on the number of grid points in the ν and μ variables has to be imposed. If MCSOR sweeps are carried out with column-major or row-major ordering (see sections 3.4.1 and 3.4.2), N_ν and N_μ must be of the form $(k/2+1)N' + (k/2+1) + 1$, where k is the employed order of finite differences and N' is another integer. Since $k = 8$ in x2dhf, we get that the number of grid points in μ and ν must be of the form $5N' + 6 = 5(N' + 1) + 1$, although different sized grids can be used for μ and ν. With the aim of enabling switching between the SOR and MCSOR relaxation methods in various steps of any calculation, the implementation in x2dhf forces the additional MCSOR grid size limitation in all calculations.

Taking the conditions arising from the use of the 7-point quadrature rule of eq. (47) as well as from MCSOR together, we thus see that the number of

28

points in μ needs to be of the form $30N + 1$, where N is an integer, since 30 is the smallest common denominator of 5 and 6. The smallest possible grid that satisfies this limitation is therefore the $N_\nu = N_\mu = 31$ grid.

This smallest possible grid is illustrated in fig. 3 together with the application of eq. (46) in two dimensions, which yields a 17-point cross-like pattern.

3.3.1. Boundary conditions

The use of eq. (46) to evaluate derivatives at grid point (x_i, y_j) requires knowledge of the values $f(x_{i'}, y_{j'})$ for $i' \in [i-4, i+4]$ and $j' \in [j-4, j+4]$. This leads to the problem that when eq. (46) is used to discretize eq. (39), one also needs to solve for grid points located within the boundary band: if the point (x_i, y_j) is close to grid boundaries, the stencil will end up operating on points that do not formally exist on the grid. This is a rather unwelcome complication, because it results in a more complex algorithm.

Laaksonen, Pyykkö, and Sundholm used a different numerical stencil for the boundary grid points than for the inner grid points: while they used central finite differences for inner grid points, they used one-sided finite differences to find the solution in the points close to the boundary. When a high-order rule is employed, this approach thus requires using a different set of rules for the points close to the boundaries.

We can exemplify this complication in one dimension with the 9-point rule of eq. (46) at the $x = 0$ boundary, employing grid points at $x_i = (i-1)h$ for $i \in [1, N]$. Assuming $N \gg 1$, we could then use the rule of eq. (46) down to $i = 5$, which would use $(f_1, \ldots, f_9)$ for the interpolation. The finite difference rules for the points $i \in [1, 4]$ would still use the same set of input values $(f_1, \ldots, f_9)$, but stencil would be different for each of these points. In more dimensions, such an algorithm requires even more complicated logic, since a point can be in or out of the boundary region in each dimension.

However, also another approach is possible. When we dealt with the model problem (eq. (42)), we knew the exact solution, and provided extra data by continuing the exact solution outside the numerical grid. Thus, if we can also provide additional boundary values for FD HF calculations, we are able to use the same stencil for all inner grid points.
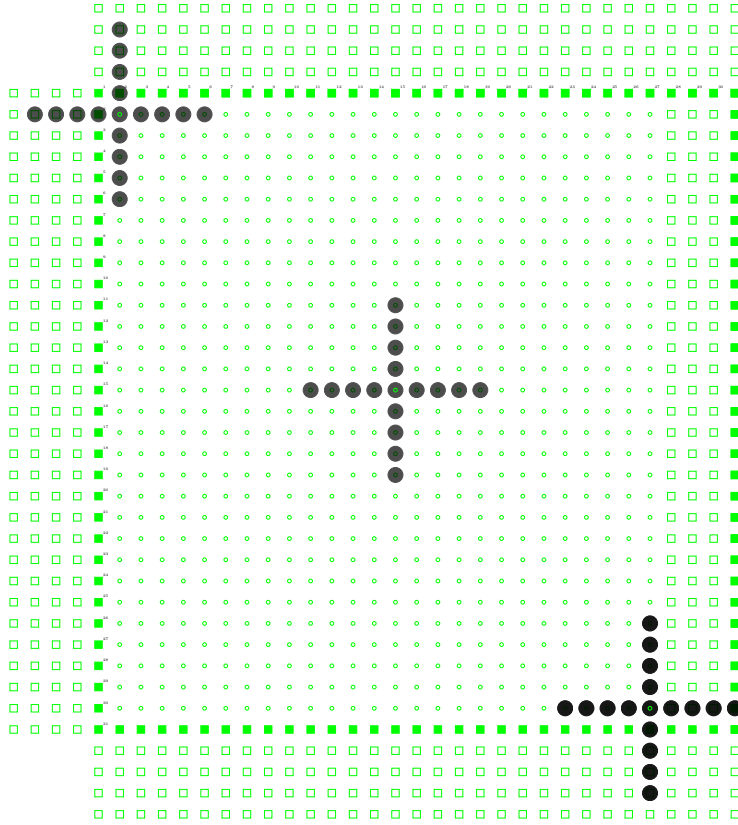
Figure 3: A visualization of a 31×31 grid for f, and the 17-point numerical stencil employed by x2dhf. Filled green squares denote the limits of the 31×31 grid, and points where the solution are found from the Poisson equation are shown as small empty green circles. Extra boundary values shown as empty green squares must be provided to be able to employ the 17-point stencil to relax the solution at every inner point. The points on the right-hand side of the grid are beyond the practical infinity μ_∞, where we assume that the orbitals and potentials vanish identically. The known behaviour of the orbitals and potentials in the large-r region close to μ_∞ is employed to determine their values at points close to the boundary at μ_∞. Note that while no data exists at the left hand segment of the grid, as illustrated by the empty regions in the upper and lower left corners of the figure, the upper and lower right corners are required for the calculation of the kinetic energy in the asymptotic region.

3.3.2. Symmetry properties of coordinate system

The calculation of some of these extra boundary values relies on knowledge of the symmetry of the coordinate system. The Cartesian coordinates in terms of (ν, μ, θ) read

$$
\begin{aligned}
x &= \frac{R}{2} \sinh(\mu) \, \sin(\nu) \, \cos(\theta) \\
y &= \frac{R}{2} \sinh(\mu) \, \sin(\nu) \, \sin(\theta) \\
z &= \frac{R}{2} \cosh(\mu) \, \cos(\nu)
\end{aligned}
\tag{48}
$$

where $\mu \in [0, \mu_{\max}]$, $\nu \in [0, \pi]$ and $\theta \in [0, 2\pi]$. It is clear from eq. (48) that (fictitiously) flipping the sign of μ or ν flips the point at (x, y, z) over to $(-x, -y, z)$. However, the same result $[(x, y, z) \to (-x, -y, z)]$ is also obtained when $\theta \to \theta + \pi$, and we know from the analytical angular solution

$$
e^{im\theta} = \cos(m\theta) + i \sin(m\theta)
\tag{49}
$$

that $\theta \to \theta + \pi$ leads to an additional $(-1)^m$ phase factor. Because of this property, we can immediately identify that flipping the sign of ν leads to

$$
f(\nu, \mu) = (-1)^m f(-\nu, \mu)
\tag{50}
$$

and also that flipping the sign of μ leads to the analogous property

$$
f(\nu, \mu) = (-1)^m f(\nu, -\mu).
\tag{51}
$$

We can identify one further symmetry condition for the $\nu \in [0, \pi]$ axis by examining eq. (48) around $\nu = \pi$. We observe that $\nu \to \pi + \nu$ flips $(x, y, z) \to (-x, -y, -z)$ while $\nu \to \pi - \nu$ leads to $(x, y, z) \to (x, y, -z)$. We thus observe that the two coordinates $(-x, -y, -z)$ and $(x, y, -z)$ differ by a (x, y) inversion, and we can write down the third symmetry equation by again using the same relation obtained above

$$
f(\pi + \nu, \mu) = (-1)^m f(\pi - \nu, \mu).
\tag{52}
$$

Although the coordinate system does not formally have points at $\mu < 0$ or $\nu < 0$, x2dhf employs extended grids that can have such values to facilitate the relaxation process: as was discussed above in section 3.3.1, the finite

difference stencil can reach points that are formally outside the grid. Knowing the symmetry of the orbitals and potentials around the μ and ν axes is therefore of great value for the numerical implementation.

From the above discussion, we observe that orbitals have definite symmetry around the μ and ν axes, and can be divided into components of even or odd symmetry with respect to this inversion: Orbitals of σ, δ, ... symmetry are even functions of (ν, μ), while orbitals of π, φ, ... symmetry are odd functions of (ν, μ).

Since Coulomb and exchange potentials arise from products of orbitals, they have analogous symmetry properties. Coulomb potentials are always of σ symmetry and thus even functions around the μ and ν axes, since there is no m dependent term in eq. (24). Exchange potentials can be of either even or odd symmetry, depending on the value of $m_a - m_b$ in eq. (23).

We observe from eqs. (50) to (52) that any odd function vanishes along the $(\nu, 0)$, $(0, \mu)$ and (π, μ) boundary lines, while even functions are finite at the boundary lines and their values on these lines need to be determined in the SCF/SOR procedure. Before discussing the rules for how this takes place in section 3.3.4, we first comment on an additional symmetry found in homoatomic molecules.

3.3.3. Symmetry in homoatomic molecules

Homoatomic molecules have an additional symmetry with respect to inversion $z \leftrightarrow -z$. It is easy to see that this symmetry leads to

$$f(\pi - \nu, \mu) = \pm f(\nu, \mu), \ \nu \in [0, \pi] \tag{53}$$

where the plus and minus signs are for gerade and ungerade solutions, respectively. In principle, this symmetry could be utilised to reduce the memory needed to store orbitals and potentials and—more importantly—the number of grid points undergoing relaxation by a factor of two. However, this would incur the additional hassle of handling boundary conditions at $\nu = \pi/2$. Therefore, the $D_{\infty h}$ symmetry is only used to explicitly force the symmetry of the orbitals in post-processing in the aims to improve SCF/SOR convergence.

3.3.4. Determination of boundary values

Since orbitals and potentials are either even or odd functions of μ and ν, the values of f on the other side of the boundary lines are known. All that

remains is then to determine the values of the orbitals and potentials on the $(\nu, 0)$, $(0, \mu)$ and (π, μ) boundary lines themselves.

We note again that interpolation is not needed for functions of odd symmetry, such as orbitals and potentials of π or φ symmetry, as such functions vanish on the boundary lines. The only thing that needs to be done is therefore to derive equations for determining the values of even functions, such as orbitals and potentials of σ and δ symmetry, on the $(\nu, 0)$, $(0, \mu)$ and (π, μ) boundary lines.

Assuming that $f(\nu_1, \mu_j) = f(\nu_1, -\mu_j)$, $f(\nu_{N_\nu}, \mu_j) = f(\nu_{N_\nu}, -\mu_j)$, $j = 2, N_\mu$, and that $f(\nu_i, \mu_1) = f(-\nu_i, \mu_1)$, $i = 2, N_\nu - 1$, and using the 9-point Lagrange interpolation formula for equally spaced abscissas, it is possible to derive formulae for updating the function values along the boundaries (see section A.13)

$$f(\nu_1, \mu_j) = \frac{1}{126} \left(210 f(\nu_2, \mu_j) - 120 f(\nu_3, \mu_j) + 45 f(\nu_4, \mu_j) \right.$$

$$\left. - 10 f(\nu_5, \mu_j) + f(\nu_6, \mu_j) \right)$$

$$f(\nu_{N_\nu}, \mu_j) = \frac{1}{126} \left(210 f(\nu_{N_\nu-1}, \mu_j) - 120 f(\nu_{N_\nu-2}, \mu_j) + 45 f(\nu_{N_\nu-3}, \mu_j) \right.$$

$$\left. - 10 f(\nu_{N_\nu-4}, \mu_j) + f(\nu_{N_\nu-5}, \mu_j) \right)$$

$$f(\nu_i, \mu_1) = \frac{1}{126} \left(210 f(\nu_i, \mu_2) - 120 f(\nu_i, \mu_3) + 45 f(\nu_i, \mu_4) \right.$$

$$\left. - 10 f(\nu_i, \mu_5) + f(\nu_i, \mu_6) \right)$$

$$i = 2, N_\nu - 1, \quad j = 2, N_\mu \qquad (54)$$

So far we have only discussed the $(\nu, 0)$, $(0, \mu)$ and (π, μ) boundaries; yet, the (ν, μ_∞) boundary line needs to be addressed, as well. Since this boundary line corresponds to points that are far away from the molecule, we assume that the orbitals and potentials vanish for $\mu > \mu_\infty$. Moreover, we will estimate the values f of the orbitals and potentials that are close to the boundary, $f(\nu_i, \mu_{N_\mu-4+k})$, $i = 1, \ldots, N_\nu$, $k = 1, \ldots, 4$, with the known asymptotic behaviour of the orbitals and potentials; see sections A.11 and A.12 for in-depth discussion.

3.3.5. Compact notation for difference formulas

One can note that the first and second derivative expressions in eq. (46) are odd and even functions of the grid points around the expansion point. The expressions for the various μ derivatives needed for FD HF can then be rearranged as

$$
\begin{aligned}
\left.\frac{\partial f}{\partial \mu}\right|_{i,j} &= \sum_{k=1}^{4} d_k^{(\mu)}\left(f(\nu_i, \mu_{j-k}) - f(\nu_i, \mu_{j+k})\right) \\
&= \sum_{k=1}^{9} \tilde{d}_k^{(\mu)} f(\nu_i, \mu_{j-5+k}) \\
\left.\frac{\partial^2 f}{\partial \mu^2}\right|_{i,j} &= \sum_{k=1}^{4} d_k^{(\mu\mu)}\left(f(\nu_i, \mu_{j-k}) + f(\nu_i, \mu_{j+k})\right) + d_5^{(\mu\mu)} f(\nu_i, \mu_j) \\
&= \sum_{k=1}^{9} \tilde{d}_k^{(\mu\mu)} f(\nu_i, \mu_{j-5+k})
\end{aligned}
\tag{55}
$$

where the coefficients $\tilde{d}_k^{(\mu)}$ and $\tilde{d}_k^{(\mu\mu)}$ are trivially identified from eq. (46). One can even take a step further and collect the μ-dependent part of the Laplacian as

$$
\left.\left(\frac{\partial^2 f}{\partial \mu^2} + \frac{\cosh \mu}{\sinh \mu}\frac{\partial f}{\partial \mu}\right)\right|_{i,j} = \sum_{k=1}^{9} D_k^{\mu}(\mu_j) f(\nu_i, \mu_{j-5+k}).
\tag{56}
$$

An analogous technique is used to evaluate the necessary derivatives over ν.

3.4. Successive overrelaxation (SOR) method

Solving eq. (39) by the finite difference discretization discussed in the previous subsection leads to a matrix equation

$$
\mathbf{Rf} = \mathbf{s}
\tag{57}
$$

where $\mathbf{f}$ and $\mathbf{s}$ are vectors of length $N_\nu N_\mu$, and N_ν and N_μ are typically in the range 10^2–10^3. The matrix $\mathbf{R}$ can thus be quite large, but it is also extremely sparse. Because of this, iterative methods are extremely attractive for the solution of eq. (57).

As was already mentioned in section 1, the orbitals and potentials are usually solved in the FD HF method with the SOR method [29, 62, 63], which is a variant of the Gauss–Seidel method for solving linear systems

of equations. The method is guaranteed to converge, if the matrix $\mathbf{R}$ is symmetric and positive-definite, and if the relaxation factor ω is within the interval $0 < \omega < 2$ [63, 64].[3]

Every SOR sweep consists of in-place updates to the elements of the solution array f_p as

$$f_p := R_{pp}^{-1} \left[(1 - \omega) R_{pp} f_p + \omega \left(s_p - \sum_{q \neq p}^{N_\nu N_\mu} R_{pq} f_q \right) \right] \tag{58}$$

in a loop over all the elements of the array, $p = 1, \ldots, N_\nu N_\mu$. Let us now write the SOR update of eq. (58) for eq. (39) with the discretization of eq. (55). The diagonal term R_{pp}, which thus yields the contribution to the grid point (ν_i, μ_j) arising from its old value, can be identified from eqs. (39) and (55) as

$$G(\nu_i, \mu_j) = A(\nu_i, \mu_j) d_5^{(\nu\nu)} + C(\nu_i, \mu_j) d_5^{(\mu\mu)} + E(\nu_i, \mu_j), \tag{59}$$

since the first derivative operators multiplying B and D in eq. (39) don't contain diagonal terms (cf. the original one-dimensional expression, eq. (46)).

Having identified the mathematical structure of the update, we can thus write down the SOR update arising from eq. (58) for the solution of eq. (39)

---

[3]A proof has been shown for the standard discretization of the Poisson equation by the second-order cross-like stencil, when the grid points are handled from the bottom to the top, and from the left to the right; we are not aware of a proof for higher-order discretizations.

with the discretization of eq. (55) explicitly as

$$
\begin{aligned}
f(\nu_i, \mu_j) :=& (1 - \omega) f(\nu_i, \mu_j) + \frac{\omega}{G(\nu_i, \mu_j)} \Bigg[F(\nu_i, \mu_j) \\
& - \sum_{k=1}^{4} \Big\{ A(\nu_i, \mu_j) d_k^{(\nu\nu)} \left(f(\nu_{i-k}, \mu_j) + f(\nu_{i+k}, \mu_j) \right) \\
& + B(\nu_i, \mu_j) d_k^{(\nu)} \ \left(f(\nu_{i-k}, \mu_j) - f(\nu_{i+k}, \mu_j) \right) \\
& + C(\nu_i, \mu_j) d_k^{(\mu\mu)} \left(f(\nu_i, \mu_{j-k}) + f(\nu_i, \mu_{j+k}) \right) \\
& + D(\nu_i, \mu_j) d_k^{(\mu)} \ \left(f(\nu_i, \mu_{j-k}) - f(\nu_i, \mu_{j+k}) \right) \Big\} \Bigg].
\end{aligned}
\tag{60}
$$

3.4.1. Update sweeps

Every update sweep consists of using eq. (60) to update the solution for $i = 2, \ldots, N_\nu - 1$ and $j = 2, \ldots, N_\mu - 4$, that is, for the interior grid points. Each SOR sweep does consecutive in-place updates to elements of the solution array $\mathbf{f}$, and the update at each point thus uses the newest available information for its neighboring points. As will be discussed below in section 3.4.3, a number of sweeps is performed on the interior grid points, thus propagating information from the outer boundary region towards the centre of the molecule, as well as from the z-axis back towards the outer boundary.

After the requested number of sweeps have been carried out, the solution is updated separately at the remaining points: the line $i = 1$ corresponding to the $\nu = 0$ boundary line, the line $i = N_\nu$ to the $\nu = \pi$ boundary line, the $j = 1$, *i.e.*, $\mu = 0$ boundary line, and the points $j \in [N_\mu - 3, N_\mu]$ belonging to the region where the values of the orbitals and potentials are estimated from their asymptotic behaviour (sections A.11 and A.12).

As the update in every relaxation step happens through the employed finite difference stencil, this means that the convergence speed depends critically on the employed grid spacing. As the convergence thus becomes the slower the larger a grid is used, it is recommended to run FD HF calculations in sequences of increasing grid size, using the solution found on the last grid size as an initial guess at each step. The solutions are then interpolated from

the previous grid to the current one.[4] Even when a converged solution on a smaller grid is used as an initial guess, thousands of sweeps may be needed to meet the specified convergence criterion.

In addition to the natural column-major (outer loop on j, inner loop on i) update that is tailored to the memory access in Fortran, x2dhf also supports a reverse column-major update, in which the columns are updated in reverse order, as well as row-major (outer loop on i, inner loop on j) updates.

In addition x2dhf implements "middle-type" sweeps, which are used by default, because they lead to a faster convergence. The ordering of the grid points in the middle-type sweeps in the SOR method is the following. In the outer loop, the μ variable loops first from $\mu_j = \mu_{(N_\mu-1)/2}$ down to $\mu_j = \mu_2$, and then from $\mu_j = \mu_{(N_\mu-1)/2+1}$ up to $\mu_j = \nu_{N_\mu-4}$. The outer loop thus specifies a fixed μ_j value. In the inner loop, the ν values loop from $\nu_i = \nu_{(N_\nu-1)/2}$ down to $\nu_i = \nu_2$, and then from $\nu_i = \nu_{(N_\nu-1)/2+1}$ up to $\nu_i = \nu_{N_\nu-1}$.

3.4.2. Multicolour SOR method

The MCSOR method was originally developed for better efficiency on vector processors [29]. The idea in the MCSOR method is that the discretization through the 17-point numerical stencil can be thought to divide the grid points into five separate colour groups. Since the stencil only connects points by up to four steps in either the horizontal or vertical directions, the relaxation at, say, a "black" grid point depends solely on its "red", "orange", "yellow", and "blue" neighbours (see fig. 4 for illustration). The relaxation of all the "black" grid points can thus be performed simultaneously on a vector processor. Once the "black" grid points have been updated, the "red", "orange", etc. grid points can be updated in a similar fashion, one colour at a time.

The parallel updates to the solution array are thus independent. In contrast, the SOR method updates points consecutively, always using the newest information for every grid point. This difference in the way SOR vs MCSOR update the values of the solution on the grid has implications for the resulting convergence of the overrelaxation procedure. In our experience, the MCSOR scheme should be avoided when the initial orbitals and potentials are of poor quality. For instance, when hydrogenic orbitals are used to initialize calcu-

---

[4]In order to facilitate this process the x2dhf program offers a special label *interp*. See the User's Guide.
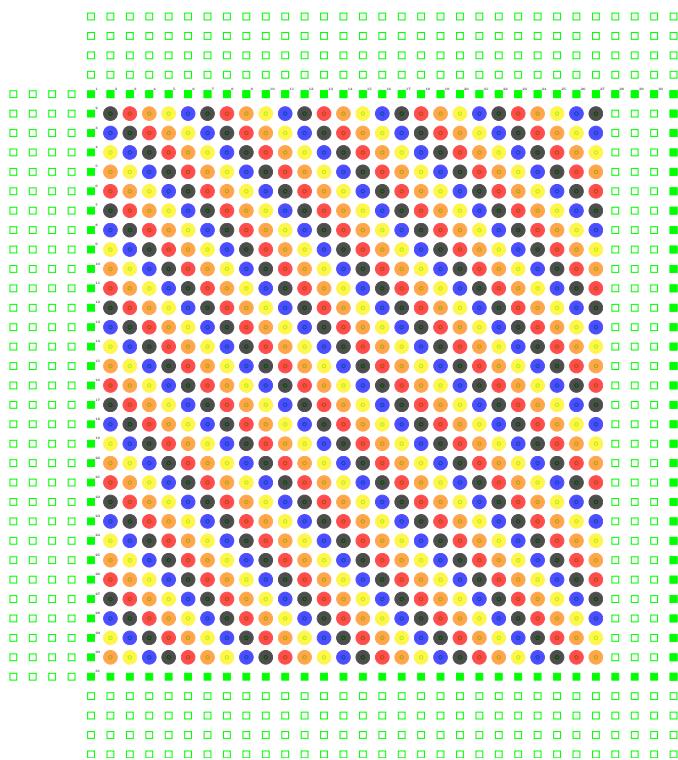
Figure 4: Discretization through the 17-point numerical stencil divides the grid points into five separate colour groups and the relaxation at, say, a black grid point depends solely on its red, orange, yellow, and blue neighbours.

lations on many-electron systems, it is better to use the SOR algorithm for the first 50–100 SCF iterations.

MCSOR can be used to obtain a parallel algorithm for use on several processors with OpenMP or Portable Operating System Interface threads (pthreads) programming. In practice, one can expect a wall-time speed-up factor of about 3 when using the MCSOR algorithm with OpenMP or pthreads for orbital relaxation, at a cost of using 5 times more processor time than an analogous calculation using a single-threaded SOR procedure.

Importantly, the speed-up factor is grid-size dependent. The performance of the MCSOR method decreases when the function value array saturates the processor's level 3 (L3) cache. Once the capacity of the L3 cache has been exhausted, the speed-up factor drops to about 2 for larger grids, and becomes fairly independent of the number of threads used for parallelisation (8 threads are used by default).

38

The ordering of the grid points in the default middle-type sweeps in MCSOR is as follows. In the outer loop, the μ variable loops first from $\mu_j = \mu_{(N_\mu - 1)/2}$ down to $\mu_j = \mu_2$, as in the SOR method. However, in the second step, the loop is handled in the opposite order to the SOR method: we loop down from $\mu_j = \nu_{N_\mu - 4}$ to $\mu_j = \mu_{(N_\mu - 1)/2 + 1}$, so that the middle values are not used and modified by different MCSOR threads at the same time, which would lead to inconsistencies.

3.4.3. Interweaving (MC)SOR and SCF

As we already discussed above in section 2.1.1, the salient feature of the FD HF method is that the iterative SCF procedure needed to solve the HF equations is tightly interwoven with the (MC)SOR iterations used to compute the potentials. The main algorithm can be summarized as follows

- initial guess for the orbitals and potentials

- loop over SCF iterations:

    - loop over orbitals o in inverse order

        * relaxation step for Coulomb V_C^o and exchange V_x^{oo} potentials for the orbital itself
        * loop over orbitals $p < o$: relaxation step for exchange potentials V_x^{op}
        * relaxation step for orbital o, using updated values for V_C^o, V_x^{oo}, and V_x^{op} for $p < o$, and previous values for V_C^p and V_x^{op} for $p > o$

- reorthogonalize orbitals using the Gram–Schmidt method

- recalculate orbital energies

- if orbital energies have changed considerably, update the potentials in the μ_∞ boundary region (see section A.11)

If the maximum change in orbital energies between successive SCF iterations has decreased by a given factor (1.15 by default; see the `multipol` keyword in the User's Guide), the boundary values for potentials at μ_∞ are re-evaluated. This approach follows from the observation that the boundary values for the potentials do not change considerably between consecutive SCF iterations,

which is why is no need to update them that frequently if the orbitals are not changing much. This approach thus saves many processor cycles.

As we discussed above in section 3.3, each relaxation employs the same numerical stencil for all the inner grid points; only the boundary lines require special handling. Each (MC)SOR relaxation of an orbital or a potential consists of N_{SOR} macroiterations, which each involve N_{mSOR} microiterations, and the algorithm for each relaxation step can be summarized as follows

- loop over N_{SOR} macroiterations ($N_{\mathrm{SOR}} = 1$ by default):

  - pad the $f(\nu_i, \mu_j)$ array with boundary values (negative μ and ν values)
  - loop over N_{mSOR} microiterations ($N_{\mathrm{mSOR}} = 10$ by default):

    1. update $f(\nu_i, \mu_j)$ according to eq. (60) (various orderings possible for grid points) in a loop over inner grid points $i \in [2, N_\nu - 1]$ and $j \in [2, N_\mu - 4]$
    2. only for even functions: compute new function values along the $(\nu, 0)$, $(0, \mu)$, and (π, μ) boundary lines from the relaxed solution in the interior grid points with eq. (54) (odd functions vanish by symmetry)

  - extract the solution from the padded array
  - only if relaxing orbitals (potentials were discussed above), update boundary values in the μ_∞ boundary region (see section A.12)

The above procedure thus determines the SCF cycle. When self-consistency has been reached, the wave function matches with the value computed from the converged potential; thereby the norm of the orbital before reorthonormalization will already be close to unity, and the relative change in the orbital eigenvalue will be close to zero. These parameters are usually defined by the user in the input data, but the default values for these parameters are 10^{-10} in x2dhf.

The distinction between the macro- and micro-iterations is a consequence of the manner in which the boundary conditions are applied. The most straightforward approach would be to relax an orbital at all inner grid points and then update the boundary values along the internuclear axis and at infinity. In practice, there is no need to update the boundary values at infinity in each SOR sweep. Consequently, the micro-iterations entail updating the

40

boundary values at the internuclear axis in each SOR sweep, followed by an update to the boundary values at infinity, thus forming a single macro-iteration. The default setting is to perform a single macro-iteration. In the case of potentials, the boundary values at infinity are updated even less frequently, as explained above.

3.4.4. Default number of (MC)SOR iterations

The default number of (MC)SOR microiterations for orbitals and potentials during a single SCF iteration, $N_{\mathrm{mSOR}} = 10$, should be satisfactory for ordinary cases, as the convergence of the FD HF solution usually depends on the overall number of (MC)SOR microiterations needed to reach a given orbital energy threshold, rather than on a judiciously chosen value for this parameter. This is illustrated in fig. 5, which shows the average change in the orbital energy between consecutive SCF iterations as a function of the total number of SOR microiterations. Various choices for N_{mSOR} lead to the same behaviour, confirming that only the total number of SOR steps taken in the calculation is relevant.

To add on the discussion in fig. 5, we note that if N_{mSOR} is too small (2–6), more time than necessary will be spent on the calculation. If N_{mSOR} is too large (e.g. 14–18), instead, the overall convergence can be somewhat faster, but the solution obtained may be distorted if the boundary conditions get "out of sync" with the orbital energies (see section 4.2.2 for discussion on the SCF algorithm).

The calculations in fig. 5 were carried out for molecules with small, medium, and large number of orbitals and potentials: FH, KrH$^+$, and TlF. Our analysis in fig. 5 rests on the average change in the orbital energy defined as

$$\Delta E = \frac{1}{N_{\mathrm{orb}}} \sum_{i=1}^{N_{\mathrm{orb}}} |\Delta \varepsilon_i| \tag{61}$$

where $\Delta \varepsilon_i$ represents the relative change in the orbital energy for a given orbital between two consecutive SCF iterations and N_{orb} is the number of occupied orbitals. It is worth noting that according to fig. 5, the orbitals and potentials are improved at a virtually constant rate of $\Delta E \approx 10^{-2}$ per SCF iteration during the first 15–20% of SOR microiterations. The remaining 80–85% of microiterations are needed to improve the accuracy of orbitals and potentials, as measured by the ΔE, by six orders of magnitude.

Figure 5: The compound error in orbital energies ΔE (eq. (61)) as a function of the total number of SOR iterations taken for three choices for the number of SOR microiterations (N_{SOR}) within each SCF iteration for FH ($3\sigma^2 1\pi^4$ configuration), KrH$^+$ ($8\sigma^2 4\pi^4 1\delta^4$ configuration), and TlF ($17\sigma^2 9\pi^4 4\delta^4 1\varphi^4$ configuration). Few differences can be seen between the results for the three choices, confirming that the main effect comes just from total number of SOR iterations taken. Note that the same N_{SOR} values are used for orbitals and potentials and that is why the labels read: `sor 8 8`, `sor 10 10` and `sor 12 12`.
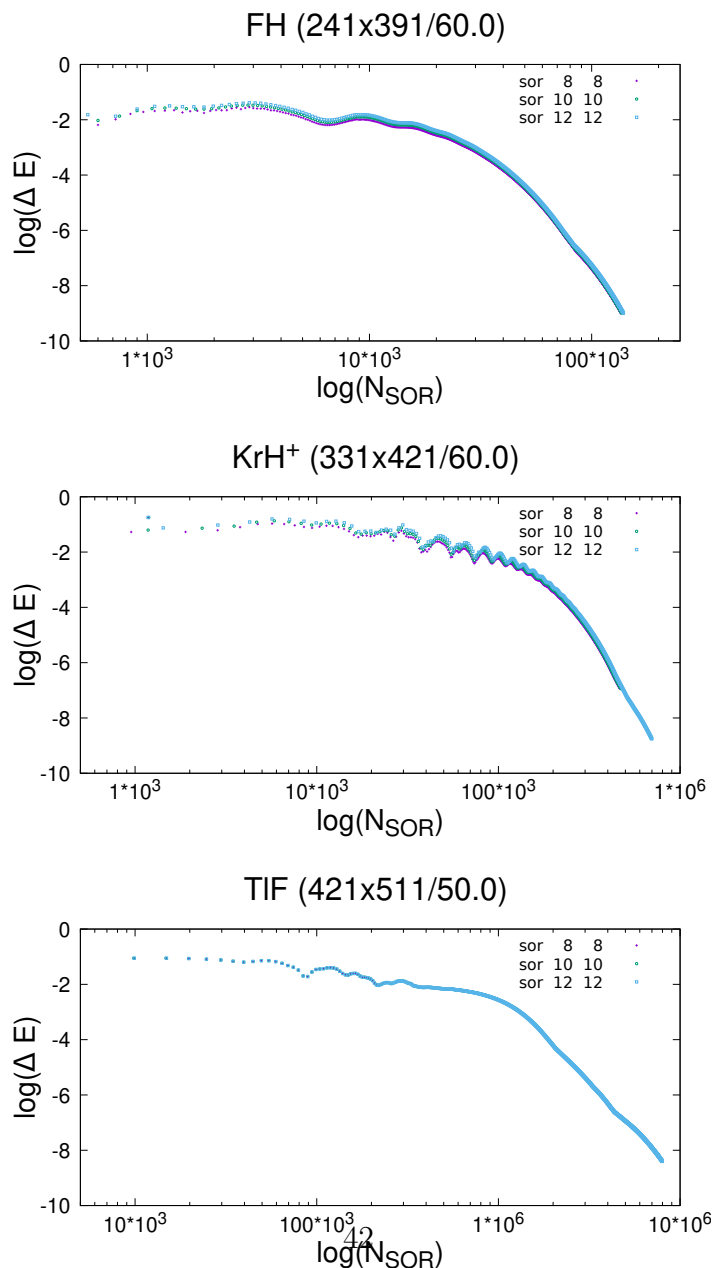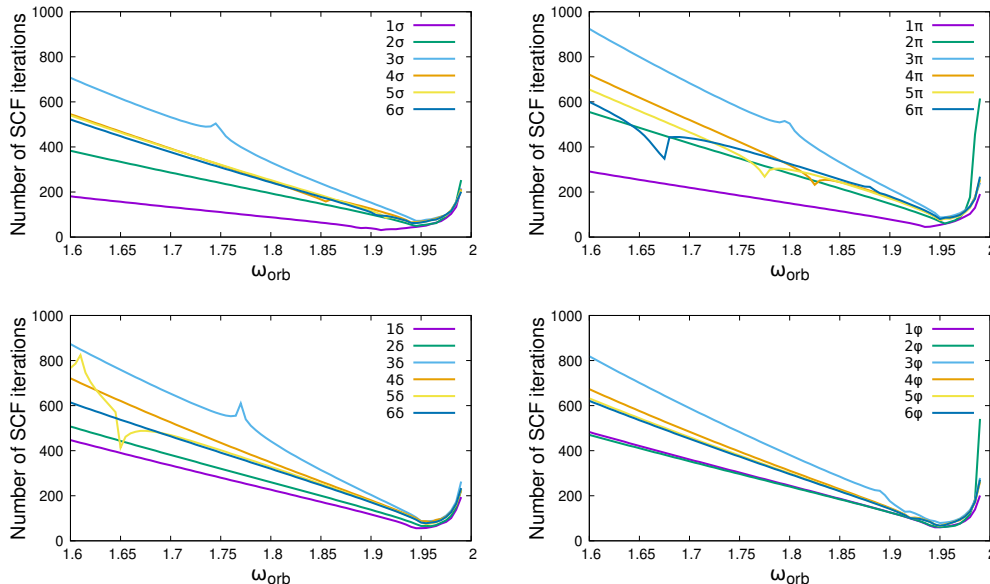
Figure 6: The number of SCF/MCSOR iterations needed to converge the Ne^{9+} orbitals as a function of ω_{orb}.

3.4.5. Choice of overrelaxation parameter

The convergence of the SOR method depends critically on the value of the overrelaxation parameter ω. To investigate the performance of various choices for the orbital overrelaxation parameter ω_{orb}, we studied the Ne^{9+} system, for which we relaxed the six lowest orbitals of the σ, π, δ, and ϕ symmetries by the SOR and MCSOR methods on a $241 \times 391/60.0a_0$ grid until the orbital energy threshold 10^{-10} was reached. 10 SOR microiterations were carried out in each iteration.

Since Ne^{9+} is a one-electron system, the sought-for orbitals have well-known exact analytical expressions and it is not necessary to compute Coulomb or exchange potentials; the SCF/SOR procedure boils down to relaxing the orbitals, orthonormalizing them, and recomputing orbital energies. As we still do want to study the efficiency of the numerical algorithm, the orbitals were initialized to those of Na^{10+}, which is also a one-electron system. The resulting guess is sufficiently close to the pursued solution, and the SOR calculations converge without difficulties for a wide range of overrelaxation parameters.
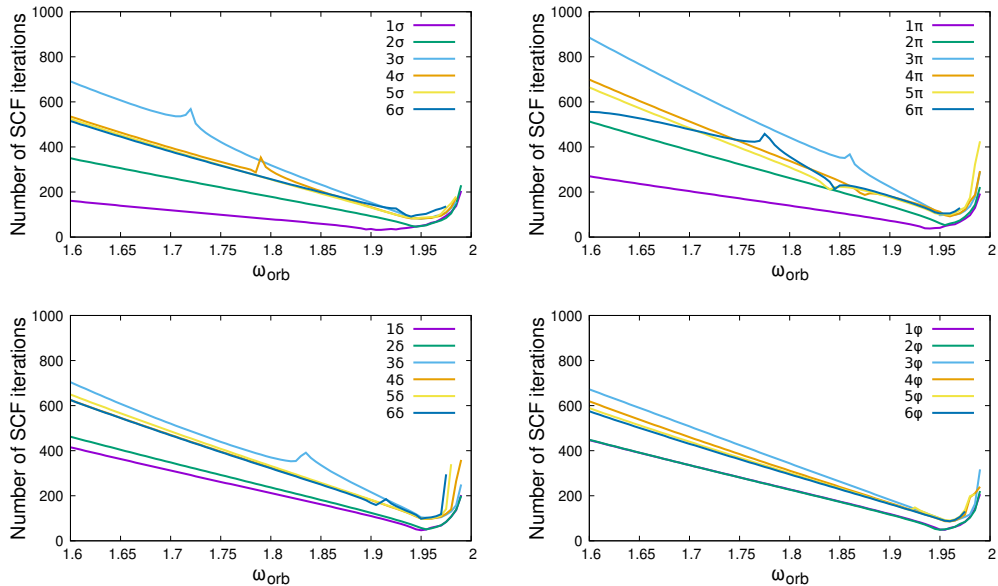
Figure 7: The number of SCF/MCSOR iterations needed to converge the Ne^{9+} orbitals as a function of ω_{orb}.

Figures 6 and 7 show the number of iterations needed to converge the orbitals as a function of the employed orbital relaxation parameter ω_{orb} for the SOR and MCSOR methods, respectively. We do not observe qualitative differences in the convergence behaviour between orbitals of different symmetries, or the relaxation algorithms used. In all cases, the optimal values of the orbital relaxation parameter ω_{orb} are virtually the same—around $\omega_{orb} \approx 1.95$—and the corresponding necessary number of SCF iterations also turn out to be similar.

A FD HF calculation also requires a relaxation parameter for the potential, ω_{pot}. The same qualitative behaviour as above is observed also when solving the HF equations of any many-electron system with respect to both relaxation parameters, ω_{orb} and ω_{pot}: the required number of SCF iterations decreases when the parameters approach their optimal values from the left, and rapidly increases when the values become too large, especially when they start to approach $\omega_{orb} = 2$ or $\omega_{pot} = 2$. This behaviour is demonstrated in the two-dimensional plots in figs. 8 and 9, which show the required number
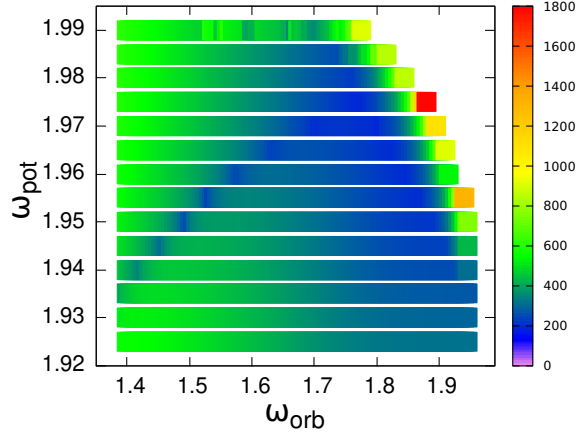
44

Figure 8: The number of SCF iterations required to converge FH on a $[91 \times 181/65.0a_0]$ grid as a function of ω_{orb} and ω_{pot}. The default value $N_{\mathrm{mSOR}} = 10$ was employed.

of SCF iterations for the FH and KrH$^+$ molecules, respectively, as a color bar on in the $(\omega_{\mathrm{orb}}, \omega_{\mathrm{pot}})$ plane.

3.4.6. Nearly optimal default values

One can show that the optimal value $\omega_{\mathrm{pot}}^{\mathrm{opt}}$ of the potential relaxation parameter for a model Poisson equation discretized by the second-order stencil is given by the formula [63]

$$\omega_{\mathrm{pot}}^{\mathrm{opt}}(N_\nu, N_\mu) = \frac{2}{1 + \sqrt{1 - \rho(N_\nu, N_\mu)^2}} \tag{62}$$

where

$$\rho(N_\nu, N_\mu) = \frac{1}{2}\left[\cos\frac{\pi}{N_\nu} + \cos\frac{\pi}{N_\mu}\right] \tag{63}$$

is the spectral radius of the corresponding matrix. We are not aware of analogous results for higher-order discretizations, or for the general elliptical
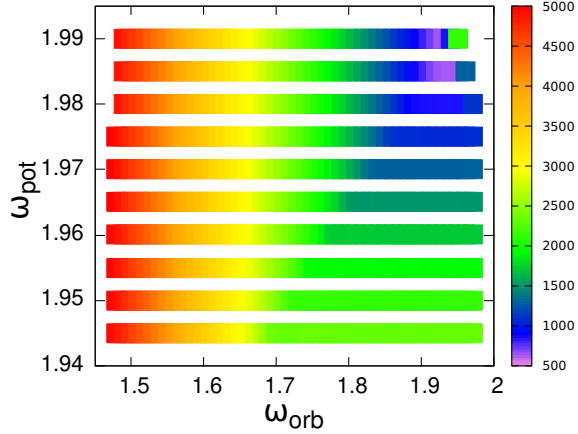
45

Figure 9: The number of SCF iterations required to converge KrH$^+$ on a $[349 \times 421/60.0a_0]$ grid as a function of ω_{orb} and ω_{pot}. The default value $N_{\mathrm{mSOR}} = 10$ was employed.

second-order PDEs like eq. (39) that arise in the FD HF method. However, it has been shown that the (nearly) optimal value of the overrelaxation parameter for the potentials in this case can be approximated by the formula

$$\omega_{\mathrm{opt}}^{\mathrm{pot}}(N_\nu, N_\mu) = \frac{2P_1}{1 + \sqrt{1 - \rho(N_\nu, N_\mu)^2}} + P_2 \tag{64}$$

where $P_1 \approx 0.603$ and $P_2 \approx 0.79$ are constants determined from numerical experiments; the current default values of x2dhf were determined in [65].

We note that the (nearly) optimal values of $\omega_{\mathrm{opt}}^{\mathrm{orb}}$ are always smaller than the corresponding $\omega_{\mathrm{opt}}^{\mathrm{pot}}$ values for a given grid size [1]. This observation initially led us to the automatic estimate

$$\omega_{\mathrm{opt}}^{\mathrm{orb}} = \omega_{\mathrm{opt}}^{\mathrm{pot}}(\omega_{\mathrm{opt}}^{\mathrm{pot}} - 1), \tag{65}$$

where it is assumed that $1 < \omega_{\mathrm{opt}}^{\mathrm{pot}} < 2$. However, this estimate turns out to be a bit too large for heavier species like Kr or Rn, as the convergence of the resulting SCF process is observed to be non-monotonic. As a remedy, we ended up further decreasing $\omega_{\mathrm{opt}}^{\mathrm{orb}}$ from eq. (65) to

$$\omega_{\mathrm{opt}}^{\mathrm{orb}} = \omega_{\mathrm{opt}}^{\mathrm{pot}}(\omega_{\mathrm{opt}}^{\mathrm{pot}} - 1) - 10^{-3} \max(Z_A, Z_B), \tag{66}$$

46

which is how the optimal value for the orbital relaxation parameter is estimated in the current version of `x2dhf`.

3.4.7. Potential for future improvements

We note that there may be room to improve the convergence of the SOR method. Bai and Chi [66] proposed a class of asymptotically optimal SOR methods. Numerical tests with the five-point finite difference discretization show that the new methods are more efficient and robust than the classical SOR method. Li and Evans [67] claim that the convergence of the SOR method can be improved if the linear system is preconditioned by Gauss–Jordan elimination. Such methods could be investigated in future versions of the `x2dhf` program.

4. Description of the program

4.1. Repository structure

`x2dhf` is freely and openly available as a GitHub repository [68] under the GNU General Public License v2.0, or later (GPL-2.0-or-later). The repository contains README.md and INSTALL files that describe how to build and run the program. An in-depth users' guide, which describes the program's input data can be found in `docs/users-guide.pdf`. The `test-sets` subdirectory contains over two hundred of examples of input data, `input*.data`, as well as the corresponding reference output of the program in the `reference.lst`. The `bin/testctl` script should be used to list and run the tests.

The `lda_orbitals` and `hf_orbitals` directories contain tabulations of LDA and HF atomic radial orbitals which can be used to initialize calculations (see section 4.2.1).

The program is built with `CMake`. The `bin` directory contains the `x2dhf` executable(s) and several Bash and Perl scripts to facilitate the usage of the program. The most important of these is the `xhf` Bash script, which should be used to run the program for a given set of input data (see `xhf -h`). The directory also contains the `pecctl` script, which facilitates calculations of potential energy curves, and the `elpropctl` script that computes electrical properties out of total energies and multipole moments evaluated at several finite field strengths.

Pseudocode 1: X2DHF (main routine)

Input: Input data defining the atomic/diatomic system to be solved
by means of HF, DFT, or an independent particle model

Output: At convergence, orbitals and corresponding orbital
energies, Coulomb/exchange potentials, multipole
moments, and CPU usage statistics

```
1  call setPrecision       // calculate floating-point precision
                           // and lengths of integer/real variables
2  call setDefaults  // set default values of constants/variables
3  call inputData        // set up calculation according to input
4  allocate    // allocate memory for orbitals, potentials, etc
                           // whose sizes are defined by input data
5  call zeroArray8     // zero out arrays with integer*8 indices
6  call initArrays            // initialise common block arrays,
                                 // one-electron potentials,
                  // integration and differentiation weights,
              // Jacobians, address arrays, mesh arrays, etc
7  call printCase     // print out details about the calculation
8  call initOrbPot        // initialise orbitals and potentials
9  call prepSCF        // normalise and orthogonalise orbitals,
                                 // calculate orbital/total energy
10 call SCF                    // perform SCF/(MC)SOR iterations
11 call printResults   // output total energy, orbital energies,
                                 // norms, CPU usage statistics
12 stop
```

48

4.2. Flow of control via pseudocodes

The large-scale structure of the program is best seen by examining the pseudocode of its main routine (see pseudocode 1). The program uses several parameters that are hard-coded to values defined in the `params` module: for example, the maximum number of grid points in the ν and μ variables and the maximum number of orbitals are fixed at compile time to values given in `params.f90`, since some arrays are statically allocated for simplicity and efficacy.

The program's execution begins by determining the employed precision of the integer and floating-point variable data types (step 1 in pseudocode 1). Next, the default values of a host of variables used to control the behaviour of the program are set (step 2 in pseudocode 1). Some of these values can, however, be modified by the input data read next from the `input.data` file by the `inputData` routine and its many subroutines (step 3 in pseudocode 1).

When the input data has been parsed, the memory requirements for the various necessary data structures[5] (section A.14 lists some of them) for the calculation can be determined, and the necessary memory is allocated (step 4 in pseudocode 1). The fixed length arrays are stored in common blocks. Necessary arrays that have the same content for any job type are then either initialized to zero (step 5 in pseudocode 1), or filled with data (step 6 in pseudocode 1).

4.2.1. Initial guess

At this stage (step 7 in pseudocode 1), the program prints out information on the type of calculation to run, and proceeds to the next stage, which is to initialise the orbitals and potentials (step 8 in pseudocode 1).

There are several options for starting the calculations from a linear combination of atomic orbitals (LCAOs), which are an attractive form for describing the molecular orbitals for a given system in compact form.

In simple cases, the most straightforward way is to define the molecular orbitals as a linear combination of hydrogenic functions located on the centres A and B. The traditional setup of `x2dhf` thus requires inputting the orbitals as linear combinations of Slater-type orbitals on the two nuclei.

---

[5]Such as the orbitals and potentials, the differentiation and integration coefficients, the A, B, etc arrays of the Fock and Poisson equations, and the scratch memory. In addition, the `(mc)sor` routine employs two integer arrays to pick up subsequent values for relaxation from the primary and extended arrays of orbitals/potentials, for example.

However, this approach becomes tedious for systems with many orbitals. As an alternative, results from the `GAUSSIAN` program can also be used to initialize molecular orbitals: the basis set used and the molecular orbital expansion coefficients are extracted from the program's output, and values of the molecular orbitals at the grid points are computed from these data.

The procedure to set up calculations has been further improved and simplified in this version of `x2dhf` by providing ready-to-use LDA (available for H–Og) and HF atomic orbitals (available for H–Ca, Ga, Br–Sr, I–Ba, Au–Pb, At–Ra) as part of the `x2dhf` distribution. Such good atomic basis functions allow for a compact representation of the guess orbitals. If expansion coefficients have not been explicitly set in the input file, `x2dhf` initializes the molecular orbitals with the HF or LDA atomic orbitals ordered in energy; if the molecule is homoatomic, the gerade and ungerade molecular orbitals are formed by equal weighting of the atomic orbitals on the two centers.

The LDA orbitals have been determined in exchange-only LDA calculations with the `HelFEM` program [50, 51, 55], while the HF atomic orbitals were obtained from a modified version of Froese-Fischer's program [69].

The special aspect of the FD HF approach is that in addition to the orbitals, an initial guess must be provided for the potentials, as well; a further complication here is that a guess for the total Coulomb and exchange potential is not enough, but separate guesses have to be formed for all the Coulomb potentials arising from single orbital densities, as well as all the exchange potentials arising from the various orbital products.

Coulomb potentials are initialized from a linear combination of Thomas–Fermi potentials at the two centres; our implementation is based on a routine from the atomic program of Desclaux [70]. However, if LDA orbitals were used to initialize the calculation, the Coulomb potentials can also be initialised with the corresponding superposition of atomic Coulomb potentials. All exchange potentials are initialised as $c_A/r_A + c_B/r_B$, where c_A and c_B are normalised LCAO coefficients.

4.2.2. SCF procedure

Having completed the guess stage, the guess orbitals are orthonormalised, and the orbital energies and the total energy are calculated (step 9 in pseudocode 1). In the next stage the SCF process is carried out (step 10 in pseudocode 1) and finally, its results are printed out (step 11) before the execution of the program ends (step 12 in pseudocode 1).

Pseudocode 2: SCF performs SCF/(MC)SOR iterations
***

Input: An initial set of (norb) orbitals and Coulomb/exchange potentials and corresponding orbital energies. Every saveSCFdata iterations total energy is recalculated and restart data are saved to disk.

Output: On convergence (or otherwise) orbitals and Coulomb/exchange potentials and orbital energies.

1 for *iscf=1* **to** *maxscf* **do**

```
                                              // SCF loop
```

2   **for** *iorb=norb* **to** *1* **do**

```
           // orbitals' loop; orbitals stored in reverse order
```

3   call potAsympt   `// set potentials at` R_∞

4   call relaxDriver   `// perform (MC)SOR iterations`

```
                              // for potentials and orbitals
```

5   call norm   `// normalise orbitals`

6   call ortho   `// orthogonalise orbitals`

7   call EaHF || EaLXC || EaDFT   `// calc orbital energy`

8   call EabHF || EabLXC || EabDFT   `// calc off-diagonal`

```
                                  // Lagrange multipliers
```

9 ΔEa(iorb)=Ea(iscf)-Ea(iscf-1)   `// monitor changes`

```
                                       // in orbital energies
```

10 ΔNa(iorb)=Na(iscf)-Na(iscf-1)   `// monitor changes`

```
                                       // in orbital norms
```

11 ΔE=max($|\Delta$Ea(1)$|$,...,$|\Delta$Ea(norb)$|$)

12 ΔN=max($|\Delta$Na(1)$|$,...,$|\Delta$Na(norb)$|$)

13   **if** *iscf>Nscf2skip* **then**

```
            // at least Nscf2skip SCF iterations are performed
```

14   **if** $\Delta E < E_{\text{threshold}}$ **or** $\Delta N < N_{\text{threshold}}$ **then**

15   **return**   `// orbital energy/norm threshold reached`

```
title FH
method hf
nuclei 9.0 1.0 1.7328
config 0
1 pi
3 sigma end
grid 200 40.0
orbpot hf
scf 2000 10 10 14 3
stop
```

Figure 10: Input data for a HF calculation on the FH molecule ($R = 1.7328a_0$) with a $200 \times 200/40a_0$ grid.

The SCF process is controlled by the SCF routine (see pseudocode 2). In each SCF iteration, the orbitals are processed in an opposite order to the one used to define the electronic configuration in `input.data`. For example, the input data for the FH molecule at the experimental equilibrium bond length $R = 1.7328a_0$ is shown in fig. 10.

With such a definition for the electronic configuration, the Fock equation for the 1σ orbital, which is the orbital with the lowest energy, is solved first.[6] The relaxation of the 1σ orbital is preceded by the relaxation of the $V_C^{1\sigma}$ potential. One also needs the exchange potential $V_x^{1\sigma 1\sigma}$; however, it is easy to see from eqs. (10) and (11) that diagonal exchange potentials for σ orbitals coincide with their Coulomb potentials: $V_x^{1\sigma 1\sigma} = V_C^{1\sigma}$. Naturally, the 1σ orbital update also depends on the Coulomb and exchange potentials of the other orbitals. However, at this stage they are treated as given.

Next, the Fock equation has to be solved for the 2σ orbital. However, the $V_x^{1\sigma 2\sigma}$ and $V_C^{2\sigma} = V_x^{2\sigma 2\sigma}$ potentials have to be determined first. Again, the potentials of the higher orbitals are used as-is.

In the same spirit, the relaxation of the 3σ orbital again begins with the relaxation of the $V_x^{1\sigma 3\sigma}$, $V_x^{2\sigma 3\sigma}$ and $V_C^{3\sigma} = V_x^{3\sigma 3\sigma}$ potentials, while fixed values are used for the $V_x^{3\sigma 1\pi}$ and $V_C^{1\pi}$ potentials.

---

[6]This also requires calculating the orbital energy and the off-diagonal Lagrange multipliers for the employed model. In DFT calculations, the functionals can be provided either by the Libxc library (`EaLXC` and `EabLXC`), or by the program itself (`EaDFT` and `EabDFT`).

Finally, the relaxation of the 1π orbital is preceded by the relaxation of the $V_C^{1\pi}$, $V_x^{1\pi 1\pi}$, $V_x^{3\sigma 1\pi}$, $V_x^{2\sigma 1\pi}$ and $V_x^{1\sigma 1\pi}$ potentials. Note that the Coulomb and exchange potentials do not coincide for non-σ orbitals, and therefore have to be computed separately. For example, the Coulomb potential $V_C^{1\pi}$ arises from a cylindrically symmetric density, while the exchange potential $V_x^{1\pi 1\pi}$ contains both same-orbital ($1\pi_{\pm 1}$–$1\pi_{\pm 1}$; $|\Delta m| = 0$) and other-orbital ($1\pi_{\pm 1}$–$1\pi_{\mp 1}$; $|\Delta m| = 2$) contributions.[7]

The `SCF` routine calls `relaxDriver` to perform relaxations of the corresponding potentials for each orbital in turn; the potentials can be relaxed in parallel (see discussion in section 4.5). The relaxation of the orbital itself is carried out subsequently (see pseudocodes 3 and 4).

Pseudocode 5 shows the details of `coulExchSOR` routine. Several arrays are prepared during the initialization phase of the program, so that a simple loop can be used to prepare the right- and left-hand sides of the Poisson equation for a particular Coulomb or exchange potential, and relax the equation by means of `maxsor1` macroiterations. The SOR routine is called in each macroiteration, performing the `maxsor2` micro iterations.

Once the potentials have been updated, the `orbSOR` routine (or its equivalents `orbSORPT` or `orbMCSOR`) is called, and the values of the orbitals are relaxed in a similar fashion to the `coulExchSOR` routine (see pseudocode 6).[8] The current values of the orbitals and the potentials are used by the proper version of Fock routine to prepare the right- and left-hand sides of the Poisson equation for the chosen method (`fockHF`, `fockDFT`, `fockLXC`, etc). The `orbAsymptGet` routine is invoked in step 14 of pseudocode 6 to get data that will be used to update the orbital values in the tail region upon completion of the relaxation (see section A.12). The relaxation itself is achieved by the call to the `SOR` routine in step 16 of pseudocode 6.

---

[7]It is important to note that, in principle, the Coulomb and exchange potentials could be evaluated directly. Nevertheless, the present approach is preferred due to the expense associated with calculating potentials via a series of integrations in two variables.

[8]Depending on the choice of the method (see User's Guide), the program can be used to solve the HF equations, the DFT equations, or the HFS equations $X\alpha$ exchange where the α parameter is calculated with the self-consistent multiplicative constant (SCMC) method. The program can also be used to solve one-electron diatomic problems (OED) and the harmonium problem (TED).

Pseudocode 3: RELAXDRIVER controls SOR/MCSOR relaxation of orbitals and potentials

---

Input: Orbital to relax (by default lpotmcsor=.FALSE. and lorbmcsor=.FALSE.).

Output: Orbital and corresponding Coulomb and exchange potentials updated by maxsor1*maxsor2 (MC)SOR iterations.

---

1 if *lpotmcsor* **then**

2 | **#ifdef** OPENMP

3 | call coulExchMCSOR   `// Coulomb/exchange potenitals`
        `// relaxed in parallel in separate`
        `// OpenMP threads via MCSOR routine`
        `// parallelised by another group of`
        `// OpenMP threads`

4 | **#elif** PTHREAD || TPOOL

5 | call coulExchSORPT   `// Coulomb/exchange potentials`
        `// relaxed in parallel in separate`
        `// p-threads by MCSORPT routine`

6 | **#else**

7 | call coulExchMCSOR tcp*[f]Coulomb/exchange potenitals
        `// relaxed one by one via single-threaded MCSOR`

8 | **#endif**

9 else

10 | **#ifdef** OPENMP

11 | call coulExchSOR `// Coulomb/exchange potenitals for`
        `// a given orbital relaxed in separate`
        `// OpenMP threads using SOR`

12 | **#elif** PTHREAD || TPOOL

13 | call coulExchSORPT   `// Coulomb/exchange potenitals`
        `// for a given orbital relaxed in`
        `// separate p-threads using SORPT`

14 | **#else**

15 | call coulExchSOR `// Coulomb/exchange potenitals for`
        `// a given orbital relaxed one by`
        `// one within main execution thread`

`// continued in` **Pseudocode 4**

Pseudocode 4: (Pseudocode 3 continued) RELAXDRIVER controls
SOR/MCSOR relaxation of orbitals and potentials

---

1 if *lorbmcsor* **then**

2   **#if** PTHREAD || TPOOL

3   call orbMCSORPT   `// relax orbital using`
                           `// mcsor_pthread or mcsor_tpool C routines`

4   **#else**

5   call orbMCSOR   `// relax orbital using`
                                   `// single-threaded MCSOR`

6   **#endif**

7 else

8   call orbSOR   `// relax orbital using SOR`

9 return

4.3. Array storage

As a major new feature in version 3.0 of `x2dhf`, the whole program has
been internally restructured in terms of Fortran modules, allowing the For-
tran compiler to check that function arguments are correctly passed between
functions in different compilation units. As a result of taking advantage of
the features of the Fortran 95 standard, the code has also been simplified and
streamlined considerably, making it much easier to modify and to extend to
new functionalities.

The refactoring has especially resulted in significant changes to the way
memory is passed around in the code, which has enabled eliminating many
potential bugs. The use of assumed-size arrays (`dimension(*)` in Fortran)
has been replaced wherever possible in favor of assumed-shape arrays
(`dimension(:)`), which also pass the array size within function calls, thus
eliminating possible out-of-bounds errors.

While older versions of the program [1, 31] passed the arrays to other rou-
tines either in their entirety, or as sub-arrays with particular data extracted,
the current version of the program employs Fortran `pointers` to access the
data structures. As is usual with scientific code development [71], refactor-
ings are usually never complete, and some parts of the program still need
further cleanup and streamlining.

The function $f(\nu, \mu)$ is represented by a 2-dimensional array $\boldsymbol{F}$ in `x2dhf`.

Pseudocode 5: COULEXCHSOR prepares data for the SOR relaxations and performs the macro and micro SOR relaxations of Coulomb and exchange potentials for a given orbital. If pragma OPENMP is used each potential is relaxed in a separate thread. Poisson equation is abbreviated as PE.

Input: Orbital number iorb.
Output: Coulomb and exchange potentials updated by maxsor1 macro and maxsor2 micro SOR iterations.

1 for *nexchpot=1* **to** *nexchpots(iorb)* **do**
```
                // loop over Coulomb/exchange potentials for
                                        // a given orbital iorb
```
2 | ib1=i1b(ins1(iorb,nexchpot))
3 | ib2=i1b(ins2(iorb,nexchpot))   // get location of orbitals
```
                    // within psi array needed for nexchpot
                                // Coulomb/exchange potential
```
4 | ibexp=ibexcp(iorb,nexchpot)   // get location of
```
            // Coulomb/exchange potential within excp array
```
5 | deltam=idelta(iorb,nexchpot)   // get difference of m
```
                // quantum numbers for the product of orbitals
```
6 | isym=isyms(iorb,nexchpot) // get the symmetry of nexchpot
```
                                                    // potential
```
7 | rhs=G*psi(ib1:)*psi(ib2:) // prepare right-hand side of PE
8 | lhs=F3+deltam*E   // prepare left-hand side of PE
```
        // with diagonal part of the diff.  operator incl.
```
| // perform maxsor1*maxsor2 SOR iterations
9 | **for** *i=1* **to** *maxsor1* **do**
10 | | call putin (isym,excp(ibexp:),work)   // immerse
```
                            // excp(ibexp:)  in work array
                        // and add extra boundary values
```
11 | | call sor (isym,work,LHS,RHS,BPOT,D,...)   // perform
```
                            // maxsor2 micro SOR iterations
```
12 | | call putout (excp(ibexp:),work)   // extract updated
```
                // excp(ibexp:)  values out of work array
```

13 return

56

Pseudocode 6: ORBSOR prepares data for the SOR relaxations and performs the macro and micro SOR relaxations of a given orbital. The program can be used to solve the HF equations, the DFT equations, or the HFS equations that involve $X\alpha$ exchange where the α parameter is calculated according to the self-consistent multiplicative constant (SCMC) method. It can also be used to solve one-electron diatomic problems (OED) or the harmonium problem (TED).

Input: Orbital number iorb.
Output: Orbital updated by `maxsor1` SOR macroiterations and
`maxsor2` SOR microiterations.

```
// Prepare LHS and RHS of Fock eq.  for a given method
```
1 if (HF.or.OED) call fockHF (iorb)

2 if (TED) call fockTED (iorb)

3 if (DFT.or.HFS.or.SCMC) call fockDFT(iorb)

4 if (LXC) then   `// use xc functionals from libxc`

5   if (lxcPolar) then

6   call fockLXCpol(iorb)

7   else

8   call fockLXCunpol(iorb)

9   endif

10 endif

11 isym=isymOrb(iorb)   `// get symmetry of orbital`

```
// perform maxsor1 macro SOR iterations
```
12 for *i=1* to *maxsor1* do

13   lhs=fock1+diag   `// add diagonal part of`
                                          `// 2`$^{\text{nd}}$` derivatives`

14   call orbAsymptGet   `// get data needed to update orbital`
                     `// in asymptotic region after relaxation`

15   call putin (isym,psi(iborb:),work)   `// immerse psi(iborb:)`
                `// into work array and add extra boundary values`

16   call sor (isym,work,LHS,RHS,B,D,...)   `// perform`
                                `// maxsor2 micro SOR iterations`

17   call putout (psi(iborb:),work)   `// extract updated`
                     `// psi(iborb:)  values out of work array`

18   call orbAsymptSet   `// update tail region of orbital`

19 **return**   57

The grid points are readily mapped into the corresponding elements of the two-dimensional array $\boldsymbol{F}$ used to store the $f(\nu_i, \mu_j)$ values in the program; see also fig. 3.

To perform SOR iterations, the $\boldsymbol{F}$ array is immersed into a larger $(N_\nu + 8) \times (N_\mu + 4)$ matrix, which has additional values along the boundaries that have been computed with knowledge of the symmetry of the function. The immersion and extraction is handled by the `putin` and `putout` routines, respectively. As discussed above, padding the solution onto the extended grid allows for an easier application of the relaxation procedure for the interior grid points.

The evaluation of the right-hand side of eq. (56) for every grid point i, j can be carried out as a series of matrix-vector multiplications of the submatrices $\boldsymbol{F}(1, j)$ and $\boldsymbol{D}^\mu(1, j)$ for every j. The evaluation of the analogous ν derivatives for a selected ν_i value and all the μ_j values can be done analogously by multiplying the corresponding submatrices $\boldsymbol{F}^\mathrm{T}(1, i)$ and $\boldsymbol{D}^\nu(1, i)$. All differentiations of the orbitals and the potentials can thus be carried out efficiently on modern hardware with a call to the `dgemv` routine included in the basic linear algebra subprograms (BLAS) library [72].

4.4. Language, unusual features and limitations

The program has been (re)written in Fortran 95. The program can be compiled as stand-alone, as it contains simplified replacements of the employed BLAS routines. Compilation is carried out with CMake. Optimized BLAS libraries should be used whenever possible (see `x2dhfctl -B`).

The command and data file structure is described in a separate document (see the User's Guide in the repository [68]). Over two hundred examples with corresponding inputs and outputs are provided by the various test sets (see `testctl -h`).

Several C routines have been added in version 3.0 to facilitate parallelisation of the SCF process and MCSOR routine via Portable Operating System Interface threads (pthreads; see section 4.5). If the multi-threaded version employing pthreads is requested, a C compiler is therefore also necessary to build the necessary extensions. OpenMP parallellism is handled with the standard Fortran extension.

The program can be compiled in quadruple precision with e.g. the `-freal--8-real-16` option of the gfortran compiler (see `x2dhfctl -r 16`). As quadruple precision is not supported by commonly available implementa-

tions of the BLAS standard at the moment, the bundled implementations have to be used for calculations in quadruple precision, instead.

4.5. Parallellization speedups

As was already discussed above in section 4.2.2, an SCF iteration begins by the relaxation of the Coulomb potential of the first orbital—which should be the one lowest in energy—and the orbital itself. The relaxation procedure then continues with higher lying orbitals. When such an orbital is to be relaxed, all the Coulomb and exchange potentials that involve the lower, already relaxed orbitals, must be updated. The higher the orbital is, the more exchange potentials must be relaxed. Therefore, if this work can be done in parallel with the relaxation of the Coulomb potential for the given orbital, a reasonable (but system dependent) speedup can be expected.

The `x2dhfctl` script that is used to build the executable binary offers three options to handle parallellization of the potential relaxation. The options `-o`, `-p` and `-t` switch on OPENMP, PTHREAD, and the TPOOL directive, respectively, which select separate routines to relax potentials with OpenMP or pthreads.

The Fortran version of the (MC)SOR routine is used when parallellism is not employed, or when the program is built with OpenMP support. Parallel relaxation of the potentials with pthreads is carried out by a C version of the (MC)SOR routine. If the program has been compiled with the pragma PTHREAD, pthreads are created whenever the routine `coulExch_pthread` is called and destroyed when the routine finishes. In contrast, if the pragma TPOOL is used, several pthreads are created when the program is started, they are used by any call to the `coulExch_tpool` routine, and only destroyed when the program ends.

The time needed to calculate the multipole moments and to relax the orbitals and potentials for the same FH, KrH$^+$ and TlF systems discussed above in fig. 5 is given in table 2 for the various parallellisation options. These data show that the relaxation of the potentials can be sped up by a factor of 3 for the smallest system, and by factor of 15-20 for the largest system when sufficiently many parallel cores are available.

Since the relaxation of a particular orbital is a single-threaded process, the speed-up factors for the relaxation of orbitals and potentials together is limited by Amdahl's law to between 2 and 8. Since the relaxation of the orbitals and potentials is the dominant step in a FD HF calculation, these

ratios are also a fair estimate of the resulting wall-time speed-ups of the whole calculation.

5. A complementary review of related literature

Having discussed the theory behind `x2dhf` in section 2, the numerical discretization and relaxation procedure in section 3, and the internal layout of the program in section 4, we proceed with a brief review of related literature. The main purpose of this section is again to augment the recent extensive review [7] by rediscussing pertinent work carried out with the `x2dhf` program, as well as to discuss the most recent advances in the field of fully numerical calculations on diatomic molecules.

5.1. Early years

For many years, the `x2dhf` program was mainly used to assist the development and calibration of sequences of universal even-tempered basis sets. This effort was initiated by Moncrieff and Wilson in the early 1990s [73–84]. In the course of that work, the FD HF method proved to be a reliable source of reference values of total energies, multipole moments, static polarizabilities and hyperpolarizabilities (α_{zz}, β_{zzz}, γ_{zzzz}, $A_{z,zz}$ and $B_{zz,zz}$) for atoms, diatomic molecules, and their ions [85–90].

5.2. Basis set convergence of total energies

`x2dhf` was also used in the literature to provide HF-limit values for examining the convergence patterns of properties calculated using the cc-pVXZ correlation-consistent basis sets of Dunning and coworkers [91–95] within the context of CBS models [96–100].

Important studies by Helgaker *et al.* [101] and Halkier *et al.* [97] demonstrated that HF energies exhibit exponential convergence both with respect to the total number of the basis functions of a given type, as well as with respect to the maximum angular momentum of the basis set, while correlation energies only converge according to an inverse power law.

The differing convergence patters of HF and post-HF calculations have ramifications for basis set design: the cc-pVXZ basis sets were constructed to allow the extrapolation of correlation energies to the CBS limit, and are thereby not optimal for CBS limit extrapolation of HF or DFT total energies. This was the rationale behind Jensen's project to build hierarchies of

Table 2: Effects of code parallelisation for the FH, KrH$^+$ and TlF systems. The system clock timings (in seconds) are given for the evaluations of the multipole moments (`mm`), relaxation of orbitals (`orbs`), relaxations of the Coulomb and exchange potentials (`pots`) and their sum (`orb+pots`). In the column labelled `-s` the timings for the single-threaded version of the code were given. The columns labelled `-o`, `-p` and `-t` give the timings obtained when the pragmas OPENMP, PTHREAD, and TPOOL were used during the compilation, respectively. The values in parentheses give the speedup.

	`-s` ST	`-o` OpenMP	`-p` PTHREAD	`-t` TPOOL
		FH		
mm	3.8	1.9	3.8	3.8
orbs	138.3	116.9	139.8	140.1
pots	351.3	112.3 (3.1)	160.0 (2.2)	128.6 (2.7)
orbs+pots	489.7	229.2 (2.1)	299.8 (1.6)	268.7 (1.8)
		KrH$^+$		
mm	9.2	1.9	9.3	9.1
orbs	81.8	83.5	84.1	83.6
pots	517.9	69.5 (7.5)	81.5 (6.4)	65.3 (7.9)
orbs+pots	599.7	153.0 (3.9)	165.6 (3.6)	148.9 (4.0)
		TlF		
mm	39.9	3.9	39.96	32.88
orbs	80.0	87.2	82.09	72.22
pots	922.6	60.5 (15.3)	63.79 (14.5)	47.29 (19.5)
orbs+pots	1002.6	147.7 (6.8)	145.89 (6.9)	119.52 (8.4)

polarization-consistent basis sets specifically tailored to facilitate CBS limit extrapolation of HF and DFT energies, dipole moments, and equilibrium distances [102–110]. Related to this effort, Jensen described obtaining significantly different or even lower HF limit energies with his new Gaussian basis sets than the FD HF values reported in the literature [56].

In an important contribution, Jensen examined the dependence of FD HF total energies on the grid size for 42 diatomic species composed of first and second-row elements and reported their energies to better than μE_h accuracy [56]. Jensen pointed out that large values for the practical infinity r_∞ (up to $r_\infty = 400 a_0$ in Jensen's study) are sometimes necessary to obtain the HF limit in FD HF calculations, as even though the orbitals have finite range, the potentials may approach their asymptotic limits only slowly.

The FD HF method was also used by Weigend *et al.* in the construction of Gaussian basis sets of quadruple zeta valence quality with a segmented contraction scheme for the H–Kr atoms [111], and by Petersson and coworkers in the development of the n-tuple-ζ augmented polarized family of basis sets (nZaP, $n = 1$–6) designed to allow extrapolating both the SCF energy and the correlation energy to their corresponding CBS limits [112].

The FD HF energies accurate to at least $1 \mu E_h$ were calculated with `x2dhf` for 27 diatomic transition-metal-containing species to investigate the convergence of the HF energies upon increasing the sizes of correlation-consistent basis sets and augmented basis sets developed for the transition atoms by Balabanov and Peterson [113, 114]. Some of these values were later revised by Lehtola [20] with calculations with the `HelFEM` program.

Sheng *et al.* determined FD HF values for He_2 to study CBS limit extrapolations of the correlation energy with the aug-cc-pVXZ orbital basis sets [115].

5.3. Basis set convergence of molecular properties

Halkier and Coriani studied the electric quadrupole moment of the FH molecule [116] by estimating the CBS limit of full configuration interaction (FCI) calculations in Gaussian basis sets. FD HF calculations were used to check that the largest employed Gaussian basis sets reproduced the HF quadrupole moment accurately.

Likewise, Pawlowski *et al.* [117] used the FD HF method to compute the HF limit dipole polarizability and second hyperpolarizability of the Ne atom to determine basis set truncation errors in Dunning's cc-pVXZ basis sets augmented with diffuse functions (aug-cc-pVXZ). Specifically, the study

considered double (d-aug), triple (t-aug), and quadruple augmentation (q-aug), finding that at least triple augmentation is required to converge the hyperpolarizability to 0.05 a.u. from the FD HF value with a 6-ζ level basis set (t-aug-cc-pV6Z). This knowledge was then used to build a Gaussian basis with an even closer agreement to the FD HF value.

Roy and Thakkar [118] computed the leading coefficients of the MacLaurin expansion of the electron momentum density from wave functions computed with the x2dhf program, finding large differences from literature values computed earlier with Slater-type orbital basis sets.

The x2dhf program was also employed by Shahbazian and Zahedi [119] to compare the convergence patterns of total energies and spectroscopic parameters in the correlation-consistent and polarization-consistent basis sets in HF calculations on a set of first-row diatomic molecules, also considering extrapolations to the CBS limit.

5.4. Miscellaneous

Accurate HF values for a set of diatomic molecules were used to proposed quality measures for Gaussian basis sets [120] and to test whether the counterpoise method can be used to correct basis set superposition effects [121].

Codes to evaluate the prolate spheroidal harmonics has been reported by Gil and Segura [122] and by Schneider and coworkers [123, 124]; the latter is used in HelFEM for the analytical evaluation of potentials [20]. Mendl proposed an efficient algorithm for two-center Coulomb and exchange integrals of prolate spheroidal orbitals [125].

Bodoor *et al.* investigated the numerical solution of two-electron pair equations of diatomic molecules, which turn out to be second order partial differential equations of 5 variables [126].

5.5. Steps towards relativistic calculations

A separate problem is the assessment of relativistic basis functions used for solving the Dirac–Fock equations. Despite some early attempts on small systems like H_2^+ [127–129]; HeH^{2+} [127]; HeH^+ [128]; and LiH, Li_2, BH, and CH^+ [130]; no general-use relativistic version of the FD HF method has yet been reported to the best of our knowledge. However, analogous relativistic finite element variants have been described in the literature [7].

Still, the two-dimensional, fully numerical finite-difference approach to the second-order Dirac equation for one-electron diatomics might be seen

as the first step towards the Dirac–Fock method [131], and FD HF can be used to indirectly assess the quality of the basis sets used for relativistic calculations.

Styszyński studied the influence of the relativistic core-valence correlation effects on total energies, bond lengths and fundamental frequencies for a series of hydrogen halide molecules (HF, HCl, HBr, HI and HAt) [132]. The results of non-relativistic HF calculations in Gaussian basis sets were compared by Styszyński and collaborators with those of FD HF calculations to assess the quality of basis sets and the dependence of spectroscopic constants on the basis set truncation errors [132–134].

5.6. Modeling irradiation processes

Calculations of the stopping powers and ranges of energetic ions in matter within the semiempirical approach developed by Ziegler, Biersack, and Littmark require the knowledge of interatomic potentials [135]. Nordlund *et al.* [136] studied repulsive potentials for C-C, Si-Si, N-Si, and H-Si systems, pioneering fully numerical HF and LDA calculations as well as calculations with numerical atomic orbital (NAO) basis sets for these systems.

Pruneda and Artacho [137] extended the analysis to C-C, O-O, Si-Si, Ca-O, and Ca-Ca systems with fully numerical HF calculations, which were supplemented with DFT calculations carried out in a NAO basis set with pseudopotentials.

Kuzmin examined relativistic effects in the potentials of the Kr-C, Xe-C, Au-C, and Pb-C diatomics with Gaussian basis sets, employing the FD HF method to validate the accuracy of the used Gaussian basis set in non-relativistic calculations [138, 139].

More recently, Lehtola [140] studied all-electron HF calculations of repulsive potentials of the He-He, He-Ne, Ne-Ne, He-Ar, Mg-Ar, Ar-Ar, and Ne-Ca systems with the `HelFEM` program, and investigated the accuracy of Gaussian basis set approaches.

Numerical orbitals obtained from the FD HF method proved to be useful in the development of a model of high-harmonic generation in diatomic molecules [141].

It turns out that the FD HF method (within the local exchange approximation) can be of some help when the multiple interatomic coulombic decay model is employed to analyse the process of neutralization and deexcitation of highly-charged ions being splashed from graphene [142]. The method was

64

used to calculate the orbital energies for C-ion separations down to a thousandth of the atomic unit. Solutions of the HF equations can also be used to describe the tunnelling ionisation of molecules within a model which relies on precise values of the asymptotic form of the valence (tunnelling) orbital [143–153].

5.7. Warning about confinement

Diatomic molecules can be studied in elliptical confinement that simulates a high pressure environment by enforcing the wave function to vanish at r_∞ [154–156]. The FD HF method was recently employed to study the $H_2{}^+$ and H_2 systems in their ground states in hard-wall confinement [157]. However, we warn that since `x2dhf` relies on solving the Poisson equation for the orbitals and potentials by imposing the boundary conditions by asymptotic expansions for the united atom in gas phase close to r_∞, the use of smaller values for r_∞ does not yield the correct confined solution, as incorrect boundary values are being imposed. Proper calculations of atoms and diatomic molecules in confinement are possible with `HelFEM`, however, as that program uses Green's functions for an exact solution to the Poisson equation for the potentials, and solves orbitals with the posed boundary conditions without imposing any assumed asymptotic behaviour. As a result, `HelFEM` yields the correct result even when hard-wall or soft confinement potentials are employed.

5.8. Density functional calculations

The FD HF approach proved useful in the DFT context to construct and test various functionals [158–165] including exchange energy functionals for excited-states [166]. Recently the FD HF results together with the machine-learning techniques have been used to test semi-local kinetic energy functionals on atoms and diatomics [167].

Makmal *et al.* described the fully numerical all-electron solution of the optimized effective potential equation for diatomic molecules in the `DARSEC` program in 2009 [168, 168], following a similar finite differences approach to `x2dhf`. The DARSEC implementation has since been employed in a number of studies on fundamental DFT [169–186].

Chávez *et al.* [187] described a Python module for embedding calculations in the prolate spheroidal coordinate system, which also employs a discretization similar to that in `x2dhf`.

Kraus examined basis set extrapolations in DFT [188, 189] with fully numerical calculations with the `HelFEM` program.

Lehtola studied the numerical behaviour of recent density functionals in non-self-consistent [190] as well as self-consistent atomic calculations [55, 61]. Many functionals were found to be numerically ill-behaved already at fixed electron density [190], while some functionals—such as most members of the Minnesota family—only exhibit pathological behaviour in self-consistent calculations, with the issues sometimes arising already for hydrogen [190], or on heavier atoms, with the Li and Na atoms causing the most problems [55].

Lehtola *et al.* studied diatomic molecules in strong magnetic fields [191] with `HelFEM`, finding large basis set truncation errors in the standard Dunning basis set series in extreme conditions. In a follow-up study, Lehtola and Åström [192] identified large errors for also atoms in strong magnetic fields. Lehtola has also recently discussed the use of fully numerical wave functions for diatomics to fit atomic orbital basis sets by the maximal overlap method [193].

6. Example results

As the review in section 5 illustrates, it has been demonstrated many times over the years that the FD HF method can produce HF-limit values of total energies, orbital energies, multipole moments, as well as (hyper)polarisabilities for various atomic and diatomic systems. As was also discussed in section 5, such results have been often used to assess the quality of basis sets and to test various schemes to improve them.

6.1. Basis set truncation errors in He_2 and other diatomics

Although Gaussian basis set (GBS) calculations can reach high accuracy for small molecules [194], typically employed basis sets suffer from truncation errors and basis set superposition errors, which are highly dependent on the property that is being studied. As discussed in section 5, various schemes have been suggested for reducing the error of the total energy, such as counterpoise (CP) methods [195] to reduce the basis set superposition error, as well as various CBS limit extrapolation techniques.

We exemplify these kinds of investigations in table 3 which shows the HF interaction energy in He_2 as a function of the internuclear distance. Results are shown for fully numerical calculations with `x2dhf`, as well as two sets of

Table 3: HF interaction energies of the helium dimer in μE_h from FD calculations [28]. For comparison, results of two GBS calculations are also shown: the raw $10s4p3d1f$ GBS values of Gutowski *et al.* [196] and GBS values from the doubly augmented cc-pVXZ basis set series (d-aug-cc-pVXZ) that have either also been extrapolated to the CBS limit with $(5\zeta,6\zeta)$ extrapolation [197], or extrapolated to the CBS limit while also including counterpoise (CP) corrections [195]. The last three columns show the differences between the values in columns 3, 4, and 5 and the FD values in column 2, respectively.

	interaction energy				basis set truncation error		
R(au)	FD[a]	GBS1[b]	GBS2$^c_{CBS}$	GBS2$^c_{CBS+CP}$	Δ	Δ_{CBS}	Δ_{CBS+CP}
3.0	13517.08	13518.21	13517.50	13517.02	1.13	0.42	-0.06
3.5	4335.76	4336.16	4336.27	4335.79	0.40	0.51	0.03
4.0	1357.88	1358.03	1358.24	1357.91	0.15	0.36	-0.14
4.5	416.54	416.60	416.75	416.55	0.06	0.21	-0.05
5.0	125.55	125.57	125.72	125.53	0.02	0.17	-0.04
5.4	47.58	47.59	47.71	47.57	0.01	0.13	-0.02
5.6	29.20	29.21	29.31	29.19	0.01	0.11	-0.02
5.8	17.88	17.89	17.97	17.88	0.01	0.08	-0.01
6.0	10.94	10.94	11.0	10.93	0.00	0.06	-0.01
6.5	3.17	3.18	3.23	3.17	0.01	0.06	-0.01
7.0	0.92	0.92	0.98	0.91	0.00	0.06	-0.01
7.5	0.26	0.26	0.30	0.26	0.00	0.04	0.00
8.0	0.08	0.06	0.07	0.08	-0.02	-0.01	0.00

[a]ref. 28, [b]ref. 196, [c]ref. 197, the (5,6) extrapolation values

GBS calculations: an old calculation of Gutowski *et al.* [196], and a newer one of Varandas [197] that includes CBS and CP corrections. The data in table 3 demonstrates the usefulness of having access to fully numerical data: while the raw, CP corrected, or CBS extrapolated data are sometimes in excellent agreement with results of fully numerical calculations, the basis set truncation error varies significantly along the studied geometries.

Figures 11 and 12 demonstrate the accuracy of distributed, universal, even-tempered basis sets (DUET) in reproducing total energy and multipole moments for a group of small, medium and large diatomic molecules [32]. Again, the numerical solution offers a way to assess the accuracy of the employed DUET basis sets, which show considerable differences across molecules.
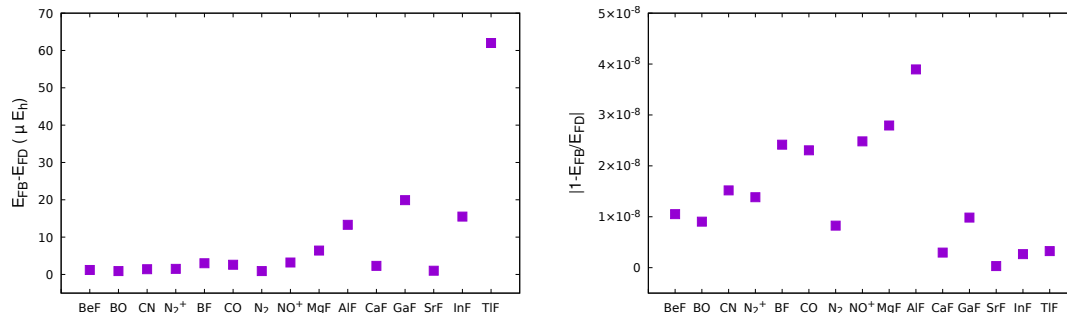
Figure 11: Absolute (μE_h, left plot) and relative errors of the total energy calculated using DUET basis sets for a range of diatomic molecules [32].

6.2. Harmonium atom

The intracule equation (eq. (37)) can be solved by the present version of the program.[9] To verify the implementation, we have solved the intracule equation for various values of ω_r and collected the results in table 4, where we have also included results of Taut [198] for comparison. The dependence of the σ ground-state energy on the ω_r parameter is also shown in Figure 13.

The Hamiltonian in eq. (37) is a combination of a repulsive Coulomb interaction with charge $1/2$ and a harmonic confinement potential, whose strength is controlled by ω_r. Unsurprisingly, the smaller the ω_r parameter is, the more extended the solution becomes, which is reflected in a poorer accuracy of the numerical solution observed in table 4.

Supplementing the results in table 4, we note that the program easily reproduces the correct solution for $\omega_r = 1/2$ ($2/\omega_r = 4$), with the energy equalling $5/8$. Higher states can also be calculated with `x2dhf`, and the energies of the first two excited σ states are obtained as $0.804\,828\,530 E_h$ and $1.021\,806\,949 E_h$.

Having established that the program finds the correct ground state for various values of ω_r, we proceed by studying higher-lying states of harmonium

---

[9]The extracule equation (eq. (38)) could also be solved with the FD HF method, but recovering well-known eigenvalues is of no special interest. However, the scheme could be easily used to find solutions of some distorted harmonic potentials.
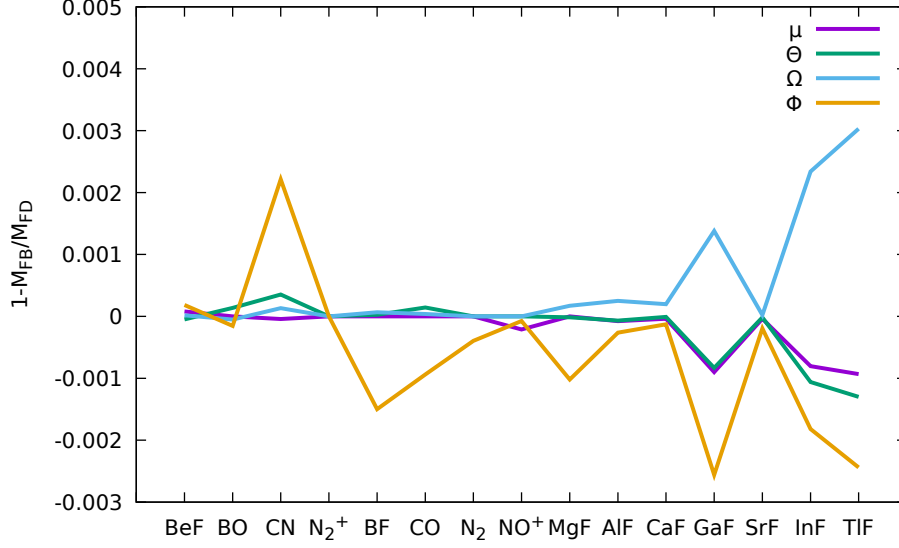
Figure 12: Relative errors of μ, Θ, Ω and Φ multipole moments calculated using DUET basis sets (M_{FB}) and FD HF method (M_{FD}) [32].

Table 4: The σ^2 ground-state energy, E, of the intracule (eq. (37)) as a function of the ω_r parameter. $|1 - N|$ denotes the norm error. The results of Taut [198] are also given for reference.

$2/\omega_r$	E/E_h	$\|1 - N\|$	$E[\text{Taut}]/E_h$	Grid
20.000 0	0.175 000 000 000	8×10^{-13}	0.175 0	$151 \times 241/100.0 a_0$
54.738 6	0.082 208 885 019	4×10^{-12}	0.082 2	$151 \times 241/100.0 a_0$
115.229	0.047 723 028 034	5×10^{-11}	0.047 7	$151 \times 271/200.0 a_0$
208.803	0.031 129 840 981	3×10^{-11}	0.031 1	$151 \times 301/350.0 a_0$
342.366	0.021 906 383	8×10^{-8}	0.021 9	$241 \times 511/550.0 a_0$
523.102	0.016 249 219	6×10^{-8}	0.016 2	$631 \times 1441/750.0 a_0$
758.124	0.012 541	5×10^{-6}	0.012 5	$631 \times 1351/450.0 a_0$
1054.54	0.009 956 947	6×10^{-8}	0.010 0	$1261 \times 2851/650.0 a_0$
1419.47	0.008 106	3×10^{-6}	0.008 1	$1261 \times 2851/650.0 a_0$

Figure 13: The log-log plot of the σ^2 ground-state energy, E (E_h), of the intracule as a function of the ω_r parameter.
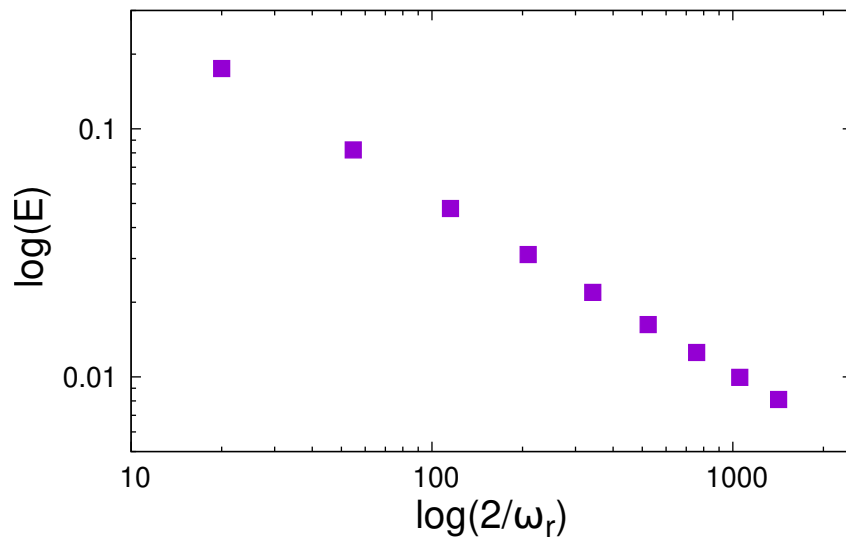
for $\omega = 1/2$. The orbital and total energies of the 12 lowest states of the σ^2, π^2, δ^2, or ϕ^2 configurations at the HF level of theory are given in table 5.

All but four of the orbitals are well converged. The outliers—the $2\sigma_g$, $2\pi_u$, $2\delta_g$ and $2\phi_u$ orbitals—have gaps of only some mE$_h$ to their higher lying neighbours (the $3\sigma_g$, $3\pi_u$, $3\delta_g$ and $3\phi_u$ orbitals). These differences are too small to be properly treated by the present implementation of the SOR method, as performing the calculations on more refined grids or in quadruple precision did not resolve the problem.

According to Kais *et al.* [54], the orbital and total energy for the lowest state are $\varepsilon_{\mathrm{HF}} = 1.227\,13\mathrm{E}_h$ a.u. and $E_{\mathrm{HF}} = 2.039\,325\mathrm{E}_h$. Kais *et al.* did not specify how their calculations were carried out; only that the `CADPAC` program [The Cambridge Analytic Derivatives Package] was used. As `CADPAC` employs Gaussian basis sets [199], it is not surprising to find that our total and orbital energies differ: our total energy is 0.89 mE$_h$ lower than that of Kais *et al.*, while our orbital energy (for which the variational principle does not apply since the potential of the orbital is different) is 49.5 mE$_h$ higher.

6.3. Ar-C at small internuclear distances

The great benefit of a fully numerical approach is that it can also be used to compute total and orbital energies for internuclear distances relevant in atom-atom or atom-ion collisions, where the behaviour at extremely small internuclear distances is of great importance. Although some important advances have been made recently [140], the reliable modeling of such bizarre systems with atomic basis set approaches remains extremely difficult.

First, the inner electronic orbitals of atoms can hybridize at small internuclear distances, while standard electronic basis sets do not contain functions to describe core orbital polarization. Moreover, the character of the atomic orbitals themselves can change: for example, at the limit $R \to 0$, the Ar-C system approaches the Cr atom, which is well known to exhibit a ground state with an occupied $3d$ orbital while Ar and C only feature occupied s and p orbitals.

Second, various electronic states are relevant when examining the range of internuclear distances relevant in collisions. Since the ground states of the Ar and C atoms are a singlet and a triplet, respectively, while the Cr atom has a septet ground state, it is clear that at least the triplet, quintet, and septet states need to be included in the consideration when studying the Ar-C collision.

Table 5: Orbital ϵ_a and total energies E of the lowest three singlet states of the σ^2, π^2, δ^2 and ϕ^2 configurations of the harmonium atom ($\omega = 1/2$) on $241 \times 271/25.0 a_0$ grid. $|1 - N|$ denotes the error of the orbital norm.

Orbital	ε_a	$E/\mathrm{E_h}$	$|1 - N|$
$2\phi_u$	3.513	6.763	1×10^{-04}
$1\phi_g$	3.037\,850\,636	5.788\,811\,079	4×10^{-16}
$2\delta_g$	3.033	5.783	2×10^{-05}
$1\phi_u$	2.580\,510\,831	4.832\,264\,681	8×10^{-15}
$1\delta_u$	2.565\,227\,220	4.816\,620\,939	9×10^{-16}
$2\pi_u$	2.563	4.815	5×10^{-05}
$1\delta_g$	2.114\,837\,213	3.867\,436\,248	3×10^{-15}
$2\sigma_g$	2.109	3.863\,979\,716	5×10^{-04}
$1\pi_g$	2.107\,519\,031	3.859\,874\,164	1×10^{-15}
$1\sigma_u$	1.692\,631\,671	2.948\,477\,552	1×10^{-15}
$1\pi_u$	1.668\,530\,193	2.923\,072\,506	2×10^{-15}
$1\sigma_g$	1.276\,676\,881	2.038\,438\,872	9×10^{-16}

The third major issue is that the linear dependencies in the atomic basis change considerably when the internuclear distance spans many orders of magnitude, giving rise to unknown truncation errors in the calculations.

In the following, we consider exchange-only LDA [38, 39] calculations on a single configuration of the triplet state of Ar-C, in which two π orbitals are fully occupied, two electrons occupy a third π orbital, and the rest of the electrons are placed on doubly occupied σ orbitals.

Figure 14 shows how the orbital energies in the Ar-C system depend on the internuclear distance $R \in [10^{-3}, 2]a_0$. The major feature to observe in the upper panel of fig. 14 is how the energy of the 1σ orbital undergoes a major change. At large R, the 1σ orbital corresponds to the $1s$ orbital of the Ar atom ($\varepsilon_{1s}^{\mathrm{Ar}} \approx -113.7\mathrm{E_h}$). Around $R \approx 0.3a_0$, the orbital appears to start experiencing the attraction of the C nucleus, as can be observed from the visibly non-zero slope of the orbital energy curve. The orbital energy decreases sharply around $R \approx 0.1a_0$, which is around the size of the Ar $1s$ orbital. The united atom limit ($\varepsilon_{1s}^{\mathrm{Cr}} \approx -213.8\mathrm{E_h}$) is finally reached for $R < 0.01a_0$, which is close to the size of the Cr $1s$ orbital.

Also the lower panel of fig. 14 contains interesting features: significant changes are especially observed in the energies of the 2σ, 3σ, 4σ, and 1π orbitals. The first three of these correspond to the Ar $2s$, C $1s$, and the Ar $2p_0$ core orbitals at large R, while the 1π orbital in Ar-C at large R contains the Ar $2p_{\pm 1}$ core orbitals. When the internuclear distance is decreased, the energies of these orbitals are strongly affected, and it is clear that hybridization is again going on between the deep-lying orbitals of Ar and C.

The highly non-monotonic behaviour of the 2σ energy in the region $R \in [0.01a_0, 1a_0]$ is especially worthwhile to notice, and it is likely an "after-effect" of the strong changes in the $1s$ orbital in that region. The 3σ and 1π orbitals show more muted changes. At small R, the 1σ and 2σ orbitals become the Cr united atom $1s$ and $2s$ orbitals, respectively, while the 3σ and 1π orbitals form the $2p$ orbital of the Cr united atom.

Many of the higher-lying orbital energies do not appear to change much in the studied region, as makes perfect sense: the outermost electrons are sufficiently far removed from the nuclei that they only experience a screened interaction.

While this calculation is performed for a fixed electronic configuration for a spin triplet, it is sufficient to highlight that calculations can be performed with `x2dhf` at small internuclear separations, although they can be troublesome to converge. A more in-depth examination of the Ar-C system would

Figure 14: DFT orbital energies of Ar-C as a function of the internuclear distance R given in a_0. All orbitals are shown in the upper panel. Since the large changes of the 1σ orbital dominate the plot, the zoomed in behaviour of the other orbitals is shown in the lower panel.
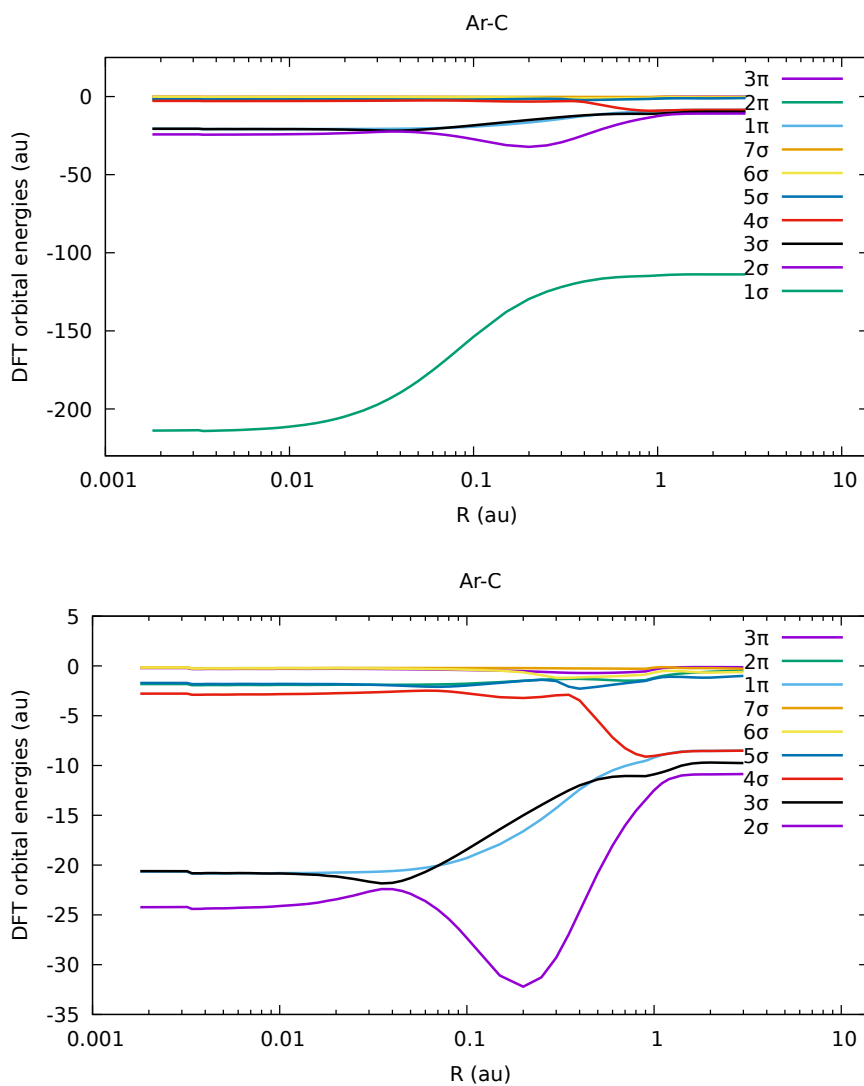
include additional spin states and configurations, such that the united Cr atom limit that also features occupied δ orbitals would also be considered, for instance.

6.4. Tests of Libxc functionality

The present version of the program allows one to perform DFT calculations with many functionals available through the Libxc library [41]. In the following, we compare total energies of the He, Be, Ne, and Kr atoms obtained by the x2dhf program to calculations performed in two ways with the HelFEM [50, 51, 55] program, while a third independent reference is provided by Engel's atomic OPMKS program [200].

Both x2dhf and HelFEM make use of Libxc [41], which is why in the following, we will exclusively employ Libxc's functional identifiers to uniquely specify the employed functionals. However, independent implementations of density functionals are employed in Engel's OPMKS program.

Comparisons for calculations that only include a correlation functional are not carried out for OPMKS, as the program appears to set the Coulomb interaction between the electrons to zero when no exchange potential has been specified. The calculations in OPMKS employed the parameters IMAX=800, RWALL=100.0, and TOLPOT=1.d-9.

Atomic calculations were carried our with the gensap program of HelFEM, which is specialized for calculations with spherical symmetric electron densities [50, 51, 55]. The calculations were carried out with the default 15-node Lagrange interpolating polynomial basis, employing 10 radial elements and the default value $r_\infty = 40a_0$. Exploratory calculations suggest that such a numerical basis set affords total energies converged to nE_h for the studied He, Be, Ne, and Kr atoms.

Atomic calculations can be carried out in the diatomic approaches employed in x2dhf and the diatomic program of HelFEM by setting $Z_B = 0$. The internuclear distance then becomes an arbitrary parameter; the calculations were run for $R = 1.7328a_0 \approx 0.917$ Å, which is the experimental equilibrium bond length of the FH molecule that was also used above in fig. 10.

As we wanted to compare the accuracy of the two methods especially devised for diatomic systems, another set of results were obtained using the diatomic program of HelFEM [20]. The numerical basis set for diatomic molecules in HelFEM is of the form of eq. (3) with an m dependent truncation parameter l_{max} for the partial wave expansion, while $X^{ml}(\mu)$ was described

by 15-node LIP elements [20]. The `HelFEM` default value of the practical infinity of $r_\infty = 40a_0$ was likewise employed for these calculations. The proxy method [20] with $\epsilon = 10^{-10}$ was used to generate a suitable numerical basis for the diatomic calculations with `HelFEM` using the `diatomic_cbasis` program. This procedure led to the following numerical basis sets: $N_{\text{elem}} = 3$ ($N_{\text{bf}}^{\text{rad}} = 42$) and $l_{\text{max}}^\sigma = 8$ for He; $N_{\text{elem}} = 3$ ($N_{\text{bf}}^\mu = 42$) and $l_{\text{max}}^\sigma = 12$ for Be; $N_{\text{elem}} = 3$ ($N_{\text{bf}}^\mu = 42$), $l_{\text{max}}^\sigma = 17$ and $l_{\text{max}}^\pi = 13$ for Ne; and $N_{\text{elem}} = 5$ ($N_{\text{bf}}^\mu = 70$), $l_{\text{max}}^\sigma = 32$, $l_{\text{max}}^\pi = 24$, and $l_{\text{max}}^\delta = 22$ for Kr; N_{elem} being the number of elements in μ and N_{bf}^μ the resulting number of numerical basis functions in μ.

There is no automatic or easy way to decide what size of a grid is needed in `x2dhf` for a particular system. The required size of the grid and the value of the practical infinity are dependent on the target accuracy of the solution, the heaviness of the individual nuclei, the overall charge state, and the examined electronic configuration. The examples in the `test-sets` subdirectory should be consulted to perform grid convergence studies. For these example calculations, the $181 \times 271/65.0a_0$ grid was used for He, Be, and Ne, and the $331 \times 511/150.0a_0$ grid was used for Kr.

A comparison of the resulting data is shown in table 6. Since both `x2dhf` and `HelFEM` use the same implementation of density functionals provided by Libxc, the results from the atomic program of `HelFEM` are expected to be the most reliable, as the one-center expansion makes the most sense for these calculations, and the atomic calculations were easy to converge to the CBS limit. The use of the same density functional implementation is known to be extremely important in studies performed at this level of accuracy, since small changes in the numerical parameters of density functionals arising from e.g. ambiguities in the original literature often result in total energy differences in the μE_h range [201].

The agreement between all four approaches is in general excellent, and even for the krypton atom an agreement with 7-8 significant figures is reached. However, since the total energy varies by four orders of magnitude between He and Kr, sub-μE_h precision has not been reached in all of the diatomic calculations.

The proxy approach used in the `diatomic` calculations in `HelFEM` was originally designed and tested for Hartree–Fock calculations [20]. We observe from the data in table 6 that although the claimed sub-μE_h precision for the choice of the numerical basis is achieved by this method in Hartree–Fock calculations, some density functional calculations with the `diatomic`

program show differences of the order of 1–3 µE$_h$ for the Ne and Kr atoms to the reference values obtained with the `gensap` atomic program.

We attribute this difference to the non-linearity of density functional approximations. However, we also note that the approach in `HelFEM` is still variational, as evinced by the `diatomic` total energies always being above the CBS limit values produced with the `gensap` program. Further calculations performed with larger numerical basis sets, *i.e.*, larger values of the $l_{\max}$ truncation parameters demonstrate that excellent agreement with results from the `gensap` program can be obtained (not shown).

Because `x2dhf` solves the Poisson equation with SOR, it can approach the CBS limit value from above or below. This behaviour is also observed in the data in table 6. For example, with the `GGA_X_B88` functional, the total energy reproduced by `x2dhf` is 26 nE$_h$ above the CBS limit value from `gensap` for Ne, while it is 21 µE$_h$ below the CBS limit value for Kr. It is thus clear that a larger grid is needed to get rid of the discrepancies observed for the krypton atom. Using a $631 \times 991/150.0a_0$ grid one gets the total energies $-2752.100\,620$E$_h$, $-2748.627\,895$E$_h$ and $-2753.851\,525$E$_h$, for the `GGA_X_B88`, `LDA_X-GGA_C_PBE`, and `HYB_GGA_XC_B3LYP` functionals, respectively, which are in µE$_h$ agreement with the reference values from the `gensap` program.

The results of this subsection demonstrate that `x2dhf` can be used to run DFT calculations with semi-local or global hybrid LDA and GGA functionals. However, the results also exemplify the need to carefully converge the calculations with respect to the grid size and the value of the practical infinity r_∞ to achieve the CBS limit in high precision. We again remind here about the double role of the practical infinity r_∞ in `x2dhf` calculations, which was discussed above in section 3.1.

Table 6: Total SCF energies of the He, Be, Ne, and Kr atoms calculated using exchange and correlation functionals from Libxc [41]. The results of the `x2dhf` (the first lines) are given together with the deviations, $E - E(\texttt{x2dhf})$, from the `diatomic` [20] program of `HelFEM`, fully numerical results from the atomic `gensap` [50, 51, 55] and from the `OPMKS` program [200]. The deviations are given in nE$_h$ units for He, Be, Ne and µE$_h$ for Kr.

Functional(s)	Approach	He	Be	Ne	Kr
HF	x2dhf	-2.861 679 996	-14.573 023 168	-128.547 098 052	-2 752.054 976
	diatomic	2	2	-5	0
				Continued on next page	

77

Table 6 – continued from previous page

Functional(s)		He	Be	Ne	Kr
	atomic	0	0	-57	-1
LDA_X [38, 39]	x2dhf	−2.723 639 793	-14.223 290 827	-127.490 740 825	-2 746.866 100
	diatomic	9	12	232	0
	atomic	0	0	-6	0
	OPMKS	0	0	-6	-1
GGA_X_PBE [202, 203]	x2dhf	-2.852 037 536	-14.545 039 137	-128.520 129 768	-2 751.653 674
	diatomic	11	561	996	4
	atomic	0	33	-67	1
	OPMKS	0	33	-67	1
GGA_X_B88 [204]	x2dhf	-2.863 379 361	-14.566 364 985	-128.590 092 756	-2 752.100 640
	diatomic	11	143	622	23
	atomic	0	-5	-26	21
	OPMKS	-79	-198	-644	17
LDA_C_VWN [205]	x2dhf	-2.052 843 324	-12.273 216 433	-117.699 882 594	-2 663.000 586
	diatomic	1	5	152	2
	atomic	0	0	0	0
LDA_C_PW [206]	x2dhf	-2.052 576 253	-12.272 556 485	-117.696 659 062	-2 662.986 395
	diatomic	2	4	152	30
	atomic	0	0	0	28
GGA_C_PBE [202, 203]	x2dhf	-1.988 501 616	-12.140 977 369	-117.314 905 038	-2 661.499 759
	diatomic	1	472	302	2
	atomic	0	-7	0	0
GGA_C_LYP [207, 208]	x2dhf	-1.992 266 386	-12.150 994 762	-117.357 415 352	-2 661.500 308
	diatomic	2	8	150	2
	atomic	0	0	0	0
LDA_X [38, 39]	x2dhf	-2.834 835 624	-14.447 209 474	-128.233 481 269	-2 750.147 940
LDA_C_VWN [205]	diatomic	9	12	240	1
	atomic	0	0	0!!!	0
	OPMKS	148	285	791	2
LDA_X [38, 39]	x2dhf	-2.834 455 181	-14.446 473 478	-128.229 917 209	-2 750.133 306
LDA_C_PW [206]	diatomic	10	13	235	1
	atomic	0	1	-6	0
	OPMKS	320!!!	701!!	2833!!!	15
LDA_X [38, 39]	x2dhf	-2.764 587 670	-14.308 185 377	-127.836 853 037	-2 748.627 924
GGA_C_PBE [202, 203]	diatomic	8	683	387	30
	atomic	0	75	-81	29
	OPMKS	0	75	-81	28
LDA_X [38, 39]	x2dhf	-2.767 057 515	-14.318 062 460	-127.873 287 501	-2 748.615 031
GGA_C_LYP [207, 208]	diatomic	9	20	222	1
	atomic	0	0	-5	0
	OPMKS	-134	-125	-97	0
GGA_X_PBE [202, 203]	x2dhf	-2.964 147 813	-14.769 959 464	-129.263 565 003	-2 754.935 906

Table 6 – continued from previous page

Functional(s)		He	Be	Ne	Kr
LDA_C_VWN [205]	diatomic	12	609	971	4
	atomic	0	59	-66	2
	OPMKS	149	344	725	4
GGA_X_PBE [202, 203]	x2dhf	-2.963 756 111	-14.769 215 227	-129.259 995 798	-2 754.921 272
LDA_C_PW [206]	diatomic	11	610	972	4
	atomic	-1	60	-66	1
	OPMKS	324	766	2778	15
GGA_X_PBE [202, 203]	x2dhf	-2.892 934 867	-14.629 947 789	-128.866 427 587	-2 753.416 110
GGA_C_PBE [202, 203]	diatomic	11	1038	1379	5
	atomic	0	73	-158	2
	OPMKS	0	73	-158	1
GGA_X_PBE [202, 203]	x2dhf	-2.895 699 125	-14.640 227 604	-128.902 927 530	-2 753.402 420
GGA_C_LYP [207, 208]	diatomic	11	550	899	3
	atomic	0	5	-66	1
	OPMKS	-142	-122	-158	3
HYB_GGA_XC_B3LYP [42]	x2dhf	-2.915 218 663	-14.673 328 221	-128.980 973 214	-2 753.851 519
	diatomic	8	151	357!!!	-5
	atomic	0	46	-24	-6
	OPMKS	20	240	731!!!	-5
HYB_LDA_XC_LDA0 [209]	x2dhf	-2.840 868 320	-14.477 351 811	-128.306 321 244	-2 750.605 900
	diatomic	7	21	-1634	-11
	atomic	0	12	-1810	-11

6.5. Kinetic potentials

If converged HF or Kohn–Sham orbitals $\phi_i(\boldsymbol{r})$ and eigenvalues ε_i are available, the total kinetic potential can be computed as [210]

$$v_k(\boldsymbol{r}) = v^P(\boldsymbol{r}) + v^W(\boldsymbol{r}) \tag{67}$$

where $v^P(\boldsymbol{r})$ and $v^W(\boldsymbol{r})$ are the Pauli and von Weizsäcker kinetic potentials defined as

$$v^P(\boldsymbol{r}) = \frac{\tau(\boldsymbol{r}) - \tau^W(\boldsymbol{r})}{\rho(\boldsymbol{r})} + \sum_i^N (\varepsilon_H - \varepsilon_i) \frac{|\phi_i(\boldsymbol{r})|^2}{\rho(\boldsymbol{r})} \tag{68}$$

$$v^W(\boldsymbol{r}) = \frac{|\nabla\rho(\boldsymbol{r})|^2}{8\rho^2(\boldsymbol{r})} - \frac{\nabla^2\rho(\boldsymbol{r})}{4\rho(\boldsymbol{r})} = \frac{\tau^W(\boldsymbol{r})}{\rho(\boldsymbol{r})} - \frac{\nabla^2\rho(\boldsymbol{r})}{4\rho(\boldsymbol{r})} \tag{69}$$

where $\tau^W(\boldsymbol{r}) = |\nabla\rho(\boldsymbol{r})|^2/8\rho(\boldsymbol{r})$, $\tau(\boldsymbol{r}) = 1/2\sum_i^N |\nabla\phi_i(\boldsymbol{r})|^2$ is the kinetic energy density, ε_H is the energy of the highest occupied molecular orbital (HOMO), and the total density is equal to $\rho(\boldsymbol{r}) = \sum_i^N q_i|\varphi_i(\boldsymbol{r})|^2$.

The FD HF method can be used to compute these properties. Plots of the HF total density ρ_{HF}, its Laplacian $\nabla^2\rho_{\mathrm{HF}}$, the Pauli kinetic potential v^P, the logarithm of the von Weizsäcker kinetic potential $\log(v^W)$, and the logarithm of their sum $\log(v^P + v^W)$ are shown in fig. 15 for the FH molecule. The values are plotted along the z axis, with the F atom displaced to $z = 0$, and the H atom to the experimental equilibrium distance $z = 1.7328a_0$.

For comparison, we also carried out exchange-only LDA [38, 39] calculations. The obtained differences to the HF data in fig. 15 are shown in fig. 16. To allow displaying the details of the changes in Δv^W and $\Delta(v^P + v^W)$, which can be both positive and negative, the logarithms of their absolute values are shown, instead. Some of the plots were also trimmed to focus on the regions with interesting changes.

Overall, fig. 16 shows that the LDA calculation reproduces the major features of the HF calculations. The axis scales in fig. 16 are orders of magnitude smaller than in fig. 15; the only difference is the plot of the density laplacian $\nabla^2\rho$, which in any case diverges at the nuclei [55].

7. Conclusions

We have carried out an extensive review of the restricted open-shell Hartree–Fock and Kohn–Sham methods for diatomic molecules, as well as its finite difference discretization. The methods can be also applied to solving orbitals for atomic model potentials, the Kramers–Henneberger atom, as well as Hooke's atom (also known as harmonium).

We have discussed in detail how the discretization takes place, and how the various boundary conditions for the solution are applied. The solution of the coupled sets of Poisson equations for the orbitals and potentials with the successive overrelaxation (SOR) method have also been presented at depth.

We have described the new, parallelised version 3.0 of `x2dhf`, the finite difference Hartree–Fock program for atoms and diatomic molecules. The program has been written mostly in Fortran 95, with some optional C extensions. The program is built with CMake. The program is hosted openly on GitHub [68], and it is provided with the open source GNU General Public License v2.0, or later (GPL-2.0-or-later).

Figure 15: The total kinetic potential for the FH molecule ($R = 1.7328a_0$) along the internuclear axis and its ingredients computed from a HF wave function. The F atom is placed at $z = 0$, while the H atom is found at $z = R$. The ingredients comprise: the total HF density, ρ_{HF}, $\nabla^2 \rho_{\text{HF}}$, the Pauli kinetic potential, v^P, the logarithm of the von Weizsäcker kinetic potential, $\log(v^W)$, and the logarithm of their sum, $\log(v^P + v^W)$.
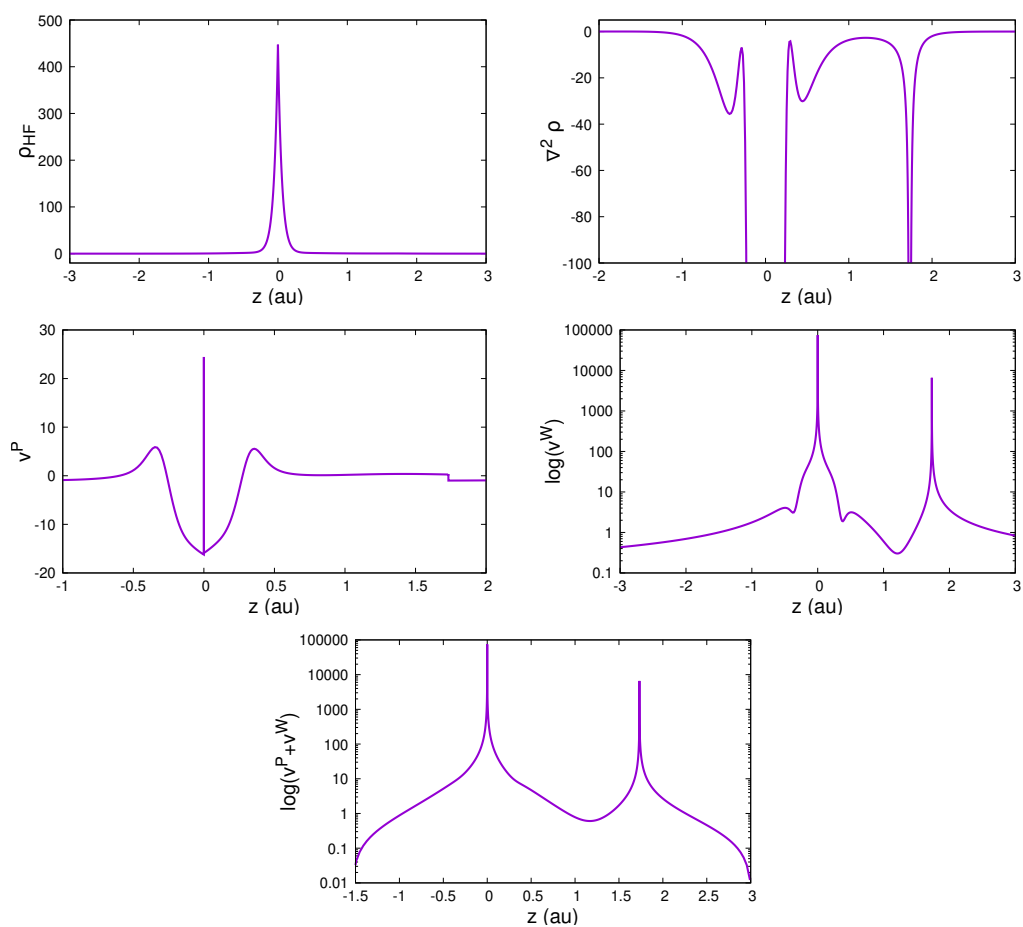
Figure 16: Differences in the DFT total kinetic potential and its ingredients compared to HF values shown in fig. 15; analogous notation is used.
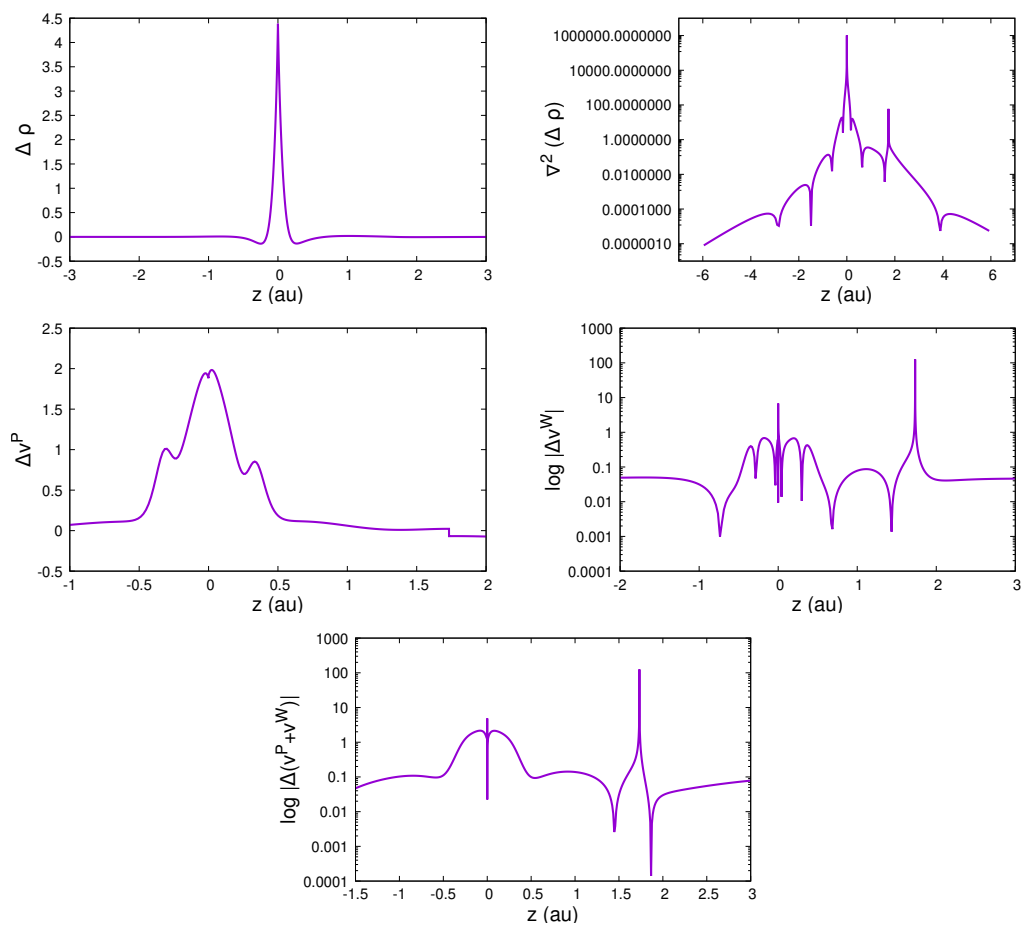
Besides extensive internal refactoring, the initialisation process of `x2dhf` has been greatly simplified by including tabulations of radial LDA and HF atomic orbitals in the program, as well as atomic LDA Coulomb potentials which afford a better initial guess to the Poisson problem. As significant new features, `x2dhf` can now also be used to solve Kohn–Sham equations with LDA and GGA functionals from the Libxc library [41], as well as to calculate molecular orbitals for the superposition of atomic potentials [48, 49].

Continuing with a discussion of the literature complementing the recent review article [7], we discussed the science that has been enabled by earlier versions of `x2dhf`, as well as recent work carried out with alternative approaches.

We exemplified the capabilities of the new version of `x2dhf` by studies of basis set truncation errors in He_2 and other diatomics, as well as calculations on harmonium and Ar-C at small internuclear distances. We verified the Libxc interface and the rectified implementation of GGA functionals by calculations on the He, Be, Ne, and Kr atoms, and found excellent agreement with reference calculations carried out with `HelFEM` and `OPMKS`. Finally, we plotted kinetic potentials from HF and exchange-only LDA calculations on the FH molecule.

This article represents the pinnacle of over 40 years of effort on the FD HF approach on diatomic molecules, much of it by the first author, who is about to retire. The considerable length of this article is a direct result of this long and extensive effort. The collaboration of the new and old generation exhibited in the authorship of this work has aimed to document in depth some of the finer details of the approach. These details may not have been explicitly written down in previous work, but they are important for achieving a thorough understanding of the FD HF approach.

Thanks to the ongoing development of mathematical methods and computer programming [71], alternative ways to perform fully numerical calculations on diatomic molecules are nowadays feasible. The use of higher-order numerical methods affords more accurate results at a similar cost, as was demonstrated on a model Poisson equation in section 3.2. The solution strategy in `HelFEM` [20] enables simpler ways to program as well as set up calculations, saving human time instead of computer time. We hope to achieve speedups in `HelFEM` calculations based on insight from `x2dhf` in future applications.

CRediT authorship contribution statement

Jacek Kobus: Conceptualization, Methodology, Software, Resources, Investigation, Validation, Formal analysis, Writing – original draft, Visualization, Project administration.

Susi Lehtola: Software, Investigation, Validation, Writing – review & editing.

Declaration of competing interest

The authors declare that they have no known competing financial interests or personal relationships that could have appeared to influence the work reported in this paper.

Data availability

Data will be made available on request.

Acknowledgements

A.8. Finite nuclear models

A detailed discussion of various nuclear charge distribution models has been published by Andrae [211]. The `x2dhf` program implements finite nuclear models following Gaussian and Fermi distributions.

A.8.1. Gaussian nuclear model

The Gaussian distribution has the form

$$\rho(r) = Z \left(\frac{\lambda}{\pi}\right)^{\frac{3}{2}} \exp\left(-\lambda r^2\right)$$

where the exponent of the normalized Gaussian-type function representing the nuclear distribution is determined by the root-mean-square radius of the

84

nuclear charge distribution via the relation $\lambda = 3/2\langle r^2\rangle$. A statistical model gives the following value for the root-mean-square radius (in fm)

$$\langle r^2\rangle^{1/2} = 0.836A^{1/3} + 0.570, \qquad A > 6 \tag{70}$$

where A is the atomic mass of a nucleus. Therefore, when the distance is expressed in atomic units we have

$$\lambda = \frac{3}{2}10^{10}\left(\frac{0.529177249}{0.836A^{\frac{1}{3}} + 0.570}\right)^2$$

For any spherically symmetric charge distribution $\rho(r)$ the potential energy is

$$-rV(r) = 4\pi\left(\int_0^r s^2\rho(s)\mathrm{d}s + r\int_r^\infty s\rho(s)\mathrm{d}s\right)$$

If $\rho(r) = \rho_0\exp(-\lambda r^2)$ then the first integral is equal to

$$\rho_0\left(\frac{-r\exp(-\lambda r^2)}{2\lambda} + \frac{\sqrt{\pi}\mathrm{erf}(\sqrt{\lambda}r)}{4\lambda^{3/2}}\right)$$

and the second to $\rho_0 r\exp(-\lambda r^2)/2\lambda$. Thus

$$-rV(r) = \rho_0\left(\frac{\pi}{\lambda}\right)^{3/2}\mathrm{erf}\left(\sqrt{\lambda}r\right) = Z\,\mathrm{erf}\left(\sqrt{\lambda}r\right)$$
$$= \frac{2Z}{\sqrt{\pi}}\left(\gamma\left(\frac{3}{2},\eta r^2\right) + \sqrt{\eta}re^{-\eta r^2}\right)$$
$$= \frac{2Z}{\sqrt{\pi}}\left(\gamma\left(\frac{3}{2},\eta r^2\right) + \sqrt{\eta}r\left(1 - \gamma(1,\eta r^2)\right)\right)$$

since $\rho_0 = Z(\lambda/\pi)^{3/2}$ (the last form of the potential can be found in Parpia's paper [212]). In the above equation $\gamma(a,x)$ is the lower incomplete gamma function, namely

$$\gamma(a,x) = \int_0^x t^{a-1}e^{-t}\mathrm{d}t$$

The potential $V(r)$ reduces to the Coulomb potential if $r \gg \sqrt{\lambda}$. In case a very tight diatomic system with finite nuclei is considered the Z_1Z_2/r con-

tribution to the total energy must be replaced by

$$\frac{Z_1 Z_2}{r} \frac{1}{\sqrt{\pi}} \gamma \left(\frac{1}{2}, \lambda_{12} r^2 \right)$$

and $1/\lambda_{12} = 1/\lambda_1 + 1/\lambda_2$ [212].

A.8.2. Fermi distribution

The Fermi distribution is more detailed than the Gaussian model and has traditionally been employed in fitting nuclear scattering data. The Fermi distribution is

$$\rho(r) = \frac{\rho_0}{1 + e^{(r-c)/a}}$$

where c is the *half-density radius* since $\rho(c) = \rho_0/2$. The parameter a is related to the nuclear *skin thickness* t through $t/a = 4 \ln 3$. It may be verified that $\rho(c - t/2) = 0.9\rho_0$ and that $\rho(c + t/2) = 0.1\rho_0$. The skin thickness is thus the interval across which the nuclear charge density drops from $0.9\rho_0$ to $0.1\rho_0$. It is a standard practice to take $t = 2.30$ fm independent of the atomic mass. The parameter c depends on the atomic mass through eq. (70) and the following relation

$$\left\langle r^2 \right\rangle \approx \frac{3}{5} c^2 + \frac{7}{5} \pi^2 a^2$$

The potential of the Fermi distribution reads

$$-rV(r) = \frac{Z}{N} \left\{ 6 \left(\frac{a}{c} \right)^3 \left[-S_3 \left(-\frac{c}{a} \right) + S_3 \left(\frac{r-c}{a} \right) \right] \right.$$
$$\left. + \frac{r}{c} \left[\frac{3}{2} + \frac{1}{2} \pi^2 \left(\frac{a}{c} \right)^2 - 3 \left(\frac{a}{c} \right)^2 S_2 \left(\frac{r-c}{a} \right) - \frac{1}{2} \left(\frac{r}{c} \right)^2 \right] \right\}$$

for $r/c < 1$ and

$$-rV(r) = \frac{Z}{N} \left\{ N + 3 \left(\frac{a}{c} \right)^2 \left[\frac{r}{c} S_2 \left(\frac{r-c}{a} \right) + 2 \left(\frac{a}{c} \right) S_3 \left(\frac{r-c}{a} \right) \right] \right\}$$

otherwise; $N = 1 + \pi^2 (a/c)^2 - 6(a/c)^3 S_3(-c/a)$ and S_k is an infinite series defined as

$$S_k(r) = \sum_{n=1}^{\infty} (-1)^n \frac{e^{nr}}{n^k}$$

86

This is the potential for the Fermi distribution used in the GRASP92 package [213], and the `x2dhf` program follows suit.

A.9. Evaluation of one- and two-particle integrals

The volume element in the (ν, μ, θ) coordinates is

$$\mathrm{d}x\mathrm{d}y\mathrm{d}z = \frac{R^3}{8}\sinh\mu\,\sin\nu\,(\cosh^2\mu - \cos^2\nu)\,\mathrm{d}\nu\mathrm{d}\mu\mathrm{d}\theta \tag{71}$$

The expression for the kinetic energy can be calculated in the (ν, μ, θ) coordinates as

$$
\begin{aligned}
E_T^a &= \int\int\int \mathrm{d}x\mathrm{d}y\mathrm{d}z\,\phi_a^*\left(-\frac{1}{2}\nabla^2\right)\phi_a \\
&= -\frac{\pi R}{2}\int\int\sqrt{(\xi^2-1)(1-\eta^2)}f_a(\nu,\mu)T(\nu,\mu)f_a(\nu,\mu)\mathrm{d}\nu\mathrm{d}\mu
\end{aligned} \tag{72}
$$

where

$$T(\nu,\mu) = \frac{\partial^2}{\partial\mu^2} + \frac{\xi}{\sqrt{\xi^2-1}}\frac{\partial}{\partial\mu} + \frac{\partial^2}{\partial\nu^2} + \frac{\eta}{1-\eta^2}\frac{\partial}{\partial\nu} - m_a^2\left(\frac{1}{\xi^2-1} + \frac{1}{1-\eta^2}\right) \tag{73}$$

The nuclear potential energy is analogously evaluated as

$$E_n^a = -\frac{\pi R}{2}\int\int\sqrt{(\xi^2-1)(1-\eta^2)}R\left\{\xi(Z_1+Z_2) + \eta(Z_2-Z_1)\right\}f_a^2\mathrm{d}\nu\mathrm{d}\mu \tag{74}$$

The two-electron Coulomb and exchange energy contributions to the total energy are obtained as

$$
\begin{aligned}
E_C^{ab} &= \int\int\int \mathrm{d}x\mathrm{d}y\mathrm{d}z\,\phi_a\frac{2}{R\xi}\tilde{V}_C^b\phi_a \\
&= \frac{\pi R^2}{2}\int\int\frac{1}{\xi}\sqrt{(\xi^2-1)(1-\eta^2)}(\xi^2-\eta^2)f_a(\nu,\mu)\tilde{V}_C^b f_a(\nu,\mu)\mathrm{d}\nu\mathrm{d}\mu \\
E_x^{ab} &= \int\int\int \mathrm{d}x\mathrm{d}y\mathrm{d}z\,\phi_a\frac{2}{R\xi}\tilde{V}_x^{ab}\phi_b \\
&= \frac{\pi R^2}{2}\int\int\frac{1}{\xi}\sqrt{(\xi^2-1)(1-\eta^2)}(\xi^2-\eta^2)f_a(\nu,\mu)\tilde{V}_x^{ab}f_b(\nu,\mu)\mathrm{d}\nu\mathrm{d}\mu
\end{aligned}
$$

The two-dimensional integration is carried out with eq. (47)

87

A.10. Interface to Libxc routines

In the following, we use the same notation as Lehtola *et al.* [41], except that orbitals are written as ϕ in our notation. In the case of the LDA, we have

$$E_{\text{xc}}^{\text{LDA}} = \int \mathrm{d}^3 r n(\mathbf{r}) e_{\text{xc}}^{\text{LDA}}(\{n_\sigma(\mathbf{r})\}) = \int \mathrm{d}^3 r \epsilon_{\text{xc}}^{\text{LDA}}(\{n_\sigma(\mathbf{r})\}) \tag{75}$$

where $n(\mathbf{r})$ is the total electron density, $e_{\text{xc}}^{\text{LDA}}(\{n_\sigma(\mathbf{r})\})$ is the xc energy density per electron evaluated by Libxc, and $\epsilon_{\text{xc}}^{\text{LDA}}(\{n_\sigma(\mathbf{r})\})$ is the resulting xc energy density. The corresponding expression for the LDA potentials reads

$$v_{\text{xc}}^\sigma = \frac{\partial \epsilon_{\text{xc}}}{\partial n_\sigma}, \tag{76}$$

and like e_{xc}, this quantity is readily computed and returned by Libxc.

The functional form of GGAs is often referred to as dependence on the density gradient

$$E_{\text{xc}}^{\text{GGA}} = \int \mathrm{d}^3 r \epsilon_{\text{xc}}^{\text{GGA}}(\{n_\sigma(\mathbf{r})\}, \{\nabla n_\sigma(\mathbf{r}))\}). \tag{77}$$

However, the gradient dependence in GGA functionals can actually be written in the form

$$E_{\text{xc}}^{\text{GGA}} = \int \mathrm{d}^3 r \epsilon_{\text{xc}}^{\text{GGA}}(\{n_\sigma(\mathbf{r})\}, \{\gamma_{\sigma\sigma'}(\mathbf{r}))\}), \tag{78}$$

where the reduced gradient is

$$\gamma_{\sigma\sigma'}(\mathbf{r}) = \nabla n_\sigma \cdot \nabla n_{\sigma'}, \tag{79}$$

and the input and output of Libxc is formulated with respect to this variable [41]. Due to the new ingredient, the GGA expression for the local potential to be employed in the orbital optimization is somewhat more involved

$$v_{\text{xc}}^\sigma = \frac{\partial \epsilon_{\text{xc}}^{\text{GGA}}}{\partial n_\sigma} - \nabla \cdot \left(2\frac{\partial \epsilon_{\text{xc}}^{\text{GGA}}}{\partial \gamma_{\sigma\sigma'}}\nabla n_\sigma + \frac{\partial \epsilon_{\text{xc}}^{\text{GGA}}}{\partial \gamma_{\sigma\sigma'}}\nabla n_{\sigma'}\right). \tag{80}$$

The GGA potential eq. (80) can be computed in two ways: by computing the divergence term by finite differences, or by evaluating the divergence analytically, which generates complicated expressions involving higher derivatives of the density functional and Hessians of the density, for example. We adopted

the former way to evaluate eq. (80), which appears to be the standard way the problem is approached also in the plane wave community, for example.

Since the total density is defined as

$$n = \sum_a q_a \varphi_a^* \varphi_a,$$

where q_a are again orbital occupation numbers, $\nabla^2 n$ can be evaluated as

$$\nabla^2 n = 2 \sum_a q_a \varphi_a^* \nabla^2 \varphi_a + 2 \sum_a q_a \nabla \varphi_a^* \nabla \varphi_a$$

When perfoming DFT calculations using generalized gradient approximation one thus needs to evaluate $\nabla^2(f^* f)$ and $\nabla f^* \nabla g$ in the (transformed) prolate spheroidal coordinates where $f(x, y, z)$ and $g(x, y, z)$ are orbitals or their densities. These densities are real functions, since they do not contain any $\exp(im_f)$ or $\exp(im_g)$ terms; this also means that the densities have σ-type symmetry. Several relevant formulae for the evaluation of various DFT potentials have been collected below to help the reader to examine, check or modify the code in x2dhf. Employing the definition of prolate spheroidal coordinates (eqs. (1), (2), (4) and (5)) and the general form of the functions (eq. (12)) one can write

$$\frac{\partial f}{\partial x} = \frac{\partial \xi}{\partial x} \frac{\partial \mu}{\partial \xi} \frac{\partial f}{\partial \mu} + \frac{\partial \eta}{\partial x} \frac{\partial \nu}{\partial \eta} \frac{\partial f}{\partial \nu} + im_f \frac{\partial \theta}{\partial x}$$

$$\frac{\partial f}{\partial y} = \frac{\partial \xi}{\partial y} \frac{\partial \mu}{\partial \xi} \frac{\partial f}{\partial \mu} + \frac{\partial \eta}{\partial y} \frac{\partial \nu}{\partial \eta} \frac{\partial f}{\partial \nu} + im_f f \frac{\partial \theta}{\partial y}$$

$$\frac{\partial f}{\partial z} = \frac{\partial \xi}{\partial z} \frac{\partial \mu}{\partial \xi} \frac{\partial f}{\partial \mu} + \frac{\partial \eta}{\partial z} \frac{\partial \nu}{\partial \eta} \frac{\partial f}{\partial \nu}$$

since $\partial f/\partial\theta = im_f f$, $\partial\theta/\partial z = 0$ (now $f \equiv f(\nu,\mu)$). We also have

$$x^2 + y^2 = \frac{R^2}{4}(\xi^2 - 1)(1 - \eta^2)$$

$$r_1 = \sqrt{x^2 + y^2 + (z + R/2)^2}$$

$$r_2 = \sqrt{x^2 + y^2 + (z - R/2)^2}$$

$$r_1 r_2 = \frac{R^2}{4}(\xi^2 - \eta^2)$$

$$x = \frac{R}{2}\sqrt{\xi^2 - 1}\sqrt{1 - \eta^2}\cos(\theta)$$

$$y = \frac{R}{2}\sqrt{\xi^2 - 1}\sqrt{1 - \eta^2}\sin(\theta)$$

$$z = \frac{R}{2}\xi\eta$$

and therefore

$$\frac{\partial\mu}{\partial x} = \frac{1}{\sqrt{\xi^2 - 1}}\frac{\partial\xi}{\partial x} \qquad \frac{\partial\mu}{\partial y} = \frac{1}{\sqrt{\xi^2 - 1}}\frac{\partial\xi}{\partial y} \qquad \frac{\partial\mu}{\partial z} = \frac{1}{\sqrt{\xi^2 - 1}}\frac{\partial\xi}{\partial z}$$

$$\frac{\partial\nu}{\partial x} = \frac{-1}{\sqrt{1 - \eta^2}}\frac{\partial\eta}{\partial x} \qquad \frac{\partial\nu}{\partial y} = \frac{-1}{\sqrt{1 - \eta^2}}\frac{\partial\eta}{\partial y} \qquad \frac{\partial\nu}{\partial z} = \frac{-1}{\sqrt{1 - \eta^2}}\frac{\partial\eta}{\partial z}$$

$$\frac{\partial\xi}{\partial x} = \frac{4}{R^2(\xi^2 - \eta^2)}\xi x \qquad \frac{\partial\xi}{\partial y} = \frac{4}{R^2(\xi^2 - \eta^2)}\xi y \qquad \frac{\partial\xi}{\partial z} = \frac{4}{R^2(\xi^2 - \eta^2)}\left(\xi z - \frac{1}{2}R\eta\right)$$

$$\frac{\partial\eta}{\partial x} = \frac{-4}{R^2(\xi^2 - \eta^2)}\eta x \qquad \frac{\partial\eta}{\partial y} = \frac{-4}{R^2(\xi^2 - \eta^2)}\eta y \qquad \frac{\partial\eta}{\partial z} = \frac{-4}{R^2(\xi^2 - \eta^2)}\left(\eta z - \frac{1}{2}R\xi\right)$$

$$\frac{\partial\theta}{\partial x} = \frac{\partial}{\partial x}\cos^{-1}\left(\frac{2x}{R\sqrt{\xi^2 - 1}\sqrt{1 - \eta^2}}\right) = \frac{2}{R}\frac{\partial}{\partial x}\left(\frac{x}{\sqrt{\xi^2 - 1}\sqrt{1 - \eta^2}}\right)\frac{1}{\sqrt{1 - \tilde{x}^2}}$$

$$\frac{\partial\theta}{\partial x} = \frac{\partial}{\partial x}\cos^{-1}\left(\frac{2x}{R\sqrt{\xi^2 - 1}\sqrt{1 - \eta^2}}\right)$$

$$= \frac{2}{R}\frac{\partial}{\partial x}\left(\frac{x}{\sqrt{\xi^2 - 1}\sqrt{1 - \eta^2}}\right)\frac{1}{\sqrt{1 - \tilde{x}^2}}$$

$$= \frac{2}{R\sin(\theta)}\frac{1}{\sqrt{\xi^2 - 1}\sqrt{1 - \eta^2}}\left(1 - \frac{4x^2}{R^2(\xi^2 - \eta^2)}\right)$$

90

where $\tilde{x} = 2x/(R\sqrt{\xi^2 - 1}\sqrt{1 - \eta^2}) = \cos(\theta)$. Likewise

$$\frac{\partial \theta}{\partial y} = \frac{\partial}{\partial y} \cos^{-1}\left(\frac{2y}{R\sqrt{\xi^2 - 1}\sqrt{1 - \eta^2}}\right)$$

$$= \frac{2}{R}\frac{\partial}{\partial y}\left(\frac{y}{\sqrt{\xi^2 - 1}\sqrt{1 - \eta^2}}\right)\frac{1}{\sqrt{1 - \tilde{y}^2}}$$

$$= \frac{2}{R\cos(\theta)}\frac{1}{\sqrt{\xi^2 - 1}\sqrt{1 - \eta^2}}\left(1 - \frac{4y^2}{R^2(\xi^2 - \eta^2)}\right)$$

since $\tilde{y} = 2y/(R\sqrt{\xi^2 - 1}\sqrt{1 - \eta^2}) = \sin(\theta)$.

In case the f and g functions are of σ-type symmetry $(m_f = m_g = 0)$ we have

$$\frac{\partial f}{\partial x} = \frac{4}{R^2(\xi^2 - \eta^2)}\left\{\frac{\xi x}{\sqrt{\xi^2 - 1}}\frac{\partial f}{\partial \mu} + \frac{\eta x}{\sqrt{1 - \eta^2}}\frac{\partial f}{\partial \nu}\right\} \tag{81}$$

$$\frac{\partial f}{\partial y} = \frac{4}{R^2(\xi^2 - \eta^2)}\left\{\frac{\xi y}{\sqrt{\xi^2 - 1}}\frac{\partial f}{\partial \mu} + \frac{\eta y}{\sqrt{1 - \eta^2}}\frac{\partial f}{\partial \nu}\right\} \tag{82}$$

$$\frac{\partial f}{\partial z} = \frac{4}{R^2(\xi^2 - \eta^2)}\left\{\frac{(\xi z - \frac{1}{2}R\eta)}{\sqrt{\xi^2 - 1}}\frac{\partial f}{\partial \mu} + \frac{(\eta z - \frac{1}{2}R\xi)}{\sqrt{1 - \eta^2}}\frac{\partial f}{\partial \nu}\right\}$$

$$\frac{\partial f}{\partial x}\frac{\partial g}{\partial x} = \left[\frac{4}{R^2(\xi^2 - \eta^2)}\right]^2\left\{\frac{\xi^2}{(\xi^2 - 1)}\frac{\partial f}{\partial \mu}\frac{\partial g}{\partial \mu} + \frac{\eta^2}{(1 - \eta^2)}\frac{\partial f}{\partial \nu}\frac{\partial g}{\partial \nu}\right.$$
$$\left. + \frac{\xi\eta}{\sqrt{\xi^2 - 1}\sqrt{1 - \eta^2}}\left(\frac{\partial f}{\partial \mu}\frac{\partial g}{\partial \nu} + \frac{\partial f}{\partial \nu}\frac{\partial g}{\partial \mu}\right)\right\}x^2$$

$$\frac{\partial f}{\partial y}\frac{\partial g}{\partial y} = \left[\frac{4}{R^2(\xi^2 - \eta^2)}\right]^2\left\{\frac{\xi^2}{(\xi^2 - 1)}\frac{\partial f}{\partial \mu}\frac{\partial g}{\partial \mu} + \frac{\eta^2}{(1 - \eta^2)}\frac{\partial f}{\partial \nu}\frac{\partial g}{\partial \nu}\right.$$
$$\left. + \frac{\xi\eta}{\sqrt{\xi^2 - 1}\sqrt{1 - \eta^2}}\left(\frac{\partial f}{\partial \mu}\frac{\partial g}{\partial \nu} + \frac{\partial f}{\partial \nu}\frac{\partial g}{\partial \mu}\right)\right\}y^2$$

$$\frac{\partial f}{\partial z}\frac{\partial g}{\partial z} = \left[\frac{4}{R^2(\xi^2-\eta^2)}\right]^2 \left\{ \frac{(\xi z - \frac{R}{2}\eta)^2}{(\xi^2-1)}\frac{\partial f}{\partial \mu}\frac{\partial g}{\partial \mu} + \frac{(\eta z - \frac{R}{2}\xi)^2}{(1-\eta^2)}\frac{\partial f}{\partial \nu}\frac{\partial g}{\partial \nu} \right.$$
$$\left. + \frac{(\xi z - \frac{R}{2}\eta)(\eta z - \frac{R}{2}\xi)}{\sqrt{\xi^2-1}\sqrt{1-\eta^2}}\left(\frac{\partial f}{\partial \mu}\frac{\partial g}{\partial \nu} + \frac{\partial f}{\partial \nu}\frac{\partial g}{\partial \mu}\right)\right\}$$

$$\nabla f \nabla g = \left[\frac{4}{R^2(\xi^2-\eta^2)}\right]^2$$
$$\left\{ \left(\frac{R^2}{4}\xi^2(1-\eta^2) + \frac{(\xi z - \frac{R}{2}\eta)^2}{(\xi^2-1)}\right)\frac{\partial f}{\partial \mu}\frac{\partial g}{\partial \mu} + \right.$$
$$\left(\frac{R^2}{4}\eta^2(1-\xi^2) + \frac{(\eta z - \frac{R}{2}\xi)^2}{(1-\eta^2)}\right)\frac{\partial f}{\partial \nu}\frac{\partial g}{\partial \nu} +$$
$$\left.\left(\frac{R^2}{4}\xi\eta\sqrt{\xi^2-1}\sqrt{1-\eta^2} + \frac{(\xi z - \frac{R}{2}\eta)(\eta z - \frac{R}{2}\xi)}{\sqrt{\xi^2-1}\sqrt{1-\eta^2}}\right)\left(\frac{\partial f}{\partial \mu}\frac{\partial g}{\partial \nu} + \frac{\partial f}{\partial \nu}\frac{\partial g}{\partial \mu}\right)\right\}$$
$$\nabla^2 f = \frac{4}{R^2(\xi^2-\eta^2)}\left(\frac{\partial^2 f}{\partial \mu^2} + \frac{\xi}{\sqrt{\xi^2-1}}\frac{\partial f}{\partial \mu} + \frac{\partial^2 f}{\partial \nu^2} + \frac{\eta}{\sqrt{1-\eta^2}}\frac{\partial f}{\partial \nu}\right)$$

In case $m_f \neq 0$, i.e., $f = e^{im_f\theta}f(\nu,\mu)$, the partial derivatives in eqs. (81) and (82) contain additional terms $im_f f \partial\theta/\partial x$ and $im_f f \partial\theta/\partial y$ and therefore now $\nabla f^*\nabla g$ and the Laplacian $\nabla^2 f$ formulae take the form

$$\nabla f \nabla g = \left[\frac{4}{R^2(\xi^2-\eta^2)}\right]^2$$
$$\left\{ \left(\frac{R^2}{4}\xi^2(1-\eta^2) + \frac{(\xi z - \frac{R}{2}\eta)^2}{(\xi^2-1)}\right)\frac{\partial f}{\partial \mu}\frac{\partial g}{\partial \mu} + \right.$$
$$\left(\frac{R^2}{4}\eta^2(1-\xi^2) + \frac{(\eta z - \frac{R}{2}\xi)^2}{(1-\eta^2)}\right)\frac{\partial f}{\partial \nu}\frac{\partial g}{\partial \nu} +$$
$$\left.\left(\frac{R^2}{4}\xi\eta\sqrt{\xi^2-1}\sqrt{1-\eta^2} + \frac{(\xi z - \frac{R}{2}\eta)(\eta z - \frac{R}{2}\xi)}{\sqrt{\xi^2-1}\sqrt{1-\eta^2}}\right)\left(\frac{\partial f}{\partial \mu}\frac{\partial g}{\partial \nu} + \frac{\partial f}{\partial \nu}\frac{\partial g}{\partial \mu}\right)\right\}$$
$$+ m_f m_g f g \frac{4}{R^4\sqrt{(\xi^2-1)(1-\eta^2)}}$$
$$\left\{ \frac{1}{\sin^2(\theta)}\left(1 - \frac{4x^2}{R^2(\xi^2-1)(1-\eta^2)}\right)^2 + \frac{1}{\cos^2(\theta)}\left(1 - \frac{4y^2}{R^2(\xi^2-1)(1-\eta^2)}\right)^2\right\}$$

$$\nabla^2 f = \frac{4}{R^2(\xi^2 - \eta^2)} \left(\frac{\partial^2 f}{\partial \mu^2} + \frac{\xi}{\sqrt{\xi^2 - 1}} \frac{\partial f}{\partial \mu} + \frac{\partial^2 f}{\partial \nu^2} + \frac{\eta}{\sqrt{1 - \eta^2}} \frac{\partial f}{\partial \nu} \right)$$
$$+ \frac{4 m_f^2 f}{R^2(\xi^2 - 1)(1 - \eta^2)}$$
$$= \frac{4}{R^2(\xi^2 - \eta^2)} \left\{ \frac{\partial^2 f}{\partial \mu^2} + \frac{\xi}{\sqrt{\xi^2 - 1}} \frac{\partial f}{\partial \mu} + \frac{\partial^2 f}{\partial \nu^2} + \frac{\eta}{\sqrt{1 - \eta^2}} \frac{\partial f}{\partial \nu} \right.$$
$$\left. + m_f^2 \left(\frac{1}{\xi^2 - 1} + \frac{1}{1 - \eta^2} \right) f \right\}$$

When $\nabla^2(f^* f)$ is needed there is no θ-dependency and the density must be treated as a σ-type orbital.

The extension of this approach to meta-GGA functionals is non-trivial, as discussed by Zahariev *et al.* [214], for instance. We note here for completeness that the need to compute expressions similar to eq. (80) can be avoided in a basis set expansion by the use of integrations by parts [215], following the work of Pople *et al.* in [216]. The integration by parts can be used to move the differentiation from the xc potential onto the basis functions, which typically have analytical derivatives, and most atomic-orbital implementations follow this approach that is easily extended to meta-GGAs, as well [217, 215]. The finite element implementation of GGAs and meta-GGAs in HelFEM also employs this technique [20, 50, 51, 55].

A.11. Boundary conditions for potentials at r_∞

The boundary conditions for the potentials $\tilde{V}^{ab}$ at the practical infinity are obtained from the multipole expansion. In particular, we have

$$\tilde{V}_C^a = \frac{R\xi}{2} \sum_{l=0}^{l_{\max}} \frac{P_{l,0}(\cos\theta)}{r^{l+1}} Q_{l,0}^{aa} \tag{83}$$

$$\tilde{V}_x^{ab} = \frac{R\xi}{2} \sum_{l=0}^{l_{\max}} (-1)^{|\Delta m|} \frac{(l - |\Delta m|)!}{(l + |\Delta m|)!} \frac{P_{l|\Delta m|}(\cos\theta)}{r^{l+1}} Q_{l,|\Delta m|}^{ab} \tag{84}$$

where $Q_{l,|m|}^{ab} = \langle \phi_a | r^l P_{l,|m|}(\cos\theta) | \phi_b \rangle$ are the multipole moments and $P_{l,|\Delta m|}$ are the associated Legendre functions. In the present version of the program, the multipole moments are computed in parallel if OpenMP support is available.

Note that the Coulomb potential in eq. (83) only contains the $\Delta m = 0$ term, because orbital densities $|\phi_a|^2$ have cylindrical symmetry ($|\exp(im\theta)|^2 = 1$), while exchange potentials arise from orbital density products $\phi_a^* \phi_b$ that are θ dependent via $\Delta m = m_a - m_b$. `x2dhf` employs the default value $l_{\max} = 4$ unless orbitals of ϕ symmetry are detected, in which case the default value is increased to $l_{\max} = 8$.

A.12. Boundary conditions for orbitals at r_∞

The asymptotic behaviour of the orbitals is used to estimate their values in the last few grid points in the μ direction, close to r_∞. The asymptotic behaviour of the orbitals of diatomic molecules can be modeled as that of the orbitals of the corresponding united atom. Therefore, one can consider the second-order differential equation [69]

$$\frac{\mathrm{d}^2 y_a}{\mathrm{d}r^2} = \left(\varepsilon_a - \frac{g_1(r)}{r} + \frac{g_2(r)}{r^2}\right) y_a = F_a(r) y_a \tag{85}$$

with $y(0) = 0$ and $y(r) \to 0$ as $r \to \infty$, where ε_a is the orbital energy, and $g_1(r)$, $g_2(r)$, and $F_a(r)$ are functions whose exact definitions are not essential here, as the details of the approach can be found in the work of Froese-Fischer [69]. The solution $y_a(r)$ to this equation exhibits exponential asymptotic decay as

$$y_a(r) \propto F_a(r)^{-1/4} \exp\left(-\int_{r_0}^{r} F_a(r')^{1/2} \mathrm{d}r'\right) \tag{86}$$

By discretizing and approximating the integral by a rectangular rule, the above equation yields the appropriate expression of the boundary condition for the orbitals at the practical infinity in the form

$$y_a(r_{i+1}) \approx y_a(r_i) \left(\frac{F_a(r_i)}{F_a(r_{i+1})}\right)^{1/4} \exp\left(-\sqrt{F_a(r_i)}(r_{i+1} - r_i)\right) \tag{87}$$

A.13. Interpolation of boundary values

The properties discussed in eqs. (50) to (52) can be used to provide the additional values along the remaining sides of the rectangular region $[\nu_1, \nu_{N_\nu}] \times [\mu_1, \mu_{N_\mu}]$. If the solution f is an odd function, it should vanish

94

along the $(0, \mu)$, (π, μ) and $(\nu, 0)$ lines, and the corresponding values are thereby set to zero.If the solution f is an even function, suitable values are calculated using the Lagrange 9-point interpolation formula for an equally spaced abscissa [218]

$$f(x_0 + ph) \approx \sum_k A_k^n(p) u_k$$

where A_k^n is the interpolation constant given for even and odd values of n by the following formulae

$$A_k^n(p) = \frac{(-1)^{\frac{1}{2}n+k}}{\left(\frac{n-2}{2} + k\right)! \left(\frac{1}{2}n - k\right)! (p - k)} \prod_{t=1}^{n} \left(p + \frac{1}{2}n - t\right),$$

$$-\frac{1}{2}(n - 2) \leq k \leq \frac{1}{2}n$$

$$A_k^n(p) = \frac{(-1)^{\frac{1}{2}(n-1)+k}}{\left(\frac{n-1}{2} + k\right)! \left(\frac{n-1}{2} - k\right)! (p - k)} \prod_{t=0}^{n-1} \left(p + \frac{n-1}{2} - t\right),$$

$$-\frac{1}{2}(n - 1) \leq k \leq \frac{1}{2}(n - 1)$$

Assuming that $f(-x_i) = f(x_i)$ and $f_k = f(x_0 + kh)$, solving f_0 from the equation for f_5 yields

$$f_0 = \frac{1}{126}(210 f_1 - 120 f_2 + 45 f_3 - 10 f_4 + f_5).$$

A.14. Assignments of the 2D arrays in the `x2dhf` code

$$\texttt{VXI}= \xi = \cosh\mu \qquad \texttt{VXISQ}= \xi^2 \qquad \texttt{VXI1}= \sqrt{\xi^2-1} \qquad \texttt{VXI2}= \frac{\xi}{\sqrt{\xi^2-1}}$$

$$\texttt{VETA}= \eta = \cos\nu \qquad \texttt{VETASQ}= \eta^2 \qquad \texttt{VETA1}= \sqrt{1-\eta^2} \qquad \texttt{VETA2}= \frac{\eta}{\sqrt{1-\eta^2}}$$

$$\texttt{BORB}= \frac{\cosh\mu}{\sinh\mu} = \frac{\xi}{\sqrt{\xi^2-1}} \qquad\qquad \texttt{BPOT}= \frac{1}{\sqrt{\xi^2-1}} - \frac{2\sqrt{\xi^2-1}}{\xi}$$

$$\texttt{D}= \frac{\cos\nu}{\sin\nu} = \frac{\eta}{\sqrt{1-\eta^2}} \qquad\qquad \texttt{E}= -\left(\frac{1}{\xi^2-1} + \frac{1}{1-\eta^2}\right)$$

$$\texttt{G}= -\frac{\pi R^3 \xi}{2}(\xi^2 - \eta^2) \qquad\qquad \texttt{F0}= R(Z_a + Z_b)\xi + R(Z_b - Z_a)\eta$$

$$\texttt{F1}= \frac{R^2}{2}(\xi^2 - \eta^2) \quad \texttt{F2}= -\frac{R}{\xi}(\xi^2 - \eta^2) \qquad \texttt{F3}= -\frac{2}{\xi^2} \qquad\qquad \texttt{F4}= \frac{R\xi}{2}$$

$$\texttt{WGT1}= \frac{\pi R}{2}\sqrt{\xi^2-1}\sqrt{1-\eta^2} \qquad \texttt{WGT2}= \frac{\pi R^2}{2}\sqrt{\xi^2-1}\sqrt{1-\eta^2}(\xi^2-\eta^2)/\xi$$

$$\texttt{WGT2*F4}= \frac{\pi R^3}{4}\sqrt{\xi^2-1}\sqrt{1-\eta^2}(\xi^2-\eta^2) = \frac{\pi R^3}{4}\sinh\mu \sin\nu(\cosh^2\mu - \cos^2\nu)$$

References

[1] J. Kobus, A finite difference Hartree–Fock program for atoms and diatomic molecules, Comput. Phys. Commun. 184 (2013) 799–811. doi:10.1016/j.cpc.2012.09.033.

[2] W. Kohn, L. J. Sham, Self-consistent equations including exchange and correlation effects, Phys. Rev. 140 (1965) A1133–A1138. doi:10.1103/PhysRev.140.A1133.

[3] S. Huzinaga, Basis sets for molecular calculations, Comput. Phys. Rep. 2 (1985) 281–339. doi:10.1016/0167-7977(85)90003-6.

[4] E. R. Davidson, D. Feller, Basis set selection for molecular calculations, Chem. Rev. 86 (1986) 681–696. doi:10.1021/cr00074a002.

[5] J. G. Hill, Gaussian basis sets for molecular applications, Int. J. Quantum Chem. 113 (2013) 21–34. doi:10.1002/qua.24355.

[6] F. Jensen, Atomic orbital basis sets, Wiley Interdiscip. Rev. Comput. Mol. Sci. 3 (2013) 273–295. doi:10.1002/wcms.1123.

[7] S. Lehtola, A review on non-relativistic, fully numerical electronic structure calculations on atoms and diatomic molecules, Int. J. Quantum Chem. 119 (2019) e25968. `arXiv:1902.01431`, `doi:10.1002/qua.25968`.

[8] C. Froese, The self-consistent field with exchange for the ground state and first excited state of Fe^{13}, Mon. Not. R. Astron Soc. 117 (1957) 615–621. `doi:10.1093/mnras/117.6.615`.

[9] E. L. Albasiny, J. R. A. Cooper, A one-centre S.C.F. wave function for the methane molecule, Mol. Phys. 4 (1961) 353–358. `doi:10.1080/00268976100100521`.

[10] E. L. Albasiny, J. R. A. Cooper, The Calculation of Electronic Properties of BH_4^-, CH_4 and NH_4^+ using One-centre Self-consistent Field Wave Functions, Proc. Phys. Soc. 82 (1963) 289–303. `doi:10.1088/0370-1328/82/2/315`.

[11] E. L. Albasiny, J. R. A. Cooper, A one-centre study of the silane molecule, Proc. Phys. Soc. 85 (1965) 1133–1142. `doi:10.1088/0370-1328/85/6/311`.

[12] E. L. Albasiny, J. R. A. Cooper, Electronic structure and properties of the ions AlH_4^- and PH_4^+, Proc. Phys. Soc. 88 (1966) 315–323. `doi:10.1088/0370-1328/88/2/306`.

[13] J. A. Keefer, J. K. Su Fu, R. L. Belford, One-center molecular calculations with unlimited radial basis. H_2, HeH^+, and LiH centered on one nucleus, J. Chem. Phys. 50 (1969) 160–173. `doi:doi.org/10.1063/1.1670774`.

[14] E. A. McCullough Jr., Seminumerical SCF calculations on small diatomic diatomic molecules, Chem. Phys. Lett. 24 (1974) 55–58. `doi:doi.org/10.1016/0009-2614(74)80212-5`.

[15] E. A. McCullough Jr., Numerical Hartree–Fock methods for diatomic molecules: a partial-wave expansion approach, Comput. Phys. Rep. 4 (1986) 265–312.

[16] A. D. Becke, Numerical Hartree–Fock–Slater calculations on diatomic molecules, J. Chem. Phys. 76 (1982) 6037–6045. `doi:10.1063/1.442958`.

[17] A. D. Becke, Numerical Hartree–Fock–Slater calculations on diatomic molecules: Addendum, J. Chem. Phys. 78 (1983) 4787–4788. `doi:10.1063/1.445285`.

[18] A. D. Becke, Local exchange-correlation approximations and first-row molecular dissociation energies, Int. J. Quantum Chem. 27 (1985) 585–594. `doi:10.1002/qua.560270507`.

[19] A. D. Becke, Completely numerical calculations on diatomic molecules in the local-density approximation, Phys. Rev. A 33 (1986) 2786.

[20] S. Lehtola, Fully numerical Hartree–Fock and density functional calculations. II. Diatomic molecules, Int. J. Quantum Chem. 119 (2019) e25944. `arXiv:1810.11653`, `doi:10.1002/qua.25944`.

[21] S. Lehtola, HelFEM—Finite element methods for electronic structure calculations on small systems, accessed 10 June 2024 (2024).
URL `http://github.com/susilehtola/HelFEM`

[22] L. Laaksonen, P. Pyykkö, D. Sundholm, Two-dimensional fully numerical solutions of molecular Schrödinger equations. I. One-electron molecules, Int. J. Quantum Chem. 23 (1983) 309–317. `doi:10.1002/qua.560230126`.

[23] L. Laaksonen, P. Pyykkö, D. Sundholm, Two-Dimensional fully numerical solutions of molecular Schrödinger equations. II. Solution of the Poisson equation and results for singlet states of H_2 and HeH$^+$, Int. J. Quantum Chem. 23 (1983) 319–323. `doi:10.1002/qua.560230127`.

[24] L. Laaksonen, P. Pyykkö, D. Sundholm, Two-dimensional fully numerical solutions of molecular Hartree–Fock equations: LiH and BH, Chem. Phys. Lett. 96 (1983) 1–3. `doi:10.1016/0009-2614(83)80104-3`.

[25] L. Laaksonen, D. Sundholm, P. Pyykkö, Two-dimensional fully numerical MC SCF calculations on H_2 and LiH: The dipole moment of LiH, Chem. Phys. Lett. 105 (1984) 573–576. `doi:10.1016/0009-2614(84)85659-6`.

[26] D. Sundholm, P. Pyykkö, L. Laaksonen, A. J. Sadlej, Nuclear quadrupole moment of lithium from combined fully numerical and discrete basis-set calculations on LiH, Chem. Phys. Lett. 112 (1984) 1–9. doi:10.1016/0009-2614(84)87030-X.

[27] L. Laaksonen, P. Pyykkö, D. Sundholm, Fully numerical Hartree–Fock methods for molecules, Comput. Phys. Rep. 4 (1986) 313–344. doi:10.1016/0167-7977(86)90021-3.

[28] J. Kobus, Finite-difference versus finite-element methods, Chem. Phys. Lett. 202 (1993) 7–12. doi:10.1016/0009-2614(93)85342-L.

[29] J. Kobus, Vectorizable algorithm for the (multicolour) successive over-relaxation method, Comput. Phys. Commun. 78 (1994) 247–255. doi:10.1016/0010-4655(94)90003-5.

[30] J. Kobus, Diatomic molecules: Exact solutions of HF equations, Adv. Quantum Chem. 28 (1997) 1–14. doi:10.1016/S0065-3276(08)60203-8.

[31] J. Kobus, L. Laaksonen, D. Sundholm, A numerical Hartree–Fock program for diatomic molecules, Comput. Phys. Commun. 98 (1996) 346–358. doi:10.1016/0010-4655(96)00098-7.

[32] J.Kobus, Finite difference Hartree–Fock method for diatomic molecules, in: G. B. E. Onate, B. Suarez (Eds.), Proceedings European Congress on Computational Methods in Applied Sciences and Engineering, ECCOMAS 2000, Barcelona, Spain, September 11-14, 2000, CIMNE, Barcelona, 2000, p. CDROM, iSBN 84-89925-70-4.

[33] A. H. Wapstra, G. Audi, The 1983 atomic mass evaluation. 1. Atomic mass table, Nucl. Phys. A 432 (1983) 1–54.

[34] G. Audi, A. H. Wapstra, The 1993 atomic mass evaluation. 1. Atomic mass table, Nucl. Phys. A 565 (1993) 1–65.

[35] P. Csavinszky, A variational approach to the solution of Poisson's equation in prolate spheroidal coordinates, Int. J. Quantum Chem. 30 (1986) 305–309. doi:10.1002/qua.560300302.

[36] P. Hohenberg, W. Kohn, Inhomogeneous electron gas, Phys. Rev. 136 (1964) B864–B871. `doi:10.1103/PhysRev.136.B864`.

[37] J. C. Slater, A Simplification of the Hartree–Fock Method, Phys. Rev. 81 (1951) 385–390. `doi:10.1103/PhysRev.81.385`.

[38] F. Bloch, Bemerkung zur Elektronentheorie des Ferromagnetismus und der elektrischen Leitfähigkeit, Z. Phys. 57 (1929) 545–555. `doi:10.1007/BF01340281`.

[39] P. A. M. Dirac, Note on exchange phenomena in the Thomas atom, Math. Proc. Cambridge Philos. Soc. 26 (1930) 376–385. `doi:10.1017/S0305004100016108`.

[40] K. Schwarz, Optimization of the statistical exchange parameter α for the free atoms H through Nb, Phys. Rev. B 5 (1972) 2466–2468. `doi:10.1103/PhysRevB.5.2466`.

[41] S. Lehtola, C. Steigemann, M. J. T. Oliveira, M. A. L. Marques, Recent developments in LIBXC—a comprehensive library of functionals for density functional theory, SoftwareX 7 (2018) 1–5. `doi:10.1016/j.softx.2017.11.002`.

[42] P. J. Stephens, F. J. Devlin, C. F. Chabalowski, M. J. Frisch, Ab initio calculation of vibrational absorption and circular dichroism spectra using density functional force fields, J. Phys. Chem. 98 (1994) 11623–11627. `doi:10.1021/j100096a001`.

[43] A. E. S. Green, D. L. Sellin, A. S. Zachor, Analytic Independent-Particle Model for Atoms, Phys. Rev. 184 (1969) 1–9. `doi:10.1103/PhysRev.184.1`.

[44] A. E. S. Green, An Analytic Independent Particle Model for Atoms – I. Initial studies, Adv. Quantum Chem. 7 (1973) 221–262. `doi:10.1016/S0065-3276(08)60563-8`.

[45] J. E. Whalen, A. E. S. Green, Analytic Independent Particle Model for Molecules, Am. J. Phys. 40 (1972) 1484–1489. `doi:10.1119/1.1986874`.

[46] K. J. Miller, A. E. S. Green, Energy levels and potential energy curves for H_2, N_2, and O_2 with an independent particle model, J. Chem. Phys. 60 (1974) 2617–2626. `doi:10.1063/1.1681415`.

[47] T. Sawada, P. S. Ganas, A. E. S. Green, Elastic scattering of electrons from N_2, Phys. Rev. A 9 (1974) 1130–1135. `doi:10.1103/PhysRevA.9.1130`.

[48] S. Lehtola, Assessment of initial guesses for self-consistent field calculations. superposition of atomic potentials: Simple yet efficient, J. Chem. Theory Comput. 15 (2019) 1593–1604. `arXiv:1810.11659`, `doi:10.1021/acs.jctc.8b01089`.

[49] S. Lehtola, L. Visscher, E. Engel, Efficient implementation of the superposition of atomic potentials initial guess for electronic structure calculations in Gaussian basis sets, J. Chem. Phys. 152 (2020) 144105. `arXiv:2002.02587`, `doi:10.1063/5.0004046`.

[50] S. Lehtola, Fully numerical Hartree–Fock and density functional calculations. I. Atoms, Int. J. Quantum Chem. 119 (2019) e25945. `arXiv:1810.11651`, `doi:10.1002/qua.25945`.

[51] S. Lehtola, Fully numerical calculations on atoms with fractional occupations and range-separated exchange functionals, Phys. Rev. A 101 (2020) 012516. `arXiv:1908.02528`, `doi:10.1103/PhysRevA.101.012516`.

[52] T. Dziubak, J. Matulewski, Recombination of an atomic system in one, two, and three dimensions in the presence of an ultrastrong attosecond laser pulse: A comparison of results obtained using a Coulomb and a smoothed Coulomb potential, Phys. Rev. A 79 (2009) 043404. `doi:10.1103/PhysRevA.79.043404`.

[53] W. C. Henneberger, Perturbation method for atoms in intense light beams, Phys. Rev. Lett. 21 (1968) 838. `doi:10.1103/PhysRevLett.21.838`.

[54] S. Kais, D. R. Herschbach, N. C. Handy, C. W. Murray, G. J. Laming, Density functionals and dimensional renormalization for an exactly solvable model, J. Chem. Phys. 99 (1993) 417–425. `doi:10.1063/1.465765`.

[55] S. Lehtola, Meta-GGA density functional calculations on atoms with spherically symmetric densities in the finite element formalism, J. Chem. Theory Comput. 19 (2023) 2502–2517. `arXiv:2302.06284`, `doi:10.1021/acs.jctc.3c00183`.

[56] F. Jensen, On the accuracy of numerical Hartree–Fock energies, Theor. Chem. Acc. 113 (2005) 187–190. `doi:10.1007/s00214-004-0618-8`.

[57] W. G. Bickley, Formulae for Numerical Differentiation, Math. Gaz. 25 (1941) 19–27. `doi:10.2307/3606475`.

[58] L. Laaksonen, P. Pyykkö, D. Sundholm, Two-dimensional fully numerical solutions of molecular Schrödinger equations. I. One-electron molecules, Int. J. Quantum Chem. 23 (1983) 309–317. `doi:10.1002/qua.560230126`.

[59] C. Runge, Über empirische Funktionen und die Interpolation zwischen äquidistanten Ordinaten, Zeit. Math. Phys. 46 (1901) 224–243.

[60] S. Lehtola, Accuracy of a recent regularized nuclear potential, J. Chem. Theory Comput. 19 (2023) 4033–4039. `arXiv:2302.09557`, `doi:10.1021/acs.jctc.3c00530`.

[61] S. Lehtola, Atomic electronic structure calculations with Hermite interpolating polynomials, J. Phys. Chem. A 127 (2023) 4180–4193. `arXiv:2302.00440`, `doi:10.1021/acs.jpca.3c00729`.

[62] J. Kobus, Vectorizable algorithm for the (multicolour) successive overrelaxation method, in: R. A. de Groot, J. Nadrchal (Eds.), Proceedings of the 4th International Conference Physics Computing '92, World Scientific, Singapore, 1993, pp. 372–373.

[63] J. Stoer, R. Bulirsch, Introduction to numerical analysis, Springer-Verlag, New York, 1980.

[64] L. A. Hageman, D. M. Young, Applied iterative methods, Academic Press, New York, 1981.

[65] B. Sobczak, Analysis of SOR convergence rate, M.Sc. Thesis, Toruń, 2002.

[66] Z. Bai, X. Chi, Asymptotically optimal successive overrelaxation methods for systems of linear equations, J. Comput. Math. 21 (2003) 603–612.

[67] C. J. Li, D. J. Evans, Preconditioning the linear system for the SOR method, Int. J. Comp. Math. 66 (1998) 101–111. `doi:10.1080/00207169808804628`.

[68] J. Kobus, S. Lehtola, x2DHF, a finite difference Hartree–Fock program for atoms and diatomic molecules, accessed 1 August 2024 (2024). URL `http://github.com/x2dhf/x2dhf`

[69] C. F. Fischer, The Hartree–Fock method for atoms. A numerical approach, Wiley, New York, 1977.

[70] J. P. Desclaux, A multiconfiguration Dirac–Fock program, Comput. Phys. Commun. 9 (1975) 31. `doi:10.1016/0010-4655(75)90054-5`.

[71] S. Lehtola, A call to arms: Making the case for more reusable libraries, J. Chem. Phys. 159 (2023) 180901. `doi:10.1063/5.0175165`.

[72] L. S. Blackford, J. Demmel, J. Dongarra, I. Duff, S. Hammarling, G. Henry, M. Heroux, L. Kaufman, A. Lumsdaine, A. Petitet, R. Pozo, K. Remington, R. C. Whaley, An updated set of basic linear algebra subprograms (BLAS), ACM Trans. Math. Soft. 28-2 (2002) 135–151. `doi:10.1145/567806.56780`.

[73] D. Moncrieff, S. Wilson, Finite basis set versus finite difference and finite element methods, Chem. Phys. Lett. 209 (1993) 423–426. `doi:10.1016/0009-2614(93)80041-M`.

[74] D. Moncrieff, S. Wilson, On the accuracy of the algebraic approximation in molecular electronic structure calculations. III. Comparison of matrix Hartree–Fock and numerical Hartree–Fock calculations for the ground state of the nitrogen molecule, J. Phys. B: At. Mol. Opt. Phys. 26 (1993) 1605–1616. `doi:10.1088/0953-4075/26/10/003`.

[75] J. Kobus, D. Moncrieff, S. Wilson, A comparison of finite basis set and finite difference methods for the ground state of the CS molecule, J. Phys. B: At. Mol. Opt. Phys. 27 (1994) 2867–2875. `doi:10.1088/0953-4075/27/14/022`.

[76] J. Kobus, D. Moncrieff, S. Wilson, A comparison of finite difference and finite basis set Hartree–Fock calculations for the ground state potential energy curve of CO, J. Phys. B: At. Mol. Opt. Phys. 27 (1994) 5139–5147. `doi:10.1088/0953-4075/27/21/008`.

[77] J. Kobus, D. Moncrieff, S. Wilson, A comparison of finite basis set and finite difference Hartree–Fock calculations for the BF, AlF and GaF molecules, Mol. Phys. 86 (1995) 1315–1330. `doi:10.1080/00268979500102761`.

[78] D. Moncrieff, J. Kobus, S. Wilson, A universal basis set for high precision electronic structure studies, J. Phys. B: At. Mol. Opt. Phys. 28 (1995) 4555–4557. `doi:10.1088/0953-4075/28/20/016`.

[79] D. Moncrieff, S. Wilson, On the accuracy of the algebraic approximation in molecular electronic structure calculations: V. Electron correlation in the ground state of the nitrogen molecule, J. Phys. B: At. Mol. Opt. Phys. 29 (1996) 2425–2451. `doi:10.1088/0953-4075/29/12/009`.

[80] D. Moncrieff, J. Kobus, S. Wilson, A comparison of finite basis set and finite difference Hartree–Fock calculations for the InF and TlF molecules, Mol. Phys. 93 (1998) 713–725. `doi:10.1080/002689798168736`.

[81] J. Kobus, D. Moncrieff, S. Wilson, A comparison of finite basis set and finite difference Hartree–Fock calculations for the open-shell $(X^2\Sigma^+)$ species BeF, BO, CN and N_2^+, Mol. Phys. 96 (1999) 1559–1567. `doi:10.1080/00268979909483098`.

[82] J. Kobus, D. Moncrieff, S. Wilson, A comparison of the electric moments obtained from finite basis set and finite difference Hartree–Fock calculations for diatomic molecules, Phys. Rev. A 62 (2000) 062503. `doi:10.1103/PhysRevA.62.062503`.

[83] J. Kobus, D. Moncrieff, S. Wilson, A comparison of finite basis set and finite difference Hartree–Fock calculations for the open-shell $(X^2\Sigma^+)$ species BeF, MgF, CaF and SrF, Mol. Phys. 98 (2000) 401–408. `doi:10.1080/00268970009483305`.

[84] J. Kobus, D. Moncrieff, S. Wilson, A comparison of finite basis set and finite difference Hartree–Fock calculations for the open-shell ($X^2\Sigma^+$) BaF and YbF, Mol. Phys. 100 (2002) 499–508. doi:10.1080/00268970110090520.

[85] J. Kobus, D. Moncrieff, S. Wilson, Comparison of the polarizabilities and hyperpolarizabilities obtained from finite basis set and finite field, finite difference Hartree–Fock calculations for diatomic molecules, J. Phys. B: At. Mol. Opt. Phys. 34 (2001) 5127–5143. doi:10.1088/0953-4075/34/24/314.

[86] J. Kobus, D. Moncrieff, S. Wilson, Electric properties of diatomic molecules: A comparison of finite basis set and finite difference Hartree–Fock calculations, J. Comput. Methods in Sci. and Eng. 4 (2004) 611–640. doi:10.5555/1411412.1411419.

[87] J. Kobus, D. Moncrieff, S. Wilson, Comparison of the polarizabilities and hyperpolarizabilities obtained from finite basis set and finite difference Hartree–Fock calculations for diatomic molecules. III. The ground states of N_2, CO and BF, J. Phys. B: At. Mol. Opt. Phys. 40 (2007) 877–896. doi:10.1088/0953-4075/40/5/005.

[88] J. Kobus, Hartree–Fock-limit values of multipole moments, polarizabilities and hyperpolarizabilities for atoms and diatomic molecules, Comp. Lett. 3 (2007) 71–113.

[89] J. Kobus, Overview of finite difference Hartree–Fock method algorithm, implementation and application, AIP Conf. Proc. 1504 (2012) 189–208. doi:10.1063/1.4771715.

[90] J. Kobus, Hartree–Fock limit values of multipole moments, polarizabilities and hyperpolarizabilities for atoms and diatomic molecules, Phys. Rev. A 91 (2015) 022501. doi:10.1103/PhysRevA.91.022501.

[91] T. H. Dunning, Gaussian basis sets for use in correlated molecular calculations. I. The atoms boron through neon and hydrogen, J. Chem. Phys. 90 (1989) 1007. doi:10.1063/1.456153.

[92] D. E. Woon, T. H. Dunning, Gaussian basis sets for use in correlated molecular calculations. III. The atoms aluminum through argon, J. Chem. Phys. 98 (1993) 1358. doi:10.1063/1.464303.

[93] D. E. Woon, T. H. Dunning, Gaussian basis sets for use in correlated molecular calculations. IV. Calculation of static electrical response properties, J. Chem. Phys. 100 (1994) 2975. doi:10.1063/1.466439.

[94] D. E. Woon, T. H. Dunning, Gaussian basis sets for use in correlated molecular calculations. V. Core-valence basis sets for boron through neon, J. Chem. Phys. 103 (1995) 4572. doi:10.1063/1.470645.

[95] A. K. Wilson, T. van Mourik, T. H. Dunning, Gaussian basis sets for use in correlated molecular calculations. VI. Sextuple zeta correlation consistent basis sets for boron through neon, J. Mol. Struct. THEOCHEM 388 (1996) 339–349. doi:10.1016/S0166-1280(96)80048-0.

[96] A. Halkier, W. Klopper, T. Halgaker, P. Jørgensen, Basis-set convergence of the molecular electric dipole moment, J. Chem. Phys. 111 (1999) 4424–4430. doi:10.1063/1.480036.

[97] A. Halkier, T. Helgaker, P. Jørgensen, W. Klopper, J. Olsen, Basis-set convergence of the energy in molecular Hartree–Fock calculations, Chem. Phys. Lett. 302 (1999) 437–446. doi:10.1016/S0009-2614(99)00179-7.

[98] F. Jensen, The basis set convergence of the Hartree–Fock energy for H_2, J. Chem. Phys. 110 (1999) 6601–6605. doi:10.1063/1.478567.

[99] K. A. Christensen, F. Jensen, The basis set convergence of the density functional energy for H_2, Chem. Phys. Lett. 317 (2000) 400–403. doi:10.1016/S0009-2614(99)01419-0.

[100] F. Jensen, The basis set convergence of the Hartree–Fock energy for H_3^+, Li_2 and N_2, Theor. Chem. Acc. 104 (2000) 484–490. doi:10.1007/s002140000174.

[101] T. Helgaker, W. Klopper, H. Koch, J. Noga, Basis-set convergence of correlated calculations on water, J. Chem. Phys. 106 (1997) 9639–9646. doi:10.1063/1.473863.

[102] F. Jensen, Polarization consistent basis sets: Principles, J. Chem. Phys. 115 (2001) 9113–9125. doi:10.1063/1.1413524.

[103] F. Jensen, Erratum: "Polarization consistent basis sets: Principles" [J]. Chem. Phys. 115 , 9113 (2001)], J. Chem. Phys. 116 (2002) 3502–3502. doi:10.1063/1.1445402.

[104] F. Jensen, Polarization consistent basis sets. II. Estimating the Kohn–Sham basis set limit, J. Chem. Phys. 116 (2002) 7372–7379. doi:10.1063/1.1465405.

[105] F. Jensen, Polarization consistent basis sets. III. The importance of diffuse functions, J. Chem. Phys. 117 (2002) 9234–9240. doi:10.1063/1.1515484.

[106] F. Jensen, Polarization consistent basis sets. IV. The basis set convergence of equilibrium geometries, harmonic vibrational frequencies, and intensities, J. Chem. Phys. 118 (2003) 2459–2463. doi:10.1063/1.1535905.

[107] F. Jensen, T. Helgaker, Polarization consistent basis sets. V. The elements Si–Cl, J. Chem. Phys. 121 (2004) 3463–3470. doi:10.1063/1.1756866.

[108] F. Jensen, Polarization consistent basis sets. 4: The elements He, Li, Be, B, Ne, Na, Mg, Al, and Ar, J. Phys. Chem. A 111 (2007) 11198–11204. doi:10.1021/jp068677h.

[109] F. Jensen, Polarization consistent basis sets. VII. The elements K, Ca, Ga, Ge, As, Se, Br, and Kr, J. Chem. Phys. 136 (2012) 114107. doi:10.1063/1.3690460.

[110] F. Jensen, Polarization consistent basis sets. VIII. The transition metals Sc–Zn, J. Chem. Phys. 138 (2013) 014107. doi:10.1063/1.4773017.

[111] F. Weigend, F. Furche, R. Ahlrichs, Gaussian basis sets of quadruple zeta valence quality for atoms H–Kr, J. Chem. Phys. 119 (24) (2003) 12753–12762. doi:10.1063/1.1627293.

[112] S. Zhong, E. C. Barnes, G. A. Petersson, Uniformly convergent n-tuple-zeta augmented polarized (nZaP) basis sets for complete basis set extrapolations. I. Self-consistent field energies, J. Chem. Phys. 129 (18) (2008) 184116. doi:10.1063/1.3009651.

[113] T. G. Williams, N. J. DeYonker, A. K. Wilson, Hartree–Fock complete basis set limit properties for transition metal diatomics, J. Chem. Phys. 128 (4) (2008) 044101. `doi:10.1063/1.2822907`.

[114] N. B. Balabanov, K. A. Peterson, All-electron correlation consistent basis sets for the 3d elements Sc–Zn, J. Chem. Phys. 123 (2005) 064107. `doi:10.1063/1.1998907`.

[115] X. Sheng, X. Xu, S. Huang, On the validity of complete basis set extrapolation formula optimized for the equilibrium distance applied to the potential energy surface for the correlation energy of the helium dimer, Int. J. Quantum Chem. 118 (2018) 325552. `doi:10.1002/qua.25552`.

[116] A. Halkier, S. Coriani, State-of-the-art ab initio calculations of the molecular electric quadrupole moments of hydrogen fluoride, Chem. Phys. Lett. 346 (2001) 329–333. `doi:10.1016/S0009-2614(01)00895-8`.

[117] F. Pawłowski, P. Jørgensen, C. Hättig, The hyperpolarizability of the Ne atom in the approximate coupled cluster triples model CC3, Chem. Phys. Lett. 391 (2004) 27–32. `doi:10.1016/j.cplett.2004.04.055`.

[118] A. K. Roy, A. J. Thakkar, Maclaurin expansions of electron momentum densities for 78 diatomic molecules: a numerical Hartree–Fock study, Chem. Phys. Lett. 362 (2002) 428–434. `doi:10.1016/S0009-2614(02)01101-6`.

[119] S. Shahbazian, M. Zahedi, Towards a complete basis set limit of Hartree–Fock method: correlation-consistent versus polarized-consistent basis sets, Theor. Chem. Acc. 113 (2005) 152–160. `doi:10.1007/s00214-005-0619-2`.

[120] D. Rappoport, Basis-set quality and basis-set bias in molecular property calculations, ChemPhysChem 12 (2011) 3404–3413. `doi:10.1002/cphc.201100502`.

[121] L. M. Mentel, E. J. Baerends, Can the counterpoise correction for basis set superposition effect be justified?, J. Chem. Theory Comput. 10 (2013) 252–267. `doi:10.1021/ct400990u`.

[122] A. Gil, J. Segura, A code to evaluate prolate and oblate spheroidal harmonics, Comput. Phys. Commun. 108 (1998) 267–278. `doi:10.1016/S0010-4655(97)00126-4`.

[123] B. I. Schneider, J. Segura, A. Gil, X. Guan, K. Bartschat, A new Fortran 90 program to compute regular and irregular associated Legendre functions, Comput. Phys. Commun. 181 (2010) 2091–2097. `doi:10.1016/j.cpc.2010.08.038`.

[124] B. I. Schneider, J. Segura, A. Gil, X. Guan, K. Bartschat, A new Fortran 90 program to compute regular and irregular associated Legendre functions (new version announcement), Comput. Phys. Commun. 225 (2018) 192–193. `doi:10.1016/j.cpc.2017.12.013`.

[125] C. B. Mendl, Efficient algorithm for two-center Coulomb and exchange integrals of electronic prolate spheroidal orbitals, J. Comput. Phys. 231 (2012) 5157–5175. `arXiv:1203.6256`, `doi:10.1016/j.jcp.2012.04.022`.

[126] K. Bodoor, J. Kobus, J. Morrison, A numerical solution of the pair equation of a model two-electron diatomic system, Int. J. Quantum Chem. 115 (2015) 868–874. `doi:10.1002/qua.24921`.

[127] L. Laaksonen, I. P. Grant, Two-dimensional fully numerical solutions of molecular Dirac equations. results for ground singlet states of H_2 and HeH^+, Chem. Phys. Lett. 112 (1984) 157–159. `doi:10.1016/0009-2614(84)85012-5`.

[128] L. Laaksonen, I. P. Grant, Two-dimensional fully numerical solutions of molecular Dirac equations. one-electron molecules, Chem. Phys. Lett. 109 (1984) 485–487. `doi:10.1016/0009-2614(84)80348-6`.

[129] D. Sundholm, P. Pyykkö, L. Laaksonen, Two-dimensional, fully numerical solutions of second-order Dirac equations for diatomic molecules. part 3, Phys. Scr. 36 (1987) 400–402. `doi:10.1088/0031-8949/36/3/004`.

[130] D. Sundholm, Two-dimensional, fully numerical solution of the molecular Dirac equation. Dirac–Slater calculations on LiH, Li_2, BH and CH^+, Chem. Phys. Lett. 149 (1988) 251–256. `doi:10.1016/0009-2614(88)85022-X`.

[131] J. Kobus, A. Kędziorski, Two-dimensional, finite-difference method of solving the Dirac equation for diatomic molecules revisited, Mol. Phys. 120 (19-20) (2022) e2092563. `doi:10.1080/00268976.2022.2092563`.

[132] J. Styszyński, Relativistic core-valence correlation effects on molecular properties of the hydrogen halide molecules, Chem. Phys. Lett. 317 (2000) 351–359. `doi:10.1016/S0009-2614(99)01392-5`.

[133] J. Styszyński, J. Kobus, Relativistic and correlation effects on spectroscopic constants of the hydrogen astatide molecule, Chem. Phys. Lett. 369 (2003) 441–448. `doi:10.1016/S0009-2614(02)02014-6`.

[134] E. Matito, J. Kobus, J. Styszyński, Bond centred functions in relativistic and non-relativistic calculations for diatomics, Chem. Phys. 321 (2005) 277–284. `doi:10.1016/j.chemphys.2005.08.023`.

[135] J. F. Ziegler, J. P. Biersack, U. Littmark, The Stopping and Range of Ions in Solids, Pergamon, New York, 1985.

[136] K. Nordlund, N. Runeberg, D. Sundholm, Repulsive interatomic potentials calculated using Hartree–Fock and density-functional theory methods, Nucl. Instrum. Methods Phys. Res., Sect. B 132 (1997) 45–54. `doi:10.1016/S0168-583X(97)00447-3`.

[137] J. M. Pruneda, E. Artacho, Short-range repulsive interatomic interactions in energetic processes in solids, Phys. Rev. B 70 (2004) 035106. `doi:10.1103/PhysRevB.70.035106`.

[138] V. Kuzmin, Range parameters of heavy ions in carbon calculated with first-principles potentials, Nucl. Instrum. Methods Phys. Res., Sect. B 249 (2006) 13–17. `doi:10.1016/j.nimb.2006.03.012`.

[139] V. Kuzmin, Calculations of range parameters for heavy ions in carbon using ab initio potentials, Surf. Coat. Tech. 201 (2007) 8388–8392. `doi:10.1016/j.surfcoat.2006.10.053`.

[140] S. Lehtola, Accurate reproduction of strongly repulsive interatomic potentials, Phys. Rev. A 101 (2020) 032504. `arXiv:1912.12624`, `doi:10.1103/PhysRevA.101.032504`.

[141] C. B. Madsen, L. B. Madsen, High-order harmonic generation from arbitrarily oriented diatomic molecules including nuclear motion and field-free alignment, Phys. Rev. A 74 (2006) 023403. `doi:10.1103/PhysRevA.74.023403`.

[142] R. A. Wilhelm, E. Gruber, J. Schwestka, R. Kozubek, T. I. Madeira, J. P. Marques, J. Kobus, A. V. Krasheninnikov, M. Schleberger, F. Aumayr, Interatomic Coulombic decay: The mechanism for rapid deexcitation of hollow atoms, Phys. Rev. Lett 119 (2017) 103401. `doi:10.1103/PhysRevLett.119.103401`.

[143] X. M. Tong, Z. X. Zhao, C. D. Lin, Theory of molecular tunneling ionization, Phy. Rev. A 66 (2002) 033402. `doi:10.1103/PhysRevA.66.033402`.

[144] L. B. Madsen, O. I. Tolstikhin, T. Morishita, Application of the weak-field asymptotic theory to the analysis of tunneling ionization of linear molecules, Phys. Rev. A 85 (2012) 053404. `doi:10.1103/PhysRevA.85.053404`.

[145] L. B. Madsen, F. Jensen, O. I. Tolstikhin, T. Morishita, Structure factors for tunneling ionization rates of molecules, Phys. Rev. A 87 (2013) 013406. `doi:10.1103/PhysRevA.87.013406`.

[146] O. I. Tolstikhin, L. B. Madsen, T. Morishita, Weak-field asymptotic theory of tunneling ionization in many-electron atomic and molecular systems, Phys. Rev. A 89 (2014) 013421. `doi:10.1103/PhysRevA.89.013421`.

[147] A. S. Kornev, B. A. Zon, Anti-stokes-enhanced tunnelling ionization of polar molecules, Laser Phys. 24 (2014) 115302. `doi:10.1088/1054-660X/24/11/115302`.

[148] J. P. Wang, S. F. Zhao, C. R. Zhang, X. X. Zhou, Determination of structure parameters in molecular tunnelling ionisation model, Mol. Phys. 112 (2014) 1102–1114. `doi:10.1103/PhysRevLett.119.103401`.

[149] A. S. Kornev, B. A. Zon, Tunneling ionization of vibrationally excited nitrogen molecules, Phys. Rev. A 92 (2015) 033420. `doi:10.1103/PhysRevA.92.033420`.

[150] A. S. Kornev, I. M. S. B. A. Zon, The influence of a permanent dipole moment on the tunneling ionization of a CO molecule, Laser Phys. 26 (2016) 055302. `doi:10.1088/1054-660X/26/5/055302`.

[151] T. Endo, A. Matsuda, M. Fushitani, T. Yasuike, O. I. Tolstikhin, T. Morishita, A. Hishikawa, Imaging electronic excitation of NO by ultrafast laser tunneling ionization, Phys. Rev. Lett. 116 (2016) 163002. `doi:10.1103/PhysRevLett.116.163002`.

[152] I. V. Kopytin, A. S. Kornev, B. A. Zon, Tunnel ionization of diatomic atmospheric gases (N_2, O_2) by laser radiation, Laser Phys. 29 (2019) 095301. `doi:10.1088/1555-6611/ab3431`.

[153] O. P. Romashenko, A. S. Kornev, B. A. Zon, Laser radiation absorption in the atmosphere of Titan, Atmos. Ocean. Optics 33 (2020) 439–442. `doi:10.1134/S1024856020050152`.

[154] E. Ley-Koo, S. A. Cruz, The hydrogen atom and the H_2^+ and HeH^+ molecular ions inside prolate spheroidal boxes, J. Chem. Phys. 74 (1981) 4603–4610. `doi:10.1063/1.441649`.

[155] H. Olivares-Pilón, S. A. Cruz, The H, H_2^+, and HeH_2^+ systems confined by an impenetrable spheroidal cavity: Revisited study via the Lagrange-mesh approach, Int. J. Quantum Chem. 117 (2017) e25399. `doi:10.1002/qua.25399`.

[156] H. de Oliveira Batael, E. Drigo Filho, Excited states for hydrogen ion molecule confined by a prolate spheroidal boxes: variational approach, Theor. Chem. Acc. 139 (2020) 129. `doi:10.1007/s00214-020-02645-5`.

[157] N. Mukherjee, C. N. Patra, A. K. Roy, Hellmann–Feynman theorem and internal pressure for atoms, molecules and plasmas under pressure, J. Phys. B: At. Mol. Opt. Phys. 56 (2023) 065001. `doi:10.1088/1361-6455/acb6dc`.

[158] S. Liu, V. K. R. López-Boada, F. De Proft, Polynomial and Padé representations for the kinetic component $T_c[\rho]$ of the correlation energy density functional, Int. J. Quantum Chem. 69 (1998) 513–522. `doi:10.1002/(SICI)1097-461X(1998)69:4<513::AID-QUA8>3.0.CO;2-Y`.

[159] E. V. Ludeña, V. V. K. R. López-Boada, E. Valderrama, J. Maldon-ado, Local-scaling transformation version of density functional the-ory: Application to atoms and diatomic molecules, J. Comput. Chem. 20 (1999) 155–183. doi:10.1002/(SICI)1096-987X(19990115)20:1<155::AID-JCC14>3.0.CO;2-2.

[160] V. V. Karasiev, Parameter-free local exchange and Padé approxima-tion for correlation: application to diatomic molecules, J. Mol. Struct. (THEOCHEM) 493 (1999) 21–28. doi:10.1016/S0166-1280(99)00221-3.

[161] V. V. Karasiev, E. V. Ludeña, A. N. Artemyev, Electronic-structure kinetic-energy functional based on atomic local-scaling transforma-tions, Phys. Rev. A 62 (2000) 062510. doi:10.1103/PhysRevA.62.062510.

[162] V. V. Karasiev, E. V. Ludeña, Self-consistent multiplicative constant method for the exchange energy in density-functional theory, Phys. Rev. A 65 (6) (2002) 062510. doi:10.1103/PhysRevA.65.062510.

[163] V. V. Karasiev, E. V. Ludeña, Asymptotically adjusted self-consistent multiplicative parameter exchange-energy-functional method: Appli-cation to diatomic molecules, Phys. Rev. A 65 (3) (2002) 032515. doi:10.1103/PhysRevA.65.032515.

[164] V. V. Karasiev, Local "hybrid" functionals based on exact-expression approximate exchange, J. Chem. Phys. 118 (19) (2003) 8576–8583. doi:10.1063/1.1568074.

[165] V. V. Karasiev, S. B. Trickey, F. E. Harris, Faster approximate force calculations via quasi-spin density exchange-correlation functionals, Chem. Phys. 330 (2006) 216–223. doi:10.1016/j.chemphys.2006.08.017.

[166] M. Hemanadhan, M. K. Harbola, Excitation energies of molecules within time-independent density functional theory, AIP Conf. Proc. 1591 (2014) 1170–1172. doi:10.1063/1.4872892.

[167] T. Wang, K. Luo, R. Lu, Semilocal kinetic energy density functionals on atoms and diatoms, J. Chem. Theory Comput. 20 (12) (2024) 5176–5187. doi:10.1021/acs.jctc.4c00532.

[168] A. Makmal, S. Kümmel, L. Kronik, Fully Numerical All-Electron Solutions of the Optimized Effective Potential Equation for Diatomic Molecules, J. Chem. Theory Comput. 5 (2009) 1731–1740. `doi:10.1021/ct800485v`.

[169] A. Makmal, R. Armiento, E. Engel, L. Kronik, S. Kümmel, Examining the role of pseudopotentials in exact-exchange-based Kohn–Sham gaps, Phys. Rev. B 80 (2009) 161204. `doi:10.1103/PhysRevB.80.161204`.

[170] A. Makmal, S. Kümmel, L. Kronik, Dissociation of diatomic molecules and the exact-exchange Kohn–Sham potential: The case of LiF, Phys. Rev. A 83 (2011) 062512. `doi:10.1103/PhysRevA.83.062512`.

[171] E. Kraisler, L. Kronik, Piecewise Linearity of Approximate Density Functionals Revisited: Implications for Frontier Orbital Energies, Phys. Rev. Lett. 110 (2013) 126403. `arXiv:1211.5950`, `doi:10.1103/PhysRevLett.110.126403`.

[172] T. Schmidt, E. Kraisler, L. Kronik, S. Kümmel, One-electron self-interaction and the asymptotics of the Kohn–Sham potential: an impaired relation, Phys. Chem. Chem. Phys. 16 (2014) 14357–14367. `doi:10.1039/c3cp55433c`.

[173] T. Schmidt, E. Kraisler, A. Makmal, L. Kronik, S. Kümmel, A self-interaction-free local hybrid functional: accurate binding energies vis-à-vis accurate ionization potentials from Kohn–Sham eigenvalues, J. Chem. Phys. 140 (2014) 18A510. `doi:10.1063/1.4865942`.

[174] E. Kraisler, T. Schmidt, S. Kümmel, L. Kronik, Effect of ensemble generalization on the highest-occupied Kohn–Sham eigenvalue, J. Chem. Phys. 143 (2015) 104105. `doi:10.1063/1.4930119`.

[175] E. Kraisler, L. Kronik, Elimination of the asymptotic fractional dissociation problem in Kohn–Sham density-functional theory using the ensemble-generalization approach, Phys. Rev. A 91 (2015) 032504. `doi:10.1103/PhysRevA.91.032504`.

[176] T. Schmidt, S. Kümmel, One- and many-electron self-interaction error in local and global hybrid functionals, Phys. Rev. B 93 (2016) 165120. `doi:10.1103/PhysRevB.93.165120`.

[177] T. Schmidt, S. Kümmel, The influence of one-electron self-interaction on *d*-electrons, Computation 4 (2016) 33. `doi:10.3390/computation4030033`.

[178] M. Banafsheh, T. Adam Wesolowski, Nonadditive kinetic potentials from inverted Kohn–Sham problem, Int. J. Quantum Chem. 118 (2017) e25410. `doi:10.1002/qua.25410`.

[179] T. Aschebrock, R. Armiento, S. Kümmel, Challenges for semilocal density functionals with asymptotically nonvanishing potentials, Phys. Rev. B 96 (2017) 075140. `doi:10.1103/PhysRevB.96.075140`.

[180] T. Aschebrock, R. Armiento, S. Kümmel, Orbital nodal surfaces: Topological challenges for density functionals, Phys. Rev. B 95 (2017) 245118. `doi:10.1103/physrevb.95.245118`.

[181] T. Aschebrock, S. Kümmel, Ultranonlocality and accurate band gaps from a meta-generalized gradient approximation, Phys. Rev. Res. 1 (2019) 033082. `doi:10.1103/PhysRevResearch.1.033082`.

[182] T. Aschebrock, S. Kümmel, Exploring local range separation: The role of spin scaling and one-electron self-interaction, J. Chem. Phys. 151 (2019) 154108. `doi:10.1063/1.5121731`.

[183] R. Garrick, A. Natan, T. Gould, L. Kronik, Exact generalized Kohn–Sham theory for hybrid functionals, Phys. Rev. X 10 (2020) 021040. `doi:10.1103/physrevx.10.021040`.

[184] M. Banafsheh, T. A. Wesolowski, T. Gould, L. Kronik, D. A. Strubbe, Nuclear cusps and singularities in the nonadditive kinetic potential bifunctional from analytical inversion, Phys. Rev. A 106 (2022) 042812. `doi:10.1103/PhysRevA.106.042812`.

[185] T. Lebeda, T. Aschebrock, S. Kümmel, First steps towards achieving both ultranonlocality and a reliable description of electronic binding in a meta-generalized gradient approximation, Phys. Rev. Research 4 (2022) 023061. `doi:10.1103/PhysRevResearch.4.023061`.

[186] R. Richter, T. Aschebrock, I. Schelter, S. Kümmel, Meta-generalized gradient approximations in time dependent generalized Kohn–Sham

theory: Importance of the current density correction, J. Chem. Phys. 159 (2023) 124117. `doi:10.1063/5.0167972`.

[187] V. H. Chávez, J. Nafziger, A. Wasserman, pyCADMium: Chemical atoms in diatomic molecules. a prolate spheroidal Python module for embedding calculations, Journal of Open Source Software 7 (2022) 4459. `doi:10.21105/joss.04459`.

[188] P. Kraus, Basis set extrapolations for density functional theory, J. Chem. Theory Comput. 16 (2020) 5712–5722. `doi:10.1021/acs.jctc.0c00684`.

[189] P. Kraus, Extrapolating DFT toward the complete basis set limit: Lessons from the PBE family of functionals, J. Chem. Theory Comput. 17 (2021) 5651–5660. `doi:10.1021/acs.jctc.1c00542`.

[190] S. Lehtola, M. A. L. Marques, Many recent density functionals are numerically ill-behaved, J. Chem. Phys. 157 (2022) 174114. `doi:10.1063/5.0121187`.

[191] S. Lehtola, M. Dimitrova, D. Sundholm, Fully numerical electronic structure calculations on diatomic molecules in weak to strong magnetic fields, Mol. Phys. 118 (2020) e1597989. `arXiv:1812.06274`, `doi:10.1080/00268976.2019.1597989`.

[192] H. Åström, S. Lehtola, Insight on Gaussian basis set truncation errors in weak to intermediate magnetic fields with an approximate hamiltonian, J. Phys. Chem. A 127 (2023) 10872–10888. `arXiv:2307.02635`, `doi:10.1021/acs.jpca.3c04531`.

[193] S. Lehtola, Importance profiles. visualization of atomic basis set requirements, Electron. Struct. 6 (2024) 015015. `doi:10.1088/2516-1075/ad31ca`.

[194] S. Lehtola, Polarized Gaussian basis sets from one-electron ions, J. Chem. Phys. 152 (2020) 134108. `arXiv:2001.04224`, `doi:10.1063/1.5144964`.

[195] S. F. Boys, F. Bernardi, The calculation of small molecular interactions by the differences of separate total energies. Some procedures

with reduced errors, Mol. Phys. 19 (1970) 553–566. `doi:10.1080/00268977000101561`.

[196] M. Gutowski, F. B. van Duijneveldt, G. Chałasiński, L. Piela, Proper correction for the basis set superposition error in SCF calculations of intermolecular interactions, Mol. Phys. 61 (1987) 233–247. `doi:10.1080/00268978700101101`.

[197] A. J. C. Varandas, Can extrapolation to the basis set limit be an alternative to the counterpoise correction? A study on the helium dimer, Theor. Chem. Account 119 (2008) 511–521. `doi:10.1007/s00214-008-0419-6`.

[198] M. Taut, Two electrons in an external oscillator potential: Particular analytic solutions of a Coulomb correlation problem, Phys. Rev. A 48 (1993) 3561–3566. `doi:10.1103/PhysRevA.48.3561`.

[199] R. D. Amos, J. E. Rice, Implementation of analytic derivative methods in quantum chemistry, Comput. Phys. Rep. 10 (1989) 147–187. `doi:10.1016/0167-7977(89)90001-4`.

[200] E. Engel, S. H. Vosko, Accurate optimized-potential-model solutions for spherical spin-polarized atoms: Evidence for limitations of the exchange-only local spin-density and generalized-gradient approximations, Phys. Rev. A 47 (1993) 2800–2811. `doi:10.1103/PhysRevA.47.2800`.

[201] S. Lehtola, M. A. L. Marques, Reproducibility of density functional approximations: How new functionals should be reported, J. Chem. Phys. 159 (2023) 114116. `doi:10.1063/5.0167763`.

[202] J. P. Perdew, K. Burke, M. Ernzerhof, Generalized gradient approximation made simple, Phys. Rev. Lett. 77 (1996) 3865–3868. `doi:10.1103/PhysRevLett.77.3865`.

[203] J. P. Perdew, K. Burke, M. Ernzerhof, Generalized gradient approximation made simple [Phys. Rev. Lett. 77, 3865 (1996)], Phys. Rev. Lett. 78 (1997) 1396–1396. `doi:10.1103/PhysRevLett.78.1396`.

[204] A. D. Becke, Density-functional exchange-energy approximation with correct asymptotic behavior, Phys. Rev. A 38 (1988) 3098–3100. `doi:10.1103/PhysRevA.38.3098`.

[205] S. H. Vosko, L. Wilk, M. Nusair, Accurate spin-dependent electron liquid correlation energies for local spin density calculations: a critical analysis, Can. J. Phys. 58 (1980) 1200–1211. `doi:10.1139/p80-159`.

[206] J. P. Perdew, Y. Wang, Accurate and simple analytic representation of the electron-gas correlation energy, Phys. Rev. B 45 (1992) 13244–13249. `doi:10.1103/PhysRevB.45.13244`.

[207] C. Lee, W. Yang, R. G. Parr, Development of the Colle–Salvetti correlation-energy formula into a functional of the electron density, Phys. Rev. B 37 (1988) 785–789. `doi:10.1103/PhysRevB.37.785`.

[208] B. Miehlich, A. Savin, H. Stoll, H. Preuss, Results obtained with the correlation energy density functionals of Becke and Lee, Yang and Parr, Chem. Phys. Lett. 157 (1989) 200–206. `doi:10.1016/0009-2614(89)87234-3`.

[209] P. Rinke, A. Schleife, E. Kioupakis, A. Janotti, C. Rödl, F. Bechstedt, M. Scheffler, C. G. Van de Walle, First-Principles Optical Spectra for F Centers in MgO, Phys. Rev. Lett. 108 (2012) 126404. `doi:10.1103/PhysRevLett.108.126404`.

[210] M. Levy, J. P. Perdew, V. Sahni, Exact differential equation for the density and ionization energy of a many-particle system, Phys. Rev. A 30 (1984) 2745. `doi:10.1103/PhysRevA.30.2745`.

[211] D. Andrae, Finite nuclear charge density distributions in electronic structure calculations for atoms and molecules, Phys. Rep. 336 (2000) 414–525. `doi:10.1016/S0370-1573(00)00007-7`.

[212] F. A. Parpia, Electric-dipole hyperfine matrix elements of the ground state of the TlF molecule in the Dirac–Fock approximation, J. Phys. B: At. Mol. Opt. Phys. 30 (1997) 3983–4001. `doi:10.1088/0953-4075/30/17/022`.

[213] F. A. Parpia, C. Froese Fischer, I. P. Grant, GRASP92: a package for large-scale relativistic atomic structure calculations, Comput. Phys. Commun. 94 (1996) 249–271. `doi:10.1016/0010-4655(95)00136-0`.

[214] F. Zahariev, S. S. Leang, M. S. Gordon, Functional derivatives of meta-generalized gradient approximation (meta-GGA) type exchange-correlation density functionals, J. Chem. Phys. 138 (2013) 244108. `doi:10.1063/1.4811270`.

[215] S. Lehtola, F. Blockhuys, C. Van Alsenoy, An overview of self-consistent field calculations within finite basis sets, Molecules 25 (2020) 1218. `arXiv:1912.12029`, `doi:10.3390/molecules25051218`.

[216] J. A. Pople, P. M. W. Gill, B. G. Johnson, Kohn–Sham density-functional theory within a finite basis set, Chem. Phys. Lett. 199 (1992) 557–560. `doi:10.1016/0009-2614(92)85009-Y`.

[217] R. Neumann, R. H. Nobes, N. C. Handy, Exchange functionals and potentials, Mol. Phys. 87 (1996) 1–36. `doi:10.1080/00268979650027630`.

[218] M. Abramowitz, L. A. S. Stegun, Handbook of Mathematical Functions, Wiley, New York, 1977.